NASA
Technical
Paper
2084

December 1982

Empirical Source Noise Prediction Method With Application to Subsonic Coaxial Jet Mixing Noise

William E. Zorumski
and Donald S. Weir

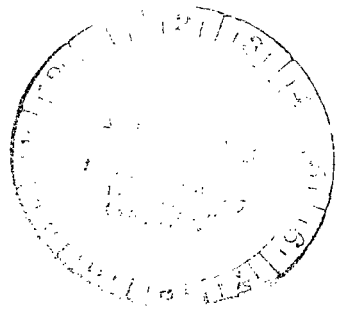

NASA

NASA
Technical
Paper
2084

1982

Empirical Source Noise Prediction Method With Application to Subsonic Coaxial Jet Mixing Noise

William E. Zorumski
Langley Research Center
Hampton, Virginia

Donald S. Weir
Kentron International, Inc.
Hampton, Virginia

NASA
National Aeronautics
and Space Administration

**Scientific and Technical
Information Branch**

CONTENTS

SUMMARY 1

INTRODUCTION 1

SYMBOLS 4

EMPIRICAL SOURCE NOISE EQUATIONS 6
Preliminary Definitions 6
Prediction Equations 7

DATA REDUCTION 11
Bicubic Splines 11
Noise Level Coordinates 12
Coordinate Constraints 13
Taylor's Series 15

COAXIAL JET MIXING NOISE 16
Organization of Data 16
Discussion of Data 18
Coaxial Jet Noise Prediction 19
Optimum Coaxial Jet 24

CONCLUDING REMARKS 29

REFERENCES 30

TABLES 31

FIGURES 41

SUMMARY

A curve-fitting technique is developed which is useful in the representation of noise sources. Noise from a given source is tabulated in a spherical coordinate system at a fixed radius from the origin. The noise, represented by mean-square pressure or by sound pressure level, is then a function of frequency, polar directivity angle, and a number of parameters which represent the physical properties of the source. The dependence of the noise on the frequency and directivity variables is represented by bicubic splines. A least-squares bicubic spline fit is made to noise data from each test of the source to find values of the noise data at the knots, or nodes, of a frequency-angle computational grid. The array of noise values at these grid points is called noise coordinates. These coordinates are associated with the parameters which describe the state of the noise source; that is, the coordinates are functions of the test parameters. The functional dependence of the coordinates on the test parameters is represented by a Taylor's series expansion of the coordinates in terms of the parameters. The coefficients in the Taylor's series, which are partial derivatives of the coordinates with respect to the various parameters, are found by a least-squares fit to data from different tests of the noise source.

The method is applied to the prediction of coaxial jet noise. The jets are axisymmetric so that a bicubic spline may be used to represent the frequency and directivity dependence. The frequency variation is represented by five intervals with natural (zero-curvature) boundary conditions. The directivity variation is also represented by five intervals but with zero-slope boundary conditions. This bicubic spline has 36 degrees of freedom or coordinates. There are five independent parameters, or dimensionless groups, which represent the flow state of a coaxial jet. Each of the 36 coordinates of the bicubic spline is represented by a third-degree Taylor's series in the 5 jet parameters. These Taylor's series each have 56 independent terms, including the constant for the origin of the expansion. Data from over 540 jet noise tests were collected to solve for the coefficients of the Taylor's series. This data base supplied over 540 equations in 56 unknowns for each of the 36 coordinates. These sets of equations were solved in the least-squares sense to produce a seven-dimensional curve fit to the jet noise data base: two dimensions for the spline and five dimensions for the Taylor's series.

INTRODUCTION

The purpose of this paper is to develop an empirical method for source noise predictions. The method is general in the sense that it may be applied to any source for which measured noise data are available. This method is limited herein to noise sources with an axis of symmetry. Extending the method to sources without symmetry is possible with only a small conceptual change, but there will be an increased requirement for data, data reduction, and computation.

This method was developed for application to aircraft noise prediction. The NASA Aircraft Noise Prediction Program (ref. 1) contains empirical methods for noise sources on conventional turbofan aircraft. The principal aircraft noise sources are the jets, the engine fans, and the engine combustion chambers. The secondary aircraft noise sources are the engine turbines and the airframe. The aircraft engine

sources are all assumed to be axisymmetric. The airframe noise is probably not axisymmetric; however, there are not enough data to define conclusively the directivity of this source. Since airframe noise is usually less than engine noise, it is frequently assumed that, in the far field, the noise from the entire aircraft is axisymmetric. The method given herein can thus be applied either to the aircraft component noise sources or to the entire aircraft.

Empirical prediction methods have three principal features: a prediction of the overall noise, a prediction of the directionality of the noise, and a prediction of the spectrum of the noise. These features appear in each of the aircraft component prediction methods given in reference 1. The general similarity of empirical prediction methods for physically different noise sources, such as an aircraft engine fan and a jet, suggests that a general formula can be given without referring to the particular physical features of the noise source. The general formula is developed in this paper.

An empirical prediction method must give an accurate description of the noise for all possible states of the source. For a particular source, its state is described by variables such as speed, temperature, and pressure. These state variables are called parameters to distinguish them from other variables, such as frequency and direction, which are associated with the noise field but not with the state of the source. Most noise-producing machines operate over a limited range of state that is not far removed from a common state called the design point. This limited range makes it possible to develop a general empirical method for source noise prediction.

An empirical prediction method gives the noise field in terms of the source parameters, or source state, and tables of constants which are uniquely related to the noise source. For example, jet noise may be predicted with a set of noise spectrum curves (functions). These curves are usually given graphically; however, for predictions with a digital computer, these graphs are converted to tables which are interpolated to give the spectrum functions (curves). Reference 1 contains tables of constants for the turbofan-powered aircraft noise sources. These tables often contain several thousand constants.

The tables used in an empirical prediction method are the end product of a data-reduction process which begins with measured source state and noise field data. The data tables used in the prediction method may be regarded as alternate forms of the original data. Emphasizing the word "reduction" in the data-reduction process implies that the smallest possible tables are desired as a basis for empirical noise prediction. One method of achieving the goal of smaller tables is to use higher-order interpolation schemes. Referring again to the example of jet noise, the tables given in reference 1 are intended for linear interpolation. By using a higher order interpolation scheme, such as cubic splines, these tables may be reduced in size; that is, they may be converted to equivalent tables with fewer entries. The selection of interpolation rules is the first step in either empirical prediction or data reduction. Empirical prediction and data reduction are inverse processes with common interpolation rules.

The goal of empirical source noise prediction is to compute a noise field which is close to the measured data. A mathematical norm is selected to give objectivity and precision to the concept of closeness. This objective definition of closeness may be used to compare different prediction methods such as a theoretical prediction and an empirical prediction. It is used first, however, in the data-reduction process in computing the tables of constants. The classical norm of distance squared

is used herein. This norm has the advantage of leading to linear equations in the data-reduction process. The resulting prediction method is said to be best in the least-squares sense.

The basic elements of the present empirical method may be summarized now. The method uses least-squares curve fits to measured data. The interpolation rules are cubic splines for noise field variables, such as frequency and direction, and Taylor's series approximations for source parameters. Taylor's series are appropriate for source parameters since these do not vary far from some standard source state values. The splines are necessary for field variables since they have a larger range of values.

The method herein is illustrated with application to the turbulent mixing noise of static subsonic coaxial jets. The flow state of a coaxial jet is a function of five source parameters. These source parameters can be chosen from a large group of interdependent parameters. Many jet noise theories use area ratio (of the outer nozzle to the inner nozzle) and the velocity and density of each stream. Empirical formulas (refs. 1, 2, and 3) often use area ratio, velocity, and total temperature of each stream. A large data base is necessary to empirically define a function of five variables.

The data base contains 65 single-jet noise tests from Lockheed-Georgia Company (work done under Air Force Contract F33615-73-C-2032 from 1972 to 1975), 146 tests of nozzles with area ratios of 0.75 and 1.2 from Pratt & Whitney Aircraft (ref. 4), and 212 tests from the NASA Lewis Research Center (refs. 5 and 6). The Lewis tests included nozzle area ratios of 1.2, 1.5, 2.0, and 3.33. The Pratt & Whitney data are unique in their coverage of the temperatures of both streams. The Lewis data cover the broadest range of source parameters, including supersonic flows in both streams. The National Gas Turbine Establishment in the United Kingdom contributed three data sets designated as data sets A, B, and C. The NGTE data set C has the largest range of area ratio, from 1.4 to 8.1, of any data set but has an ambient temperature outer stream. The Societe Nationale d'Etude et de Construction de Motuers d'Aviation in France also contributed a subsonic jet data set. This data base has over 800 separate jet noise tests with around 200 000 individual sound pressure level (SPL) measurements.

The National Aeronautics and Space Administration (NASA) has a continuing research program for the development of noise prediction methods. The first jet noise prediction methods developed under this program were by Stone (ref. 7). Stone has produced prediction formulas for a wide range of nozzle types - including rectangular nozzles and thrust reversers - and flow states. Stone's formulas have served as the best coaxial noise predictions of NASA for over 6 years. They are a blend of classical theory and keen personal insight derived from a regrettably small amount of jet noise data.

The inverted-flow nozzle, a concept developed for possible application to supersonic transport aircraft, was not covered by the 1974 prediction methods of Stone. Therefore, Stone developed separate formulas for this flow state (ref. 8) with the Lewis data base (refs. 5 and 6). In this latter method, Stone used the idea of two spectra, one from the outer premerged stream and one from the merged stream. Stone's inverted-flow method is similar to Jaeck's method (refs. 2 and 3) in the application of this idea of two additive spectra. About the same time, Pao (ref. 9) and Russell (ref. 10) developed a formula for inverted-flow jet mixing noise. Pao and Russell used the Pratt & Whitney data set and, like Stone and Jaeck, assumed an addition of two spectra. The Stone and Pao-Russell methods differ in the following

way: Stone defined the premerged and merged spectra through modifications of the empirical spectral curves from his 1974 method, whereas Pao and Russell used the rule that the premerged and merged spectra have similar shapes but different peak locations and amplitudes. All these methods are included in the NASA Aircraft Noise Prediction Program (ANOPP) (ref. 1) so that there is some ambiguity in the predictions of this program for the case of inverted-flow jets. The method developed herein is intended to replace these present ANOPP methods for coaxial jet noise.

This paper is divided into three major sections. The first section gives some preliminary definitions and notations which are helpful later. This first section also gives four strategies for making empirical noise predictions. Data reduction is discussed in the second section. It is shown how the data-reduction process is related to the format of the noise prediction method being developed. In the third section, one of these prediction strategies is applied to the data base for coaxial jet noise, and an explicit prediction method is derived for the data base. The third section concludes with a discussion of the concept of an optimum coaxial jet.

SYMBOLS

A	area, m^2
c	speed of sound, m/s
c_p	specific heat at constant pressure, $m^2/K\text{-}s^2$
$D(\theta)$	directivity of power
D_ℓ	order of derivative in Taylor's series
$\mathcal{D}$	directivity of power in frequency band
d	diameter of jet, m
E	cubic spline basis function
f	frequency, Hz
J	energy flux
$\mathcal{J}$	energy flux in frequency band
k,m,m',n,i,j,ℓ,ℓ'	integers
L	level
M	number of basis functions in spline fit on frequency
$\dot{m}$	mass-flow rate, kg/s
N	number of basis functions in spline fit on direction
P	power, W

P_ℓ	distinct permutations of independent variables in derivatives in Taylor's series
Φ	power in frequency band, W
p	pressure, Pa
$\langle p^2 \rangle$	mean-square acoustic pressure
R	gas constant, $m^2/K\ s^2$
$\mathfrak{R}$	relative spectrum
r	spherical radius
S	spectrum of energy flux
$\mathfrak{S}$	spectrum of energy flux in given direction
T	temperature, K
V	velocity, m/s
X	derivative multiplier
x	transformed prediction parameter
α	prediction parameter
γ	ratio of specific heats
Δ	noise level coordinate
$\delta_{mm'}$	Kronecker delta function
η	logarithmic frequency parameter
Θ	cubic spline basis function
θ	polar directivity angle, deg
Λ	derivative
λ	eigenvalue
ν	Helmholtz number
ρ	density, kg/m^3
ϕ	azimuthal directivity angle, deg
Ω	solid angle, sr

Subscripts:

e	equivalent
ref	reference
t	total
1	primary stream
2	secondary stream
∞	ambient

Abbreviations:

GALAC	Lockheed-Georgia Company
LeRC	NASA Lewis Research Center
NGTE	National Gas Turbine Establishment (United Kingdom)
P&W	Pratt & Whitney Aircraft
SNECMA	Societe Nationale d'Etude et de Construction de Motuers d'Aviation (France)
SPL	sound pressure level

EMPIRICAL SOURCE NOISE EQUATIONS

Preliminary Definitions

Noise is typically measured in terms of sound pressure level $L\langle p^2\rangle$ or in terms of mean-square pressure $\langle p^2\rangle$. These two variables are related by

$$L\langle p^2\rangle = 10 \log_{10} \frac{\langle p^2\rangle}{p_{ref}^2} \quad dB \left(re\ p_{ref}^2\right) \tag{1}$$

In the following discussion, it is necessary to switch frequently between these measures, so that a compact notation is desirable. Consequently, levels are usually given in units of bels (B) rather than in decibels (dB). The factor of 10 in equation (1) is not used when the level is in bels. Local atmospheric quantities are used for reference constants to simplify further the data analysis. As an example, the sound pressure level can be given as

$$L\langle p^2\rangle = \log_{10} \frac{\langle p^2\rangle}{\rho_\infty^2 c_\infty^4} \quad B \left(re\ \rho_\infty^2 c_\infty^4\right) \tag{2}$$

Spherical coordinates as shown in figure 1 are used to specify the position of the noise sensor relative to the source, which is nominally at the origin of the

coordinate system. The surface area of the source A establishes a length scale which, together with the ambient density ρ_∞ and the ambient speed of sound c_∞, can be used to form reference variables as required by the analysis. All data are assumed to be in the far field so that the pressure varies inversely with radius r. It is also assumed that any atmospheric absorption effects have been removed from the measured data.

The acoustic intensity, like the mean-square pressure $\langle p^2 \rangle$, varies inversely with the square of radius; however, the acoustic energy flux per unit solid angle J is independent of radius in the far field of a nonabsorbing medium. It is expressed as

$$J = \frac{r^2 \langle p^2 \rangle}{\rho_\infty c_\infty} \tag{3}$$

The energy flux in a frequency band with Helmholtz number $\nu = f\sqrt{A}/c_\infty$ is denoted by $\mathcal{J}(\nu)$ so that the total flux is given by a summation

$$J = \sum_{\nu} \mathcal{J}(\nu) \tag{4}$$

It is understood that the summation in equation (4) is over a contiguous set of bands. The acoustic power P is the integral over all directions of the energy flux

$$P = \int J \, d\Omega \tag{5}$$

where $d\Omega$ is the differential solid angle. Equation (5) holds for bands as well as total quantities. The reference quantity for power is $\rho_\infty c_\infty^3 A$ so that the power level is

$$LP = \log_{10} \frac{P}{\rho_\infty c_\infty^3 A} \quad B \left(re \; \rho_\infty c_\infty^3 A \right) \tag{6}$$

Equation (5) may be used for the energy flux level since the solid angle, measured in steradians, is dimensionless.

Prediction Equations

Empirical methods of noise prediction, which predominate in current practice, are essentially curve fits to measured data for various noise sources. The source state is characterized by a set of parameters α_k which control the amount of noise generated. A parameter α could be the throttle position of an engine or the velocity of a jet. A prediction variable such as the band energy flux $\mathcal{J}(\nu)$ may depend on the direction in which the noise is emitted from the source as well as a large number of source parameters.

Purely empirical prediction depends on multidimensional curve fitting. The curve fits may be made directly to the prediction variable; however, it is sometimes

useful to define related variables to separate the prediction process into several steps. Three methods of subdividing an empirical prediction equation for the band energy flux $\mathcal{J}(\nu)$, which is equivalent to the band mean-square pressure, are given herein. The effects of band number and direction are considered in this section, and the influence of the parameters is suppressed. The effect of the source parameters is considered in a subsequent section.

Prediction equations may be based on the following identities:

$$\mathcal{J}(\nu,\theta) = P \frac{J(\theta)}{P} \frac{\mathcal{J}(\nu,\theta)}{J(\theta)} \tag{7}$$

$$\mathcal{J}(\nu,\theta) = P \frac{\Phi(\nu)}{P} \frac{\mathcal{J}(\nu,\theta)}{\Phi(\nu)} \tag{8}$$

$$\mathcal{J}(\nu,\theta) = P \frac{J(\theta)}{P} \frac{\Phi(\nu)}{P} \frac{P\ \mathcal{J}(\nu,\theta)}{\Phi(\nu)\ J(\theta)} \tag{9}$$

The factor $J(\theta)/P$ is a measure of the distribution of the energy flux over the spherical directions θ. It is denoted by the symbol $D(\theta)$; that is

$$D(\theta) = \frac{J(\theta)}{P} \tag{10}$$

and, from its definition, satisfies the condition

$$\int_{\Omega} D(\theta)\ d\Omega = 1 \tag{11}$$

The directivity level LD is a negative number because of the constraint equation (eq. (11)). For axisymmetric sources which are assumed here, the solid angle is

$$d\Omega = 2\pi \sin\theta\ d\theta \tag{12}$$

The directivity index is a comparison of the directed energy flux to the average energy flux through the spherical surface around the source. The factor $\Phi(\nu)/P$ is the power spectrum denoted by $S(\nu)$

$$S(\nu) = \frac{\Phi(\nu)}{P} \tag{13}$$

This factor is a measure of the way the acoustic power is distributed over frequency bands and satisfies the condition

$$\sum_{\nu} S(\nu) = 1 \tag{14}$$

The factor $\mathcal{J}(\nu,\theta)/J(\theta)$ is the spectrum of the energy flux in a given direction,

$$\mathcal{S}(\nu,\theta) = \frac{\mathcal{J}(\nu,\theta)}{J(\theta)} \tag{15}$$

and the ratio $\mathcal{J}(\nu,\theta)/\mathcal{P}(\nu)$ is the directivity of the power in a frequency band,

$$\mathcal{D}(\nu,\theta) = \frac{\mathcal{J}(\nu,\theta)}{\mathcal{P}(\nu)} \tag{16}$$

These variables satisfy integral conditions

$$\sum_{\nu} \mathcal{S}(\nu,\theta) = 1 \qquad \text{(for all } \theta\text{)} \tag{17}$$

and

$$\int_{\Omega} \mathcal{D}(\nu,\theta)\, d\Omega = 1 \qquad \text{(for all } \nu\text{)} \tag{18}$$

The most complicated group in equation (9) is a measure of the difference between the spectrum and directivity factors,

$$\mathcal{R}(\nu,\theta) = \frac{P\ \mathcal{J}(\nu,\theta)}{\mathcal{P}(\nu)\ J(\theta)} \tag{19}$$

By associating different variables in equation (19), it follows that

$$\mathcal{R}(\nu,\theta) = \frac{\mathcal{D}(\nu,\theta)}{D(\theta)} \tag{20}$$

and

$$\mathcal{R}(\nu,\theta) = \frac{\mathcal{S}(\nu,\theta)}{S(\nu)} \tag{21}$$

The form chosen in equation (20) shows that $\mathcal{R}$ is a measure of the difference between the directivity of an energy flux band and the directivity of the total energy flux. The form in equation (21) shows that $\mathcal{R}$ is a measure of the difference between the energy flux spectrum in a given direction and the power spectrum.

In terms of these variables, three possible prediction equations are

$$\mathcal{J}(\nu,\theta) = P\ D(\theta)\ \mathcal{S}(\nu,\theta) \tag{22}$$

$$\mathcal{J}(\nu,\theta) = P\ S(\nu)\ \mathcal{D}(\nu,\theta) \tag{23}$$

$$\mathcal{J}(\nu,\theta) = P\ D(\theta)\ S(\nu)\ \mathcal{R}(\nu,\theta) \tag{24}$$

It is a matter of individual preference which, if any, of these prediction equations are used in making curve fits to the data. They have the advantage of separating effects so that different qualities of the noise source can be studied independently. It is easier to consider a single integrated measure of noise, such as total power P, than to look collectively at $\mathcal{J}(\nu,\theta)$, a variable which is two-dimensional for fixed values of the source parameters. On the other hand, the total prediction formula may eventually require all dimensions, such as introduced by $\mathcal{R}(\nu,\theta)$ in equation (24).

It is possible that the number of source parameters affecting $\mathcal{R}(\nu,\theta)$ may be less than the number affecting the power P; therefore, some savings in the number of dimensions are possible in the curve-fitting process. The use of the separated terms in the prediction equation also facilitates approximation. Many empirical formulas are based on the assumption that $\mathcal{R} = 1$. The physical interpretation of this mathematical condition is that directivity effects and spectral effects are separable.

The constraint conditions on the separate terms in the prediction equation must always be imposed and can be troublesome, as is seen later. The relative spectrum $\mathcal{R}(\nu,\theta)$ satisfies three constraints, not all of which are independent,

$$\int D(\theta)\ \mathcal{R}(\nu,\theta)\ d\Omega = 1 \qquad \text{(for all } \nu) \tag{25}$$

$$\sum_{\nu} S(\nu)\ \mathcal{R}(\nu,\theta) = 1 \qquad \text{(for all } \theta) \tag{26}$$

$$\sum_{\nu} \int S(\nu)\ D(\theta)\ R(\nu,\theta)\ d\Omega = 1 \tag{27}$$

In terms of a prediction of the sound pressure level in decibels, the prediction equation (eq. (24)) becomes

$$SPL(\nu,\theta) = 10 \log_{10} \mathcal{J}(\nu,\theta) + 10 \log_{10} \frac{A}{r^2} + 20 \log_{10} \frac{\gamma p_\infty}{p_{ref}} \quad dB \tag{28}$$

This sound pressure level is corrected easily to standard atmospheric conditions by using the value 197 for the last term in equation (28). The level $L_{\mathcal{J}}$ in equation (28) is derived from equation (24) as

$$L_{\mathcal{J}}(\nu,\theta) = \log_{10} P + \log_{10} D(\theta) + \log_{10} S(\nu) + \log_{10} \mathcal{R}(\nu,\theta) \quad B\ (re\ \rho_\infty c_\infty^3 A) \tag{29}$$

DATA REDUCTION

It is assumed that the preliminary steps of removing absorption and reflection effects from the noise data have been completed and that the measured data are available as energy flux spectra $\mathcal{J}(\nu,\theta)$ (re $\rho_\infty c_\infty^3 A$) for a number of tests of the noise source. The data-reduction process involves two further steps. The first step is to fit smooth curves through the energy flux spectra by using bicubic splines. The curve fits for each test are defined by a discrete set of coordinates whose values are established by the curve-fitting process. Each of these coordinates is potentially a function of all the source parameters. The second step in the data-reduction process is to fit curves, by using multidimensional Taylor's series with the source parameters as independent variables, to each of the coordinates defined by the first data-reduction step.

Bicubic Splines

The theory of cubic splines is well developed for one-dimensional functions. One method of extending this theory to multiple dimensions is to use tensor products of unidimensional functions. The method used here is fully developed by De Boor (refs. 11 and 12) for two dimensions and will be described briefly. The source is assumed to have an axis of symmetry so that the energy flux spectrum is a function of only two variables: the band Helmholtz number ν and polar direction angle θ. If the data are given in constant-percentage bands, such as 1/3 octave, a logarithmic frequency variable,

$$\eta = \log \nu \tag{30}$$

is useful.

Cubic splines are defined by De Boor in terms of basis functions. A basis function for the frequency variable η is defined on the interval (η_0,η_M) in terms of cubic polynomials on subintervals (η_{m-1},η_m), with $m = 1, 2, \ldots, M$. The points η_m are called nodes or knots. The basis functions are of class C^2; that is, they have continuous derivatives up to and including the second derivative. These continuity conditions relate the constants of the cubic polynomial for each subinterval so that, if the slope of the basis function is given at η_0 and η_M, the basis function is defined completely by these slopes and its values at the $m + 1$ node points. A set of $M + 1$ basis functions is defined by

$$E_m(\eta_{m'}) = \delta_{mm'} \tag{31}$$

together with the end slope conditions. De Boor uses the end conditions of zero slope for each basis function $E_m(\eta)$, with $m = 0, 1, \ldots, M$, and adds two basis functions: $E_{M+1}(\eta)$ which has a unit slope at $\eta = \eta_0$ and E_{M+2} which has a unit slope at $\eta = \eta_M$. Both these additional basis functions have values of zero at each node. A slightly different definition of the basis functions is used herein. Each basis function is required to satisfy the same homogeneous boundary condition at each end of the interval (η_0,η_M). The boundary condition may involve only the derivatives of the function but not the function itself. The conditions of zero curvature were used at the ends of the range of the frequency variable, and conditions of zero slope were used at the ends of the range of the polar angle variable. When these boundary conditions are applied to each basis function, there is the same number $M + 1$ of

basis functions as there are node points. Figure 2 depicts basis functions $E_m(\eta)$ as defined herein.

Noise Level Coordinates

Since the noise variables such as $\langle p^2 \rangle$ and $\mathcal{J}$ are positive, the noise variables such as $S(\eta)$ must be positive also. This condition is guaranteed if the curve fit is made with a noise level variable such as $L\langle p^2 \rangle$, $L\mathcal{J}$, and LS. The following expressions for the levels of equation (29) are used:

$$LS(\eta) = \sum_{m=0}^{M} E_m(\eta)\, LS_m \tag{32}$$

$$LD(\theta) = \sum_{n=0}^{N} \Theta_n(\theta)\, LD_n \tag{33}$$

$$L\mathcal{P}(\eta,\theta) = \sum_{m=0}^{M} \sum_{n=0}^{N} E_m(\eta)\, \Theta_n(\theta)\, L\mathcal{P}_{mn} \tag{34}$$

$$L\mathcal{J}(\eta,\theta) = \sum_{m=0}^{M} \sum_{n=0}^{N} E_m(\eta)\, \Theta_n(\theta)\, L\mathcal{J}_{mn} \tag{35}$$

The level coordinates such as $L\mathcal{J}_{mn}$ are the levels at the node points of the splines as shown in figure 3. Assuming that $L\mathcal{J}(\eta_i, \theta_j)$, with $i = 1, 2, \ldots, I>M$ and $j = 1, 2, \ldots, J>N$, has been measured in a test, equation (35) can be solved in the least-squares sense for the band energy flux levels $L\mathcal{J}_{mn}$ at standardized node points (η_m, θ_n). The total power level is calculated by

$$LP = \log_{10} \int_{\Omega} \sum_{\nu} \text{antilog}\left[L\mathcal{J}(\eta,\theta)\right] d\Omega \tag{36}$$

where $L\mathcal{J}$ is given by equation (35). The power level at each band node point η_m is

$$L\mathcal{P}_m = \log_{10} \int_{\Omega} \text{antilog}\left[L\mathcal{J}(\eta_m,\theta)\right] d\Omega \tag{37}$$

and the energy flux at each direction node point θ_n is

$$LJ_n = \log_{10} \sum_{\nu} \text{antilog}\left[L\mathcal{J}(\eta,\theta_n)\right] \tag{38}$$

where $L\mathcal{J}(\eta_m,\theta)$ and $L\mathcal{J}(\eta,\theta_n)$ are given by simplified forms of equation (35) which hold at the node points.

The node point levels for each of the variables in the prediction equations are then computed by simple algebraic formulas as follows:

$$LD_n = LJ_n - LP \tag{39}$$

$$LS_m = LP_m - LP \tag{40}$$

$$L\mathcal{S}_{mn} = L\mathcal{J}_{mn} - LP \tag{41}$$

$$L\mathcal{D}_{mn} = L\mathcal{J}_{mn} - LS_m - LP \tag{42}$$

$$L\mathcal{R}_{mn} = L\mathcal{J}_{mn} - LD_n - LS_m - LP \tag{43}$$

Coordinate Constraints

The set of coordinates $\mathcal{J}_{mn}$ contains $(M + 1)(N + 1)$ elements which completely describe the noise field for a given test through equation (35). The additional coordinates given by equations (39) through (43) offer alternate means of representing the noise field by the prediction equations (22), (23), and (24); however, the elements of these alternate coordinates are not all independent. They must satisfy the integral constraints of equations (11), (14), (17), (18), (25), and (26). If methods were developed for predicting these alternate coordinates, there would be no guarantee that the predicted values would satisfy the constraint equations. An independent subset of each set of alternate coordinates must be selected and the constraint equations must be used to define the remaining elements of the set.

Each of the summation expressions (eqs. (32) to (35)) for the level variables can be given as a product expression for the variables by taking antilogs of the equations as follows:

$$S(\eta) = \prod_{m=0}^{M} S_m^{E_m(\eta)} \tag{44}$$

$$D(\theta) = \prod_{n=0}^{N} D_n^{\Theta_n(\theta)} \tag{45}$$

$$\mathcal{R}(\eta, \theta) = \prod_{m=0}^{M} \prod_{n=0}^{N} \mathcal{R}_{mn}^{E_m(\eta)\,\Theta_n(\theta)} \tag{46}$$

$$\mathcal{J}(\eta, \theta) = \prod_{m=0}^{M} \prod_{n=0}^{N} \mathcal{J}_{mn}^{E_m(\eta)\,\Theta_n(\theta)} \tag{47}$$

The product forms should not be used for computation because repeated exponentiation and multiplication is much slower than the multiplications and additions in the summation forms for the levels. The product forms facilitate some proofs of identities which are needed in the process of satisfying the constraints on the main variable coordinates. Since the sum of the basis functions is a curve fit to the constant 1 (ref. 12, p. 110),

$$\sum_{m=0}^{M} E_m(\eta) = 1 \tag{48}$$

it follows that

$$S(\eta) = S_0 \prod_{m=1}^{M} (S_m/S_0)^{E_m(\eta)} \tag{49}$$

The function $S(\eta)$ satisfies a summation constraint (eq. (14)) so that the $M + 1$ coordinates S_m are not independent. The spectrum value S_0 can be designated as the dependent variable with the M variables (S_m/S_0) being independent. The value of S_0 is found from

$$LS_0 = -\log_{10} \sum_{\eta} \text{antilog} \sum_{m=1}^{M} E_m(\eta)\, L \frac{S_m}{S_0} \tag{50}$$

The independent coordinates $L(S_m/S_0)$ may be used for tabulation and curve fitting of empirical data. Equation (50) gives the dependent coordinate LS_0 which in turn allows evaluation of all spectrum levels by the identity

$$LS_m = L \frac{S_m}{S_0} + LS_0 \qquad (m = 1,2,\ldots,M) \tag{51}$$

A similar procedure is used to find the directivity coordinate LD_0

$$LD_0 = -\log_{10} 2\pi \int_0^{\pi} \sin\theta \; \text{antilog} \sum_{n=1}^{N} \Theta_n(\theta)\, L \frac{D_n}{D_0}\, d\theta \tag{52}$$

The spectrum constraints on the coordinates $\mathcal{S}_{mn}$ may be satisfied along each line of nodes where n is constant by using $\mathcal{S}_{0n}$ as the dependent coordinate and solving for $\mathcal{S}_{0n}$ in terms of $\mathcal{S}_{mn}/\mathcal{S}_{0n}$. A similar procedure applies for the directivity coordinates $\mathcal{D}_{mn}$ along each line of nodes where m is constant.

This direct solution process is not possible for the dependent coordinates of the relative spectrum. However, if MN values of the array R_{mn} are stored, then the constraint equations (eqs. (25), (26), and (27)) give $M + N + 1$ nonlinear equations for the missing values of the $(M + 1)(N + 1)$ array R_{mn}. The disadvantage of these nonlinear equations must be weighed against the advantages of the symmetric prediction equation (24) as compared with the prediction equations (22) and (23).

Figure 4 shows four schemes for saving independent noise level coordinates for a single test. The set which is used depends on the desired prediction equation;

however, each set is only an alternate scheme for representing the energy flux spectrum level $L_{\mathcal{J}}(\eta,\theta)$.

Taylor's Series

Each of the noise level coordinates is a function of the noise source parameters. An empirical approximation to these level coordinate functions may be found by testing the noise source with a matrix of source parameters and fitting curves through the reduced data. A Taylor's series is a convenient multidimensional function for this curve fit because a noise source typically operates with source parameter values which are not far removed from some standard source condition. This standard condition is the origin of the Taylor's series expansion. Since the noise levels are measured on a logarithmic scale, the source parameters may also be given logarithmically. A factor of 100 for a source parameter range, say from 0.1 to 10, translates to the logarithmic range (-1,1) of this same parameter used as an argument of the Taylor's series.

The symbol Δ is used to denote any noise level coordinate. This level can be relative to a reference constant or can be relative to this same coordinate from another experiment or theory. The use of a level coordinate relative to a theoretically predicted value is a useful technique for evaluating the theory. If the theory correctly predicts the experimental data, then the relative coordinate Δ should have a value of 0 and the Taylor's series fit to these data will have null values for the constant and all derivatives.

The independent source parameters are given by the following equation:

$$x_i = \log_{10} \frac{\alpha_i}{(\alpha_{ref})_i} \tag{53}$$

so that the Taylor's series for Δ is

$$\Delta \approx \sum_{r=0}^{N_r} \frac{1}{r!} \left(\sum_{i=1}^{N_i} x_i \frac{\partial}{\partial x_i} \right)^r \Delta \tag{54}$$

The approximate equation (54) will be applied later to an empirical study of coaxial jet noise which has five independent source parameters. A third-degree approximation ($N_r = 3$) has 55 independent derivatives in the Taylor's series as shown in table I. The approximate series (eq. (54)) is expanded into a linear sum as

$$\Delta = \sum_{\ell=1}^{N_\ell} \Lambda_\ell X_\ell \tag{55}$$

where

$$X_\ell = \frac{P_\ell}{D_\ell!} x_i x_j x_k \tag{56}$$

In equation (55), Λ_1 stands for the constant term in the Taylor's series; $\Lambda_2, \Lambda_3, \ldots, \Lambda_6$ stand for the first derivatives with respect to each of the five parameters; and N_ℓ is 56 to allow for the constant and all derivatives. The parameter subscripts i, j, and k are functions of ℓ as given in table II. The order of the derivative D_ℓ is a count of the nonzero occurrence of the subscripts i, j, and k. The integer function P_ℓ is the number of permutations of the distinct subscripts. These functions are given in table II. In computing X_ℓ by equation (56), the convention is used that $x_0 = 1$ and x_i with $i = 1, 2, \ldots, 5$, is defined by equation (53). Given a number of experiments where a noise coordinate and the source parameters α are measured, equation (55) may be solved, usually in the least-squares sense, for the derivatives Λ_ℓ. This solution, repeated for each noise coordinate, gives a prediction method for the coordinates and hence for the noise field.

COAXIAL JET MIXING NOISE

A large data base has been collected to develop an empirical prediction method for coaxial jet mixing noise. This method is intended to replace the methods for jet mixing noise. The noise prediction method for a single jet is based primarily on the GALAC data. The noise prediction method for a coaxial jet is based on these GALAC data as well as the added data sets from LeRC (refs. 5 and 6), P&W (ref. 4), NGTE, and SNECMA. These data sets are briefly summarized in table III, and an indication is given of the amount of data used in this analysis. There are 842 jet noise tests in this data base; however, only the subsonic tests, 540 in all, were used herein.

Organization of Data

The data sets, as received, are organized in several different ways. The NGTE data set A has a test matrix with primary jet velocity V_1 and velocity ratio V_2/V_1 as independent test parameters. The primary jet total temperature $T_{t,1}$ was held fixed at about 700K for most tests and the secondary temperature was equal to ambient. Area ratios A_2/A_1 of 2, 4, and 6 were tested by NGTE. The NGTE data set C tests have the same independent variables with area ratios of 1.5, 2.0, 4.0, and 8.0. The NGTE data set C includes inverted-flow cases where V_2/V_1 ranged up to 1.4 but the secondary stream was still at ambient temperature.

The P&W and LeRC data are organized around nozzle pressure ratios and total temperatures. P&W used two area ratios, 0.75 and 1.2; LeRC used area ratios of 1.2, 1.5, 2.0, and 3.33. In these tests, the pressure ratio ranged from 1 to over 4.0 and the temperature ranged from 1 to over 3 times ambient temperature.

The SNECMA data are organized around nozzle pressure ratio and total temperature with a single area ratio of 3.5. The GALAC single jet data also have nozzle pressure ratio and total temperature as test parameters.

The way in which the test matrices are organized is to some degree arbitrary; however, there is a tendency for the data to be grouped according to area ratio, nozzle pressure ratio, and total temperature. The other geometric variable which appears is primary plug size, A_0/A_1, where A_0 is the plug area. The pressure and temperature variables are natural because they are easily monitored during experiments. The variables more often used for acoustic correlations, V/c_∞ and V_2/V_1, are of course functions of the experimental variables. Based on a review of the

available data sets, an organization of the data based on the actual experimental variables - A_2/A_1, p_t/p_∞, and T_t/T_∞ - appears to be more convenient.

A review of the data base also suggests that the test variables are arranged in roughly geometric proportions such that they will appear evenly spaced on a logarithmic scale. For example, the NGTE data set C used area ratios of 1.5, 2.0, 4.0, and 8.0. The number 1.5 is near $\sqrt{2}$. The LeRC area ratios were 1.2, 1.5, 2.0, and 3.3. These ratios may be associated with $2^{1/4}$, $2^{2/4}$, $2^{4/4}$, and $2^{7/4}$. In both cases, the area ratios are fractional powers of 2, that is, $2^{m/4}$. Similar trends are apparent in the pressure ratio and total temperature. LeRC used pressure ratios of 1.0, 1.2, 1.4, 1.6, 1.8, 2.2, and 3.0, with total temperature of 1, 2, 3, and 4 times ambient. The total pressure ratios tend to be grouped in either a subsonic range, $0 < p_t/p_\infty < 1.863$, or in a supersonic range, $1.863 < p_t/p_\infty < 3.470$. There are usually far fewer variations of temperature than of pressure ratio. Usually only 1 or 2 temperatures are examined at each pressure ratio. For example, the LeRC data contain mostly temperatures of 3 and 4 times ambient with relatively few tests having ambient or 2 times ambient temperature. These observations suggest that jet noise tests may be conveniently classified by the following procedure.

Area ratio.- Area ratios A_2/A_1 should be assigned to a group with nominal value of 2^{n-4}, where $n = U, 1, 2, \ldots, 7$. The symbol U indicates undefined and is used to designate a single-stream jet; U can be thought of as $-\infty$ if the single-stream jet is considered to have an area ratio of zero. However, it is equally valid to regard the single-stream jet as representing all area ratios as long as the two streams are identical in pressure ratio and temperature. The geometric mean limits of each area ratio group are shown in table IV. The classification scheme for area ratio can also be used for plug size if the plug size is given as A_0/A_1, where A_0 is the plug area. No plug is designated by 0, a small plug by 1, and so on up to a high-radius-ratio case where $A_0/A_1 = 8$. Because of the smaller number of tests available for this variable, it may be best to use only even-value indices for plug size.

Total pressure ratio p_t/p_∞.- The total pressure ratio may be grouped in relation to the critical pressure ratio of the nozzle. If a typical value of γ is assumed to be 1.35, the critical pressure ratio is 1.863. It is proposed to separate the subsonic range into four subranges which are geometrically related to the critical pressure ratio. The boundaries of these subranges are given by fractional power $n/4$ of the critical pressure ratio and the geometric means are fractional powers $(2n-1)/8$, where $n = 1, 2, \ldots$. The classification scheme is shown in table V. Note that a pressure ratio of 1.000 is excluded from the classification since a jet with pressure ratio of 1 does not exist. If a coaxial jet is operated with a pressure ratio of 1 in one stream, then it is regarded as a single jet with pressure ratio and temperature ratio equal to the values in the active stream. The area ratio is undefined and, if the active stream is the outer stream, the central nozzle is regarded as a plug.

Total temperature ratio T_t/T_∞.- Typical values of the total temperature are 1, 2, and 3 times the ambient temperature. Some data, such as the LeRC data set, have temperatures to nearly 4 times ambient. In general, there are fewer temperature variations in the data base than in other variables; this suggests that fewer groups may be used in classifying the temperature. A geometrically related set of three groups is proposed as shown in table VI. The index indicates a geometric mean temperature $T_t/T_\infty = 2^{n-1}$. No symbol is needed for graphic display, as is shown later.

Classification code.- The indices for geometry and stream conditions may be used to form a six-digit classification code for a noise test as follows:

$$\underbrace{(A_2/A_1,\ A_0/A_1)}_{\text{Geometry}} \quad \underbrace{(p_{t,1}/p_\infty,\ T_{t,1}/T_\infty)}_{\text{Primary}} \quad \underbrace{(p_{t,2}/p_\infty,\ T_{t,2}/T_\infty)}_{\text{Secondary}}$$

The first two symbols are geometries, the next two are for the primary stream, and the last two represent the secondary, that is the outer, stream. An example of a single-stream jet code would be

U13232

This code begins with the undefined symbol U which indicates a single-stream jet with identical inner and outer stream conditions. The second symbol indicates a plug with area between 0.088 and 0.177 of the jet area. The last four digits must have the repeating pattern since there is only a single stream or two identical streams. The digit 3 indicates a total pressure ratio between 1.365 and 1.594, and the digit 2 indicates a total temperature between 1.414 and 2.828 times ambient.

It is possible to use the digit 0 to represent the undefined number. This may be more convenient for computer sorting of data. The example code would then appear as

013232

and is interpreted in exactly the same manner as long as it is recognized that 0 means undefined.

This code could be extended to include wind-tunnel or flight data by appending a digit for the free-stream Mach number. Let the Mach number be 1/10 of the last digit. Then the example jet code with a flight Mach number of 0.3 would be seven digits as follows:

0132323

Discussion of Data

GALAC data.- The test points for the GALAC circular jet are classified graphically in figure 5. Circular symbols are used to indicate a circular jet or a jet with identical streams. The number inside of the symbol shows the number of times that this nominal condition is repeated. Since the streams are identical, the test points fall on the diagonal of the figure. The majority of the 65 test points are in the subsonic region. Within each pressure ratio category, there are test points within each of the temperature categories. These data are adequate to define a function which is cubic in pressure ratio and quadratic in temperature.

NGTE data sets.- The test points for NGTE data set A are shown in figure 6. These test points are predominantly subsonic. The outer stream is always cold and the inner stream always has a moderate temperature. There is a good distribution of area ratio shown by the multiple symbols in figure 6. The test points include circular jets which fall on the diagonal as well as dissimilar stream test points.

In general, the test matrix forms a banded pattern around the diagonal. The distance of the test point away from the diagonal is a measure of the difference between the pressure ratios of the streams. This difference variable is actually the ratio of the stream total pressures $p_{t,2}/p_{t,1}$ since the coordinate system is on a geometric scale. The banded pattern of these data may be adequate to define a function which is cubic in geometric mean pressure ratio and quadratic in the ratio of pressure ratios. The pattern of test points is repeated at area ratios of 4.0 and 6.0. These three area ratios may be used to define a quadratic function of area ratio. The NGTE data set B (fig. 7) contains test points off the diagonal which will better define the effect of different pressure ratios; however, only one area ratio is represented. The NGTE data set C (fig. 8) data have a good distribution of area ratios from about 1.5 to 8.0. These test points define a function which is cubic in both pressure ratios and in area ratio. The temperatures are essentially fixed, however, with a moderate temperature primary stream and a cold secondary stream.

P&W data.- The test points for the P&W data are displayed in figure 9. These data are unique because temperature effects were studied in detail. These points define quadratic variation in temperature for both streams. The four groups of temperature points at different pressure ratios may be used to define linear variations (in two dimensions) of the temperature effects with pressure ratio. Unfortunately, the effect of area ratio variation cannot be determined from these data.

LeRC data.- The test points for the LeRC data in figure 10 show a distribution in all variables. The four area ratios could be used to define a cubic polynominal, although it may be better to limit this variable to second degree since the range of area ratio is only from about 1 to 3. At an area ratio of 1.2, three temperature test points are located at each of several pressure ratios; these three points define linear variations in the two temperatures. A pattern of three temperature points is also found at an area ratio of 3.3 so that a linear variation of the temperature effect with area ratio may be defined by these data.

SNECMA data.- The test points for the SNECMA data are displayed in figure 11. This comparatively small data set could generate a function which is quadratic in geometric mean pressure ratio and linear in the temperature without coupling between the two effects. An independent variation in the quotient of pressure ratio could also be obtained from these data.

Coaxial Jet Noise Prediction

The form of the prediction equation selected for coaxial jet noise is obtained by combining equations (28) to (30) as

$$SPL(\eta,\theta) = 10 \log_{10} P + 10 \log_{10} D(\theta) + 10 \log_{10} S(\eta) + 10 \log_{10} \mathcal{R}(\eta,\theta)$$

$$+ 10 \log_{10} \frac{A}{r^2} + 20 \log_{10} \frac{\gamma p_\infty}{p_{ref}} \quad dB \tag{57}$$

The functions P, D, S, and $\mathcal{R}$ are defined by equations (5), (10), (13), and (19) with the assumption of an axisymmetric noise field. The reference area A for the coaxial jet is defined as

$$A = \frac{\dot{m}_e}{\rho_\infty c_\infty} \tag{58}$$

where $\dot{m}_e$ is the total mass-flow rate of the jet. The source to observer distance is r and the frequency variable η is the logarithm of the Strouhal number defined as

$$\eta = \log_{10} \frac{f d_e}{V_e} \tag{59}$$

where d_e and V_e are the diameter and velocity of the equivalent jet.

The single equivalent jet has the same mass flow, energy flow, and thrust as the coaxial jet. The mass flow of the single equivalent jet is

$$\dot{m}_e = \dot{m}_1 + \dot{m}_2 \tag{60}$$

where

$$\dot{m} = \rho A V \tag{61}$$

The conditions of equivalence of mass flow and thrust give

$$V_e = \frac{\dot{m}_1 V_1 + \dot{m}_1 V_2}{\dot{m}_1 + \dot{m}_2} \tag{62}$$

Since the gas constant for air is not significantly changed by the addition of a small amount of combustion products, the equivalent temperature can be defined from the total energy flow as

$$T_e = \frac{\dot{m}_1 [\gamma_1/(\gamma_1 - 1)] T_1 + \dot{m}_2 [\gamma_2/(\gamma_2 - 1)] T_2}{\dot{m}_1 [\gamma_1/(\gamma_1 - 1)] + \dot{m}_2 [\gamma_2/(\gamma_2 - 1)]} \tag{63}$$

where

$$\frac{\gamma}{\gamma - 1} = \frac{c_p}{R} \tag{64}$$

The equivalent ratio of specific heats is defined from the mixing of the gases of each stream as

$$\frac{\gamma_e}{\gamma_e - 1} = \frac{\dot{m}_1[\gamma_1/(\gamma_1 - 1)] + \dot{m}_2[\gamma_2/(\gamma_2 - 1)]}{\dot{m}_1 + \dot{m}_2} \tag{65}$$

Because the fully expanded jet static pressure is equal to the ambient static pressure, the equivalent jet density is

$$\rho_e = \rho_\infty \left[\frac{T_e}{T_\infty} - \frac{\gamma_e - 1}{2} \left(\frac{V_e}{c_\infty} \right)^2 \right]^{-1} \tag{66}$$

The equivalent area is

$$A_e = \frac{\dot{m}_e}{\rho_e V_e} \tag{67}$$

and the equivalent jet diameter is

$$d_e = \left(\frac{4A_e}{\pi} \right)^{1/2} \tag{68}$$

The process for developing a coaxial jet noise prediction based on equation (57) for the data base is as follows:

1. Compute the band energy flux in a given direction $\mathcal{J}(f,\theta)$ from the mean-square acoustic pressure data $\langle p^2(f,\theta) \rangle$ for each subsonic test by using equation (3).

2. Convert the frequency values f to frequency parameter values η with equation (59).

3. Determine the energy flux coordinates $\mathcal{J}_{mn}$ for standard values of η_m and θ_n to express $\mathcal{J}(\eta,\theta)$ in the bicubic spline form of equation (35). The standard node point values of η_m and θ_n are shown in figure 3. These coordinates are found by solving equation (35) in a least-squares sense for the coordinates $\mathcal{J}_{mn}$ from the given values of η, θ, and $\mathcal{J}(\eta,\theta)$ for each test.

4. Compute the power level LP from equation (36), the directivity coordinate levels LD_n from equation (39), the spectrum coordinate levels LS_m from equation (40), and the relative spectrum coordinate levels $L\mathcal{R}_{mn}$ from equation (43).

5. Apply the coordinate constraints for LS_m and LD_n as presented in equations (50) and (52).

6. From the tabulated values of the nozzle pressure ratios $p_{t,1}/p_\infty$ and $p_{t,2}/p_\infty$, total temperature ratios $T_{t,1}/T_\infty$ and $T_{t,2}/T_\infty$, and area ratio A_2/A_1, build a Taylor's series expansion for each of the 36 noise level coordinates (P, 5 values of D_n, 5 values of S_m, and 25 values of $\mathcal{R}_{mn}$). Each series has the form of equation (55), with the source parameters x_i defined as

$$\left.\begin{aligned} x_1 &= \log_{10}(p_{t,1}/1.365p_\infty) \\ x_2 &= \log_{10}(p_{t,2}/1.365p_\infty) \\ x_3 &= \log_{10}(T_{t,1}/2T_\infty) \\ x_4 &= \log_{10}(T_{t,2}/2T_\infty) \\ x_5 &= \log_{10}(A_2/A_1) \end{aligned}\right\} \tag{69}$$

The derivative terms to be included in the series are selected based on the classification codes for each independent variable. For example, it takes values of x_1 in three classification intervals with values of $x_2, \ldots, x_5$ in the same interval to compute $\partial^2\Delta/\partial x_1^2$. A subset of the 56 possible derivatives is selected in this manner. The Taylor's series expansion is then determined by solving equation (55) with this subset of derivatives in a least-squares sense for each of the 36 noise coordinates.

Once the process of building the noise prediction method is completed, the following steps are required to make a prediction with this method:

1. Calculate the source parameters given by equation (69).

2. Calculate the 36 noise coordinates using equation (55).

3. Compute the values of S, D, and $\mathcal{R}$ for the desired values of η and θ from the noise coordinates by using equations (32), (33), and (34).

4. Compute the SPL from equation (57).

Single jet validation.- This prediction method was first applied to the GALAC single jet data set as a test and validation of the method. Taylor's series expansions of the 36 noise coordinates for the subsonic cases were made by using the jet pressure ratio p_t/p_∞ and total temperature ratio T_t/T_∞. The following table is a summary of the standard deviations of the third-order Taylor's series fit to the data:

Acoustic power, 10LP, dB	0.8
Directivity level coordinates, $10LD_n$, dB	0.6
Power spectrum coordinates, $10LS_m$, dB	0.6
Relative spectrum coordinates, $10L_{mn}$, dB	1.5
Average standard deviation, dB	1.1

Based on these Taylor's series expansions, predictions were made of the SPL for selected tests in the GALAC data base. In addition, predictions were made with the

single jet method (ref. 1) for comparison. The proposed prediction method should provide accuracy comparable to the prediction method of reference 1 for it to be a feasible method to apply to coaxial jets.

A sample of the results of the single jet validation of the prediction method is shown in figure 12. Results are shown for directivity angles θ of 120° and 150° and nominal total temperature ratios T_t/T_∞ of 1.0 and 3.5 for various values of velocity ratio V/c_∞. It can be seen from the figures that the accuracy of the two prediction methods is comparable. With this successful completion of the validation of the prediction method, the formulation of a coaxial jet prediction method was pursued.

Coaxial jet validation.- The empirical source noise prediction method was applied to the entire subsonic coaxial jet noise data base and to each of the six data sets separately. First-, second-, and third-order Taylor's series expansions were made to compare the effect of order on prediction accuracy. A summary of the standard deviations for each of the coordinate fits for the Taylor's series expansions is given in table VII. Missing entries in the table correspond to cases where insufficient parameter variation exists in the data base to evaluate a series of that order. It can be seen from the table that the third-order fit provides a significant gain in accuracy over the first- and second-order fits. In addition, the error comparison indicates that there is a consistency of quality of fit among data sets.

The prediction method based on the third-order Taylor's series expansion to all data sets is recommended for use at this time. The data base provided sufficient data to evaluate 43 terms of the Taylor's series for the 36 noise coordinates as given by equation (55). Table VIII gives the definition of the terms for all Taylor's series and table IX gives the derivative values for each of the 36 coordinates.

Test cases for the validation of the noise prediction method for the subsonic coaxial jet were selected from each data set. Comparisons were made between the third-order prediction based on all data sets and the third-order prediction based on the single data set from which the test case was selected to compare the error within data sets to the error among data sets. Test cases were selected to isolate the effects of various parameters on the noise prediction.

The effect of primary jet temperature on the sound pressure level, with data from the NGTE data set A, is shown in figure 13. The data show a minor effect of primary jet temperature over a range of total temperature from 1.0 to 3.1. Neither the absolute level nor the spectral shape is significantly affected by primary jet total temperature. The agreement between data and predictions is good and indicates that these data are self-consistent and that the NGTE data set A is consistent with the entire data base.

The effect of primary jet velocity on the sound pressure level, with data from the NGTE data set B, is shown in figure 14. The data show a significant effect of primary jet velocity over a range of velocity ratio from 0.7 to 1.4. The absolute noise level increases with primary jet velocity as expected. In addition, the spectral shape has a sharper peak as the primary jet velocity increases. The data and the individual set prediction agree quite well; this indicates a consistency with the data set. The difference between the prediction based on the NGTE data set B and the prediction based on all data sets indicates that the NGTE data set B tends to be lower in sound pressure level than the data base as a whole.

The effect of area ratio on the sound pressure level, with data from the NGTE data set C, is shown in figure 15. The data show a significant decrease in the sound pressure level as the area ratio increases from 2.0 to 8.0. This decrease is to be expected since the outer stream is slower than the inner stream. In addition, the frequency at which the peak sound pressure level occurs decreases with increasing area ratio; this is due to the changing equivalent jet diameter in the Strouhal number scaling. Agreement between the data and predictions is very good in this case.

The ability of this empirical method to accurately predict noise for a wide range of test conditions is demonstrated in figure 16 with the LeRC data set. A near-circular jet is compared to two coaxial jets, one with a hot and fast inner stream and the other with a hot and fast outer stream. It is easily seen that the prediction method accurately predicts the sound pressure level over this wide range of test conditions.

The effect of secondary jet temperature on the sound pressure level is shown in figure 17 by using data from the P&W data set. For a variation of total temperature ratio from 1.4 to 3.1, with other parameters held constant, little variation in the sound pressure level is seen. Note that the agreement between data and predictions is excellent in this figure.

The effect of changing thrust on the sound pressure level is shown in figure 18 by using the SNECMA data set. The prediction method provides accurate estimates in all three cases even though the noise level varies by more than 20 dB.

The results in figures 12 to 18 show that the empirical source noise prediction method can be accurately and efficiently used to predict subsonic jet noise. Its applicability to other noise sources is yet to be determined. Furthermore, the Taylor's series form for the noise coordinate curve fit can be useful for further research into the noise problem, such as the optimum coaxial jet analysis discussed in the next section.

Optimum Coaxial Jet

Expressing noise coordinates, such as acoustic power, in a Taylor's series form facilitates design studies of the effect of the jet flow state parameters on the noise. In particular, a study of the coaxial benefit, defined herein as the difference in acoustic power produced by a coaxial jet and an equivalent circular jet, can be performed readily. The equivalent circular jet is one which has the same mass flow, momentum flow (thrust), and total enthalpy flow as the coaxial jet.

A second-order Taylor's series expansion was used for the acoustic power P of the entire subsonic data base in terms of the equivalent jet velocity V_e and total temperature T_e and the coaxial jet velocity ratio V_2/V_1, total temperature ratio T_2/T_1, and area ratio A_2/A_1. There are two types of terms in this series expansion. The sum of terms including only V_e or T_e or both is the acoustic power of the equivalent circular jet. The negative sum of all remaining terms is the coaxial jet benefit defined by the relation

$$\Delta LP = LP_e - LP = -\sum_{\ell'} \Lambda_{\ell'} X_{\ell'} \tag{70}$$

where the summation over ℓ' includes all coefficients X_ℓ as defined by equation (56) which contain the parameters V_2/V_1, T_2/T_1, and A_2/A_1. The resulting expression is written in quadratic form as

$$\Delta LP = [x_i]\{\Delta_{,i}\} + \frac{1}{2}[x_i][\Delta_{,ij}]\{x_j\} \tag{71}$$

where

$$x_1 = \log_{10}(V_e/c_\infty) \tag{72a}$$

$$x_2 = \log_{10}(T_e/2T_\infty) \tag{72b}$$

$$x_3 = \log_{10}(V_2/V_1) \tag{72c}$$

$$x_4 = \log_{10}(T_2/T_1) \tag{72d}$$

$$x_5 = \log_{10}(A_2/A_1) \tag{72e}$$

The particular values of $\Delta_{,i}$ and $\Delta_{,ij}$ for this data base are

$$\{\Delta_{,i}\} = \begin{Bmatrix} 0 \\ 0 \\ 11.25 \\ 0.65 \\ -4.23 \end{Bmatrix} \tag{73}$$

and

$$[\Delta_{,ij}] = \left[\begin{array}{cc:ccc} 0 & 0 & 4.26 & -2.43 & -4.23 \\ 0 & 0 & -7.16 & -36.32 & 3.52 \\ \hdashline 4.26 & -7.16 & 33.78 & -34.01 & 19.32 \\ -2.43 & -36.32 & -34.01 & -15.44 & -10.34 \\ -4.23 & 3.52 & 19.32 & -10.34 & 14.79 \end{array}\right] \tag{74}$$

The matrices in equations (73) and (74) are partitioned to separate the equivalent jet terms x_1 and x_2 from the coaxial jet ratio terms x_3, x_4, and x_5. Coefficients of only x_1 or x_2 or both are identically zero because of the definition of coaxial benefit.

Stationary values of ΔLP are found by setting the partial derivatives with respect to x_i equal to zero, that is

$$\left\{\frac{\partial \Delta LP}{\partial x_i}\right\} = \{0\} \tag{75}$$

This condition results in a set of simultaneous linear equations for the stationary point $\{x_i^0\}$ as follows:

$$[\Delta_{,ij}]\{x_i^0\} = -\{\Delta_{,i}\} \tag{76}$$

This stationary point may give an optimum (maximum) value for the coaxial benefit ΔLP.

The characteristics of the stationary point of the coaxial benefit function are obtained by solving for the eigenvalues of the matrix $[\Delta_{,ij}]$. These eigenvalues and their eigenvectors are defined by

$$[\Delta_{,ij}][x_{j\alpha}] = [x_{j\alpha}][\lambda_\alpha] \tag{77}$$

With the data in equation (74), the eigenvalues are

$$[\lambda_\alpha] = \begin{bmatrix} -55.83 & 0 & 0 & 0 & 0 \\ 0 & -1.34 & 0 & 0 & 0 \\ 0 & 0 & 5.50 & 0 & 0 \\ 0 & 0 & 0 & 20.84 & 0 \\ 0 & 0 & 0 & 0 & 64.05 \end{bmatrix} \tag{78}$$

and the eigenvectors are

$$[x_{j\alpha}] = \begin{bmatrix} 0.01 & -0.92 & 0.39 & -0.03 & 0.07 \\ 0.54 & -0.02 & -0.02 & 0.81 & 0.21 \\ 0.34 & 0.21 & 0.34 & -0.40 & 0.75 \\ 0.77 & -0.07 & -0.15 & -0.40 & -0.47 \\ -0.01 & -0.33 & -0.84 & -0.12 & 0.41 \end{bmatrix} \tag{79}$$

The matrix of eigenvectors is orthonormal so that its transpose is equal to its inverse

$$[x_{j\alpha}]^T = [x_{j\alpha}]^{-1} \tag{80}$$

where the superscript T indicates transpose. The properties of the stationary point are found by introducing generalized coordinates $\{a_\alpha\}$, which are amplitudes of the eigenvectors, by the transformation

$$\{x_j\} = [x_{j\alpha}]\{a_\alpha\} \tag{81}$$

This transformation allows an explicit solution for the stationary point $\{a_\alpha^0\}$ in generalized coordinates as

$$\{a_\alpha^0\} = -[\lambda^{-1}_\alpha][x_{i\alpha}]^T \{\Delta_{,i}\} \tag{82}$$

In the present case, this solution is

$$\{a_\alpha^0\} = \begin{Bmatrix} 0.08 \\ 2.79 \\ -1.32 \\ 0.21 \\ -0.10 \end{Bmatrix} \tag{83}$$

and the transformation (eq. (81)) gives the stationary point in the original coordinates $\{x_j^0\}$ as

$$\{x_j^0\} = \begin{Bmatrix} -3.09 \\ 0.16 \\ 0.02 \\ 0.01 \\ 0.14 \end{Bmatrix} \tag{84}$$

This stationary point is well outside the range of the present data base. The coordinate $x_1 = -3.09$ corresponds to an equivalent jet velocity V_e of about $10^{-3}c_\infty$. The quadratic form for the coaxial benefit may be written in generalized coordinates as

$$\Delta LP = \frac{1}{2}\sum_{\alpha=1}^{5} \lambda_\alpha \left(a_\alpha - a_\alpha^0\right)^2 + \frac{1}{2}\sum_{\alpha=1}^{5} \lambda_a \left(a_\alpha^0\right)^2 \tag{85}$$

The value of the benefit at the stationary point is the second term in equation (85). If the stationary point is an optimum, or maximum value, then all eigenvalues λ_α must be negative. The data of equation (78) indicate that only two of the five eigenvalues are negative so that the stationary point is a five-dimensional saddle point. Since the stationary point of the quadratic approximation is a saddle point outside the range of the data base, there appears to be no generally optimum coaxial jet.

Figure 19 shows a contour plot of the coaxial benefit ΔLP as a function of velocity ratio and temperature ratio for nominal values of the equivalent velocity, equivalent total temperature, and area ratio. This contour shows a saddle point in the velocity ratio and temperature ratio. Contour plots at other values of equivalent velocity, equivalent temperature, and area ratio have similar saddle characteristics. The figure shows the general trend that if the velocity ratio increases, the coaxial benefit increases. Similarly, it shows that keeping the temperature ratio near 1 increases the coaxial benefit.

Although a general search for an optimum point fails, the search technique is still useful for design. The jet state parameters are subject to design constraints which reduce the number of dimensions in the optimization problem. If certain parameters are prescribed, then a stationary point may exist in the space of the remaining parameters. Pao (ref. 9) has estimated contours of equal coaxial benefit by plotting values derived from the P&W data base (ref. 4) in the space of equivalent velocity and velocity ratio. Pao estimated a maximum benefit of about 4 dB at an equivalent velocity V_e of about $1.8c_\infty$ and a velocity ratio of V_2/V_1 near 2.0. The area ratio of the P&W data is near 1 and the jets were heated so that, for purposes of a simple comparison with Pao's result, x_2 and x_5 may be set to 0 in the present analysis. Pao did not consider temperature ratio so that x_4 is set to 0 also. The

quadratic form (eq. (71)) then contains only x_1 and x_3. A fit to the P&W data set using only these two parameters yields

$$\{\Delta_{,i}\} = \begin{Bmatrix} 0 \\ -4.70 \end{Bmatrix} \tag{86}$$

$$[\Delta_{,ij}] = \begin{bmatrix} 0 & 68.11 \\ -68.11 & -73.77 \end{bmatrix} \tag{87}$$

and it is understood that i and j take on values of 1 and 3 only.

The eigenvalues and eigenvectors of the matrix in equation (87) are

$$[\lambda_\alpha] = \begin{bmatrix} -114.30 & 0 \\ 0 & 40.57 \end{bmatrix} \tag{88}$$

and

$$[x_{i\alpha}] = \begin{bmatrix} -0.51 & 0.86 \\ 0.86 & 0.51 \end{bmatrix} \tag{89}$$

The eigenvalues in equation (87) indicate a saddle point rather than a maximum. The generalized coordinates of this stationary point are

$$\{a^0_\alpha\} = \begin{Bmatrix} 0.03 \\ -0.06 \end{Bmatrix} \tag{90}$$

and the actual coordinates are

$$\{x_i\} = \begin{Bmatrix} -0.07 \\ 0.00 \end{Bmatrix} \tag{91}$$

The value of the benefit at this stationary point is 0.

The plot of the coaxial benefit contours from Pao (ref. 9) is reproduced in figure 20. Note that insufficient data exist to determine whether the contours actually close. Pao used the dashed lines to indicate that existence of an extremum was speculative. The location of the stationary point given in equation (91) corresponds to V_e = 290 m/s and V_2/V_1 = 1.0, which is at the lower left edge of figure 20. A contour of the Taylor's series expansion for these data is shown in figure 21. By comparing the two figures, it can be seen that the contours in figure 20 can be interpreted to represent the positive lobe of the saddle shown in figure 21. The results of both Pao and this paper clearly show that a significant coaxial benefit occurs for the higher values of both equivalent velocity V_e and velocity ratio V_2/V_1. This analysis shows however that there is no maximum coaxial benefit within the range of the data. A maximum can only be defined by the addition of design constraints which limit the jet state parameters to some region of the contour plane. Since the coaxial benefit function is a saddle, the maximum benefit must lie on the boundary of this design region.

CONCLUDING REMARKS

An unbiased representation of a noise data base is important for empirical noise prediction and for validation of theoretical prediction methods. The method given in the present paper is one objective approach to the development of empirical predictions. The application of this method to the prediction of coaxial jet noise shows that it is a powerful and efficient technique which can represent a large number of physical effects.

The combination of bicubic splines for acoustic field variables and Taylor's series for flow state parameters provides an economical scheme for reducing a large noise data base to a reasonably small table of constants. In the case of jet noise, a large data base with over 100 000 data elements was reduced to a table of slightly over 1000 constants. The data were reduced literally by a factor of 100.

This method of data reduction and prediction requires a large data base. The data base must result from tests which are well distributed in the space of state parameters. This means that each state parameter must be independently varied in the test program which generates the data base. If the proper combination of state parameters is not available, then it will not be possible to find all derivatives in the Taylor's series. This was the case in the analysis of coaxial jet noise where only 43 of the 56 possible terms could be found out of a data base which contained 540 tests. A carefully planned test program would have required only 56 tests, but the data used were gathered from independent laboratories in different nations so that many of the points in the parameter space were essentially repeated while others were overlooked.

The methods used here are self-evaluating in the sense that the standard deviation of the curve fits to the data is found at the same time as the curve fit. The least-squares norm used in the curve fitting process is a classical measure of agreement which results in linear equations for the constants in the curve fits. In applying this method to coaxial jet noise, a standard deviation of 1.2 dB was found for the curve fit to the data base of 540 tests.

The Taylor's series representation of state parameters facilitates optimization studies such as the search for a minimum noise jet given as an example herein. The second-order Taylor's series defines stationary points and their properties through classical eigenvalue analysis. Although the search for an optimum coaxial jet failed in the general case because the stationary point was a saddle, it still defined optimum directions in the state space for the reduction of coaxial jet noise. The minimum noise jet depends on design constraints on the jet state parameters.

The analysis of this data set confirms the concept that inverted-flow jets are less noisy than equivalent single-stream jets at the higher equivalent velocities. Within the range of data used here, there can be as much as 6 dB benefit from the high-speed inverted-flow jet. On the other hand, there is a low velocity region where conventional coaxial jets are quieter than their equivalent single jets. The low speed benefit in the range of the data is limited to about 2 dB.

Langley Research Center
National Aeronautics and Space Administration
Hampton, VA 23665
September 22, 1982

REFERENCES

1. Zorumski, William E.: Aircraft Noise Prediction Program Theoretical Manual. NASA TM-83199, Part 2, 1981.

2. Jaeck, Carl L.: Empirical Jet Noise Predictions for Single and Dual Flow Jets With and Without Suppressor Nozzles. Volume I - Single Flow Subsonic and Supersonic Jets. Doc. No. D6-42929-1, Boeing Co., [Apr. 7, 1976].

3. Jaeck, Carl L.: Empirical Jet Noise Predictions for Single and Dual Flow Jets With and Without Suppressor Nozzles. Volume II - Dual Flow Subsonic and Supersonic Jets. Doc. No. D6-42929-2, Boeing Co., [Aug. 1, 1977].

4. Kozlowski, Hilary; and Packman, Allan B.: Aerodynamic and Acoustic Tests of Duct-Burning Turbofan Exhaust Nozzles. NASA CR-2628, 1976.

5. Goodykoontz, Jack H.; and Stone, James R.: Experimental Study of Coaxial Nozzle Exhaust Noise. NASA TM-79090, [1979]. (Also available as AIAA Paper 79-0631.)

6. Stone, James R.; Goodykoontz, Jack H.; and Gutierrez, Orlando A.: Effects of Geometric and Flow-Field Variables on Inverted-Velocity-Profile Coaxial Jet Noise and Source Distributions. NASA TM-79095, [1979]. (Also available as AIAA Paper 79-0635.)

7. Stone, James R.: Interim Prediction Method for Jet Noise. NASA TM X-71618, 1974.

8. Stone, James R.: An Empirical Model for Inverted-Velocity-Profile Jet Noise Prediction. NASA TM-73838, 1977.

9. Pao, S. Paul: A Correlation of Mixing Noise From Coannular Jets With Inverted Flow Profiles. NASA TP-1301, 1979.

10. Russell, James W.: A Method for Predicting the Noise Levels of Coannular Jets With Inverted Velocity Profiles. NASA CR-3176, 1979.

11. De Boor, Carl: Bicubic Spline Interpolation. J. Math & Phys., vol. 41, 1962, pp. 212-218.

12. De Boor, Carl: A Practical Guide to Splines. Springer-Verlag, c.1978.

TABLE I.- INDEPENDENT DERIVATIVES OF FIVE-DIMENSIONAL TAYLOR'S SERIES

First derivatives				
$\Delta_{,1}$	$\Delta_{,2}$	$\Delta_{,3}$	$\Delta_{,4}$	$\Delta_{,5}$
Second derivatives				
$\Delta_{,11}$				
$\Delta_{,21}$	$\Delta_{,22}$			
$\Delta_{,31}$	$\Delta_{,32}$	$\Delta_{,33}$		
$\Delta_{,41}$	$\Delta_{,42}$	$\Delta_{,43}$	$\Delta_{,44}$	
$\Delta_{,51}$	$\Delta_{,52}$	$\Delta_{,53}$	$\Delta_{,54}$	$\Delta_{,55}$
Third derivatives				
$\Delta_{,111}$				
$\Delta_{,211}$	$\Delta_{,221}$			
$\Delta_{,311}$	$\Delta_{,321}$	$\Delta_{,331}$		
$\Delta_{,411}$	$\Delta_{,421}$	$\Delta_{,431}$	$\Delta_{,441}$	
$\Delta_{,511}$	$\Delta_{,521}$	$\Delta_{,531}$	$\Delta_{,541}$	$\Delta_{,551}$
	$\Delta_{,222}$			
	$\Delta_{,322}$	$\Delta_{,332}$		
	$\Delta_{,422}$	$\Delta_{,432}$	$\Delta_{,442}$	
	$\Delta_{,522}$	$\Delta_{,532}$	$\Delta_{,542}$	$\Delta_{,552}$
		$\Delta_{,333}$		
		$\Delta_{,433}$	$\Delta_{,443}$	
		$\Delta_{,533}$	$\Delta_{,543}$	$\Delta_{,553}$
			$\Delta_{,444}$	
			$\Delta_{,544}$	$\Delta_{,554}$
				$\Delta_{,555}$

TABLE II.- LINEAR INDEX TO DERIVATIVES

ℓ	i	j	k	$[D_\ell!/P_\ell]$	ℓ	i	j	k	$[D_\ell!/P_\ell]$
1	0	0	0	1	29	4	2	1	1
2	1	0	0	1	30	5	2	1	1
3	2	0	0	1	31	3	3	1	2
4	3	0	0	1	32	4	3	1	1
5	4	0	0	1	33	5	3	1	1
6	5	0	0	1	34	4	4	1	2
7	1	1	0	2	35	5	4	1	1
8	2	1	0	1	36	5	5	1	2
9	3	1	0	1	37	2	2	2	6
10	4	1	0	1	38	3	2	2	2
11	5	1	0	1	39	4	2	2	2
12	2	2	0	2	40	5	2	2	2
13	3	2	0	1	41	3	3	2	2
14	4	2	0	1	42	4	3	2	1
15	5	2	0	1	43	5	3	2	1
16	3	3	0	2	44	4	4	2	2
17	4	3	0	1	45	5	4	2	1
18	5	3	0	1	46	5	5	2	2
19	4	4	0	2	47	3	3	3	6
20	5	4	0	1	48	4	3	3	2
21	5	5	0	2	49	5	3	3	2
22	1	1	1	6	50	4	4	3	2
23	2	1	1	2	51	5	4	3	1
24	3	1	1	2	52	5	5	3	2
25	4	1	1	2	53	4	4	4	6
26	5	1	1	2	54	5	4	4	2
27	2	2	1	2	55	5	5	4	2
28	3	2	1	1	56	5	5	5	6

TABLE III.- COAXIAL JET NOISE DATA BASE

Area ratio	Source	Tests	Polar angles	1/3-octave bands	SPL
*U	GALAC	65	19	24	456
	NGTE A	29	7	23	161
	NGTE B	3	8	24	192
	NGTE C	55	8	27	216
	P&W	25	8	30	240
	LeRC	21	8	30	240
	SNECMA	4	15	28	420
0.75	P&W	58	9	30	270
1.20	P&W	11	9	30	270
	LeRC	35	8	30	240
1.50	NGTE C	74	8	27	216
	LeRC	22	8	30	240
2.00	NGTE A	50	7	23	161
	NGTE C	82	8	27	216
	LeRC	33	8	30	240
3.33	LeRC	35	8	30	240
3.52	SNECMA	31	15	28	420
4.00	NGTE A	50	7	23	161
	NGTE B	13	8	24	192
	NGTE C	56	8	27	216
6.00	NGTE A	50	7	23	161
8.00	NGTE C	40	8	27	216
	Total	842			

*U indicates undefined.

TABLE IV.- AREA RATIO A_2/A_1 CLASSIFICATION

Index	A_2/A_1		
	Lower limit	Geometric mean	Upper limit
U	0	Undefined	∞
1	0.088	1/8	0.177
2	0.177	1/4	0.354
3	0.354	1/2	0.707
4	0.707	1	1.414
5	1.414	2	2.828
6	2.828	4	5.657
7	5.657	8	11.314

TABLE V.- TOTAL PRESSURE RATIO p_t/p_∞ CLASSIFICATION

[γ = 1.35]

Index	p_t/p_∞		
	Lower limit	Geometric mean	Upper limit
1	>1.000	1.081	1.168
2	1.168	1.263	1.365
3	1.365	1.475	1.594
4	1.594	1.723	1.863
5	1.863	2.013	2.176
6	2.176	2.352	2.542
7	2.542	2.748	2.970
8	2.970	3.210	3.470

TABLE VI.- TOTAL TEMPERATURE RATIO T_t/T_∞ CLASSIFICATION

Index	T_t/T_∞		
	Lower limit	Geometric mean	Upper limit
1	0.707	1	1.414
2	1.414	2	2.828
3	2.828	4	5.657

TABLE VII.- STANDARD DEVIATIONS OF TAYLOR'S SERIES EXPANSIONS

Description	All data sets	LeRC data set	NGTE data set A	NGTE data set B	NGTE data set C	P&W data set	SNECMA data set
Third-order fit:							
Acoustic power	1.6	1.4	1.0	1.2	1.5	0.7	
Overall directivity	0.9	1.1	0.5	0.3	0.6	0.8	
Power spectrum	1.1		0.5		1.1	0.8	
Relative spectrum	1.2		0.5		0.9	1.1	
Total	1.2	1.5	0.5	0.5	0.9	1.0	
Second-order fit:							
Acoustic power	2.2	1.7	1.5	1.4	2.4	0.8	0.7
Overall directivity	1.0	1.1	0.6	0.3	0.7	1.1	0.2
Power spectrum	1.3	1.3	0.6		1.1	1.0	0.4
Relative spectrum	1.4	1.6	0.5		1.0	1.3	0.3
Total	1.3	1.5	0.6	0.6	1.1	1.2	0.3
First-order fit:							
Acoustic power	3.5	2.4	2.8	3.1	3.9	1.6	0.8
Overall directivity	1.4	1.3	0.9	0.5	0.8	2.0	0.2
Power spectrum	2.0	1.5	0.9		1.6	1.5	0.4
Relative spectrum	1.7	1.7	0.7		1.3	1.6	0.3
Total	1.8	1.6	0.9	1.3	1.5	1.7	0.4

TABLE VIII.- DERIVATIVE MULTIPLIERS

Definitions:

$x_1 = \log_{10}(p_{t,1}/1.365p_\infty)$

$x_2 = \log_{10}(p_{t,2}/1.365p_\infty)$

$x_3 = \log_{10}(T_{t,1}/(2T_\infty))$

$x_4 = \log_{10}(T_{t,2}/(2T_\infty))$

$x_5 = \log_{10}(A_2/A_1)$

Derivative index, ℓ	Derivative multiplier, X_ℓ	Derivative index, ℓ	Derivative multiplier, X_ℓ
1	1	29	$x_1x_2x_4$
2	x_1	30	$x_1x_2x_5$
3	x_2	31	$x_1x_3x_3/2$
4	x_3	32	$x_1x_3x_4$
5	x_4	33	$x_1x_3x_5$
6	x_5	34	$x_1x_4x_4/2$
7	$x_1x_1/2$	35	$x_1x_4x_5$
8	x_1x_2	36	$x_1x_5x_5/2$
9	x_1x_3	37	$x_2x_2x_2/6$
10	x_1x_4	38	$x_2x_2x_3/2$
11	x_1x_5	39	$x_2x_2x_4/2$
12	$x_2x_2/2$	40	$x_2x_2x_5/2$
13	x_2x_3	41	$x_2x_3x_3/2$
14	x_2x_4	42	$x_2x_3x_4$
15	x_2x_5	43	$x_2x_3x_5$
16	$x_3x_3/2$	44	$x_2x_4x_4/2$
17	x_3x_4	45	$x_2x_4x_5$
18	x_3x_5	46	$x_2x_5x_5/2$
19	$x_4x_4/2$	47	$x_3x_3x_3/6$
20	x_4x_5	48	$x_3x_3x_4/2$
21	$x_5x_5/2$	49	$x_3x_3x_5/2$
22	$x_1x_1x_1/6$	50	$x_3x_4x_4/2$
23	$x_1x_1x_2/2$	51	$x_3x_4x_5$
24	$x_1x_1x_3/2$	52	$x_3x_5x_5/2$
25	$x_1x_1x_4/2$	53	$x_4x_4x_4/6$
26	$x_1x_1x_5/2$	54	$x_4x_4x_5/2$
27	$x_1x_2x_2/2$	55	$x_4x_5x_5/2$
28	$x_1x_2x_3$	56	$x_5x_5x_5/6$

TABLE IX.- DERIVATIVE VALUES

Index, ℓ	Derivatives values, Λ_ℓ, for 10 $\log_{10}$ of -								
	P	D(30)	D(60)	D(90)	D(120)	D(150)	S(-1.0)	S(-0.5)	S(0.0)
1	-44.7	-19.6	-17.7	-15.1	-10.1	-5.6	-14.1	-9.5	-15.8
2	64.9	-85.2	-72.3	-44.9	-27.7	11.5	9.7	4.5	8.0
3	52.8	-11.6	-10.4	-9.3	-6.4	0	8.3	-8.8	-2.4
4	27.9	-18.8	-19.6	-20.9	-16.5	-4.5	1.7	5.6	-7.1
5	14.4	-9.0	-10.2	-13.1	-13.1	-9.8	2.9	-2.9	-1.8
6	-1.4	-12.3	-12.0	-12.6	-11.7	-7.5	-7.2	0.2	5.5
7	-211.3	83.4	132.3	264.7	214.7	-183.5	-12.7	-291.7	333.1
8	-409.9	-134.8	-114.7	-81.9	-13.5	38.7	106.2	155.5	8.3
9	135.8	-136.9	-96.2	-13.2	35.9	2.6	-40.6	-48.5	110.0
10	-80.9	-94.2	-62.6	13.0	11.9	13.4	63.5	-3.2	45.0
11	-43.1	44.4	25.5	3.2	7.5	-23.2	-12.2	-13.2	13.1
12	134.6	135.5	119.3	105.2	25.1	-108.5	7.6	-222.2	51.8
13	-135.6	-2.5	-6.3	-16.8	-23.8	-11.2	32.2	17.9	-15.7
14	75.3	-21.6	-13.7	-3.9	13.1	-28.8	-14.1	4.4	-8.1
15	51.4	-29.4	-20.7	-7.0	-3.7	-23.0	43.5	20.0	-15.2
16	23.6	114.1	76.8	15.0	19.1	-35.4	-55.4	-31.0	12.8
17	-19.1	13.7	4.3	-12.6	-18.2	-17.5	17.0	9.8	-13.4
18	1.0	-28.5	-22.9	-10.0	-0.7	-31.3	-1.8	-1.1	-1.9
19	44.5	-63.9	-63.1	-51.6	-51.0	10.2	-69.0	-28.3	33.2
20	0	0	0	0	0	0	0	0	0
21	-13.3	-0.8	-2.9	-4.2	-9.0	-19.9	14.4	-3.0	-7.0
22	-1 326.3	2524.2	2825.1	2446.1	3722.3	1574.2	-5289.4	2337.2	-1131.7
23	5 145.7	-263.4	-131.5	198.1	77.3	-302.6	-2658.9	-1077.2	288.4
24	-2 052.9	1370.9	839.6	-354.7	-807.3	-355.7	290.5	186.0	-1144.1
25	0	0	0	0	0	0	0	0	0
26	406.0	-23.9	-49.3	-97.4	-114.0	51.6	-329.0	-87.6	-88.0
27	806.5	518.1	564.1	535.4	185.1	40.5	1294.9	1190.1	-705.5
28	844.6	-63.7	-28.9	40.6	50.9	-65.3	108.4	-96.2	117.7
29	0	0	0	0	0	0	0	0	0
30	-388.0	247.5	187.9	82.2	-43.3	-30.0	-15.6	-108.7	-12.7
31	-223.4	-101.6	-106.8	-168.5	-277.0	-99.4	233.1	274.6	-212.1
32	0	0	0	0	0	0	0	0	0
33	85.5	10.0	2.5	-13.9	-27.8	-29.1	-56.2	-23.1	-65.7
34	0	0	0	0	0	0	0	0	0
35	0	0	0	0	0	0	0	0	0
36	-28.8	-73.5	-46.4	-17.5	-41.9	10.5	0	0	0
37	-15 062.4	-974.4	-989.6	-1102.3	-1502.9	348.0	-5794.5	-1153.7	1770.6
38	116.1	138.1	152.2	161.4	-18.9	166.4	177.7	402.3	-82.5
39	0	0	0	0	0	0	0	0	0
40	609.1	-225.9	-212.0	-193.3	-73.0	112.5	-173.8	275.3	-135.0
41	221.6	-235.0	-206.2	-184.3	7.6	25.3	17.1	81.8	-27.4
42	-193.2	152.9	122.3	76.9	-33.3	-21.9	111.2	-96.7	64.6
43	-214.3	100.5	69.6	22.7	-31.5	8.9	-0.5	8.4	23.8
44	-51.9	520.5	423.5	274.5	148.5	-244.1	368.3	168.4	-179.8
45	0	0	0	0	0	0	0	0	0
46	18.9	-11.5	-18.0	-27.4	-34.8	17.8	0	0	0
47	0	0	0	0	0	0	0	0	0
48	58.7	64.6	44.8	-0.6	-1.6	-26.9	-197.9	-1.0	-31.4
49	33.2	-159.1	-111.8	-34.9	-23.8	2.6	51.4	-14.2	-31.7
50	18.0	100.6	68.6	3.6	32.5	-25.7	-132.7	7.0	92.4
51	84.5	-79.1	-60.7	-33.7	-15.0	-1.3	-23.7	22.6	-17.4
52	-6.6	-15.4	-15.6	-23.9	-37.4	40.1	0	0	0
53	0	0	0	0	0	0	0	0	0
54	0	0	0	0	0	0	0	0	0
55	0	0	0	0	0	0	0	0	0
56	0	0	0	0	0	0	0	0	0

TABLE IX.- Continued

Index, ℓ	Derivatives values, Λ_ℓ, for 10 $\log_{10}$ of -								
	S(0.5)	S(1.0)	$\mathcal{R}$(-1.0,30)	$\mathcal{R}$(-0.5,30)	$\mathcal{R}$(0.0,30)	$\mathcal{R}$(0.5,30)	$\mathcal{R}$(1.0,30)	$\mathcal{R}$(-1.0,60)	$\mathcal{R}$(-0.5,60)
1	-18.7	-24.5	-3.0	-3.9	3.9	3.1	4.9	-3.4	-3.4
2	-12.7	-53.1	-24.0	8.4	4.0	12.2	50.9	-21.4	4.0
3	26.6	3.0	-15.7	0.6	2.5	-12.9	-9.0	-16.4	0.6
4	-14.8	-16.3	4.0	-3.8	0.6	9.3	18.6	4.2	-2.0
5	0.7	6.9	6.1	3.7	2.1	-2.1	-6.1	2.9	2.6
6	5.6	1.6	4.5	4.1	-0.8	-4.8	-2.2	5.9	1.5
7	517.2	250.6	340.2	287.7	-255.9	-247.9	-212.7	325.2	217.9
8	-176.4	-347.1	159.5	121.2	58.0	68.9	128.5	163.3	86.1
9	84.2	13.3	137.9	23.7	-8.2	35.0	-63.8	96.1	5.0
10	30.1	-60.4	5.9	18.0	3.1	-8.3	1.0	9.0	13.4
11	36.9	-32.6	51.7	14.7	-15.5	-47.2	-9.4	67.5	7.9
12	220.9	281.2	-102.3	172.0	-99.2	-209.4	-340.2	-50.5	116.8
13	-27.5	-38.7	-6.4	24.1	0.7	-22.1	16.8	1.3	19.7
14	41.7	-38.4	-7.0	-5.6	20.9	-45.4	-18.3	-10.3	-3.0
15	-5.2	-55.6	-17.4	13.6	29.1	3.5	14.8	-11.6	7.3
16	46.1	95.4	-56.4	-18.4	-60.9	-25.1	65.9	-31.7	-13.7
17	-26.4	2.2	-22.5	-10.6	1.7	17.1	11.0	-11.6	-3.5
18	12.1	-21.8	11.0	15.6	10.4	-11.6	-2.5	11.9	7.0
19	0.6	64.5	37.2	-4.2	-39.2	35.8	-11.9	11.2	-4.6
20	0	0	0	0	0	0	0	0	0
21	-3.7	-12.6	-7.7	-3.0	-0.4	1.0	0.8	-0.2	-0.3
22	-154.8	4728.9	14 897.0	-1466.0	-581.5	-2710.2	-5637.2	12 303.9	-1938.7
23	1462.1	1999.7	-714.3	-1230.3	129.4	-79.3	285.6	-1 191.5	-1015.2
24	-203.6	-118.3	-418.6	425.6	603.0	-1625.4	-1209.4	-215.0	302.9
25	0	0	0	0	0	0	0	0	0
26	-650.5	1014.7	-1 030.2	-710.1	103.8	806.4	236.9	-1 394.5	-401.4
27	-443.6	-394.3	-319.3	-371.6	499.2	-178.1	-341.6	211.2	-229.8
28	-123.8	-94.7	169.2	-115.3	-112.5	348.7	-153.0	-11.0	-161.5
29	0	0	0	0	0	0	0	0	0
30	62.5	320.2	-130.2	-114.6	-94.8	-76.1	-57.2	-94.2	-47.8
31	-161.9	-158.0	-663.7	56.1	468.4	193.1	-682.2	-477.1	91.9
32	0	0	0	0	0	0	0	0	0
33	-90.2	126.0	-199.0	-119.0	-79.0	126.1	115.3	-196.2	-53.2
34	0	0	0	0	0	0	0	0	0
35	0	0	0	0	0	0	0	0	0
36	0	0	0	0	0	0	0	0	0
37	-2005.7	3561.4	4 723.1	2228.6	-2045.6	2159.2	-3284.9	2 028.6	2186.2
38	49.6	426.7	58.7	-261.0	159.5	280.1	205.6	-118.5	-167.7
39	0	0	0	0	0	0	0	0	0
40	-348.7	240.0	-90.1	-423.0	95.3	560.9	419.2	-441.7	-282.6
41	-542.2	-443.6	331.5	-219.9	-58.8	175.3	228.7	435.9	-213.7
42	142.9	228.5	-18.7	90.7	-45.6	-128.5	-300.8	-95.3	61.2
43	16.8	89.2	-44.5	-97.9	-25.6	-22.5	-57.6	-11.5	-63.3
44	-42.7	288.3	-422.3	-332.2	13.1	-131.4	-122.8	-294.2	-217.4
45	0	0	0	0	0	0	0	0	0
46	0	0	0	0	0	0	0	0	0
47	0	0	0	0	0	0	0	0	0
48	-53.3	-3.5	-77.8	42.1	-63.7	86.0	280.7	-42.4	39.5
49	-12.4	-46.9	67.4	38.1	9.9	39.2	6.7	-0.9	30.3
50	22.8	203.5	-193.1	-111.4	-83.0	4.5	30.1	-125.9	-79.1
51	-1.4	-75.5	5.1	7.1	33.5	7.7	40.3	5.4	-1.2
52	0	0	0	0	0	0	0	0	0
53	0	0	0	0	0	0	0	0	0
54	0	0	0	0	0	0	0	0	0
55	0	0	0	0	0	0	0	0	0
56	0	0	0	0	0	0	0	0	0

TABLE IX.- Continued

Index, ℓ	Derivatives values, Λ_ℓ, for 10 $\log_{10}$ of -								
	$\mathcal{R}(0.0,60)$	$\mathcal{R}(0.5,60)$	$\mathcal{R}(1.0,60)$	$\mathcal{R}(-1.0,90)$	$\mathcal{R}(-0.5,90)$	$\mathcal{R}(0.0,90)$	$\mathcal{R}(0.5,90)$	$\mathcal{R}(1.0,90)$	$\mathcal{R}(-1.0,120)$
1	3.7	3.6	5.7	-4.6	-2.4	3.5	4.1	6.6	-4.9
2	5.0	13.7	45.2	-12.9	-5.6	4.3	19.0	39.2	-18.7
3	1.0	-13.5	-6.1	-13.7	0.3	-0.9	-15.9	0.9	-9.6
4	2.6	9.6	13.7	4.1	1.4	6.1	9.7	4.9	4.9
5	1.0	-1.4	-6.1	-2.1	0.8	-0.7	-0.2	-6.0	-1.2
6	-1.9	-4.1	2.1	4.2	-1.4	-3.0	-3.4	6.0	1.4
7	-257.8	-278.0	-93.8	73.7	129.8	-257.9	-333.8	4.3	34.7
8	71.6	74.1	124.5	130.9	37.8	105.5	76.5	90.5	62.7
9	-22.9	18.6	-9.4	-11.8	-30.4	-49.2	-0.5	83.9	-67.2
10	6.5	-9.0	29.5	-28.1	12.6	14.0	-4.0	61.7	-26.2
11	-16.5	-40.2	26.6	31.1	13.8	-13.5	-35.1	46.7	10.3
12	-114.2	-164.6	-234.2	-130.1	58.8	-136.2	-114.3	-166.9	-122.2
13	2.4	-16.2	18.9	-4.4	19.4	8.2	-10.3	5.3	-6.8
14	17.1	-39.0	3.0	-0.5	-2.2	9.7	-26.6	52.3	-4.1
15	24.1	3.3	21.7	-13.3	0.2	18.1	-0.4	23.4	-16.2
16	-52.6	-38.0	17.1	19.4	-7.2	-45.0	-64.1	-64.3	66.2
17	5.3	16.2	0.5	6.3	8.9	11.8	13.3	-19.2	6.3
18	5.8	-11.0	10.4	4.2	-5.5	-1.3	-9.8	27.5	-5.7
19	-35.9	26.0	-42.9	5.4	-17.6	-35.6	18.0	-66.1	1.4
20	0	0	0	0	0	0	0	0	0
21	1.0	1.5	-1.1	-1.1	7.3	4.2	-0.3	-13.3	-2.7
22	-656.7	-1986.1	-3945.2	5555.3	-1375.2	326.5	-1426.6	-3274.7	9914.3
23	-67.0	110.9	49.7	-940.5	-862.2	-536.3	619.9	400.3	-982.9
24	470.4	-1134.5	-753.2	324.6	276.7	328.0	-451.2	-200.4	153.6
25	0	0	0	0	0	0	0	0	0
26	81.0	626.9	-513.1	-545.6	-298.1	-109.3	538.3	-748.4	-189.2
27	553.4	-165.0	-40.2	104.6	345.2	831.9	-348.2	-275.2	228.2
28	-98.8	351.1	-11.7	-319.1	-266.2	-105.7	356.6	226.6	-58.7
29	0	0	0	0	0	0	0	0	0
30	-88.1	-94.1	-107.8	-25.3	58.7	-84.4	-114.7	-176.4	52.6
31	428.8	202.8	-528.5	-13.5	119.1	394.9	224.9	-183.1	-491.3
32	0	0	0	0	0	0	0	0	0
33	-46.4	98.2	-39.7	-31.6	15.2	-2.1	58.0	-212.2	61.3
34	0	0	0	0	0	0	0	0	0
35	0	0	0	0	0	0	0	0	0
36	0	0	0	0	0	0	0	0	0
37	-1671.6	1699.6	-4729.8	2504.9	742.4	-1871.0	2056.9	-3170.8	2800.4
38	170.4	81.2	-132.7	86.9	-106.1	183.0	-154.5	-317.1	348.6
39	0	0	0	0	0	0	0	0	0
40	143.9	447.4	64.0	-91.6	-298.8	139.5	395.8	115.9	163.3
41	-33.8	253.0	350.8	246.5	-152.5	29.3	328.1	292.1	-50.8
42	-58.0	-97.9	-220.8	-229.3	10.5	-89.4	-52.0	-90.1	-88.5
43	-14.5	-10.7	-43.2	13.8	-2.0	4.4	5.7	-31.1	-14.4
44	44.9	-115.2	-0.4	-170.9	-1.7	94.8	-76.7	158.4	35.3
45	0	0	0	0	0	0	0	0	0
46	0	0	0	0	0	0	0	0	0
47	0	0	0	0	0	0	0	0	0
48	-41.5	47.7	135.1	111.3	16.9	-14.0	-19.6	-68.9	140.5
49	17.6	30.4	-4.8	-59.8	4.4	25.2	29.6	19.8	-40.6
50	-73.0	-16.9	-52.5	29.5	-32.4	-60.3	-52.9	-181.4	72.5
51	25.2	2.6	42.6	28.6	-19.8	10.4	-3.0	59.5	24.9
52	0	0	0	0	0	0	0	0	0
53	0	0	0	0	0	0	0	0	0
54	0	0	0	0	0	0	0	0	0
55	0	0	0	0	0	0	0	0	0
56	0	0	0	0	0	0	0	0	0

TABLE IX.- Concluded

Index, ℓ	Derivatives values, A_ℓ, for 10 $\log_{10}$ of -								
	$\mathcal{R}(-0.5,120)$	$\mathcal{R}(0.0,120)$	$\mathcal{R}(0.5,120)$	$\mathcal{R}(1.0,120)$	$\mathcal{R}(-1.0,150)$	$\mathcal{R}(-0.5,150)$	$\mathcal{R}(0.0,150)$	$\mathcal{R}(0.5,150)$	$\mathcal{R}(1.0,150)$
1	-2.2	4.5	3.6	3.1	2.1	0.9	-4.2	-9.3	-6.6
2	2.0	-2.2	15.1	22.8	-14.5	-5.5	7.8	-19.4	-53.0
3	-3.5	-0.7	-15.5	25.2	7.9	-0.9	2.6	24.8	39.0
4	0.5	7.0	6.8	4.9	-2.4	0.1	-7.4	-14.1	-11.8
5	-1.6	-0.2	0.5	-5.1	-0.1	0.8	-4.4	-2.3	-5.9
6	-2.5	-4.0	-2.8	6.0	0.5	0.4	5.3	-1.1	0.1
7	244.1	-257.1	-449.0	-65.2	290.0	39.0	400.9	686.0	819.0
8	14.2	63.4	47.0	60.2	-114.8	-48.5	-9.7	-113.8	8.2
9	1.2	-42.8	-21.0	3.5	34.4	42.7	60.5	113.9	99.4
10	57.9	-9.4	-47.9	-7.8	17.3	14.2	25.0	30.3	57.0
11	10.8	-9.6	-36.7	32.5	16.8	-3.5	30.3	17.1	79.0
12	59.6	-96.0	-49.5	-150.3	16.2	50.7	-23.7	139.2	-197.8
13	13.0	6.1	4.3	15.8	-39.3	-13.4	19.7	9.2	-40.3
14	-9.4	4.9	-21.3	69.3	21.7	-24.8	29.9	51.5	142.5
15	-6.5	13.6	1.9	30.5	-10.6	-7.7	-1.1	-13.8	5.7
16	17.4	-38.5	-59.6	-67.2	42.0	39.1	14.4	-20.5	-1.0
17	4.4	10.1	8.3	-7.7	-10.2	-12.6	-8.5	2.5	24.8
18	-3.6	0.1	-9.7	22.4	-2.4	-3.1	15.9	4.0	27.7
19	-26.0	-38.7	23.9	-11.6	-47.9	-4.3	21.5	57.5	-84.2
20	0	0	0	0	0	0	0	0	0
21	4.7	5.3	3.6	-6.8	-0.8	-1.7	-1.6	8.9	16.1
22	1688.2	1181.3	-2335.8	-6456.1	6464.2	2015.2	-3440.0	-369.1	3865.9
23	-1396.8	-761.1	967.1	648.8	1522.4	221.3	201.2	-629.5	-3362.3
24	-221.3	188.9	-146.9	698.3	-552.7	-1147.2	163.9	-227.3	311.6
25	0	0	0	0	0	0	0	0	0
26	-372.0	-65.1	736.9	-630.6	-392.9	307.3	-757.4	-260.4	-2224.6
27	890.3	938.5	-977.5	-783.3	376.2	-327.3	-462.8	-1007.2	5478.0
28	-147.4	-85.1	394.3	-73.3	-92.0	307.9	-181.6	-430.7	-1200.9
29	0	0	0	0	0	0	0	0	0
30	81.6	-12.0	-88.5	-137.8	104.1	46.9	3.0	26.9	226.6
31	-363.9	233.6	257.6	359.5	-369.0	-438.6	-8.7	264.9	687.3
32	0	0	0	0	0	0	0	0	0
33	-24.0	15.3	90.5	-97.7	-1.1	47.4	-167.6	-55.8	-270.3
34	0	0	0	0	0	0	0	0	0
35	0	0	0	0	0	0	0	0	0
36	0	0	0	0	0	0	0	0	0
37	-802.9	-2492.2	3110.6	-1708.1	-1270.4	-254.6	581.6	92.3	-8360.8
38	107.4	78.1	-357.7	-173.4	235.5	-160.6	-75.1	122.3	1253.1
39	0	0	0	0	0	0	0	0	0
40	-209.2	117.6	241.6	58.9	-54.3	-14.8	-33.8	-170.8	-381.2
41	-1.9	184.2	392.7	-226.7	-83.8	26.1	-106.0	-27.1	-476.4
42	46.7	-96.5	-28.9	-4.1	-162.8	123.1	-2.1	48.9	-308.7
43	4.7	2.8	-3.0	-39.6	-15.4	20.6	-9.0	2.8	78.6
44	265.0	164.9	-195.1	-332.8	107.0	-14.1	81.1	-5.3	905.6
45	0	0	0	0	0	0	0	0	0
46	0	0	0	0	0	0	0	0	0
47	0	0	0	0	0	0	0	0	0
48	46.1	-5.9	5.1	19.8	100.5	-28.1	37.2	-16.9	1.4
49	29.7	24.2	-2.8	17.0	-9.2	-17.3	-83.7	-45.4	-13.5
50	-27.0	-80.1	-16.0	-229.5	127.5	17.1	-12.6	12.6	29.2
51	-18.6	11.3	7.3	52.8	30.9	5.0	26.4	-10.3	14.6
52	0	0	0	0	0	0	0	0	0
53	0	0	0	0	0	0	0	0	0
54	0	0	0	0	0	0	0	0	0
55	0	0	0	0	0	0	0	0	0
56	0	0	0	0	0	0	0	0	0

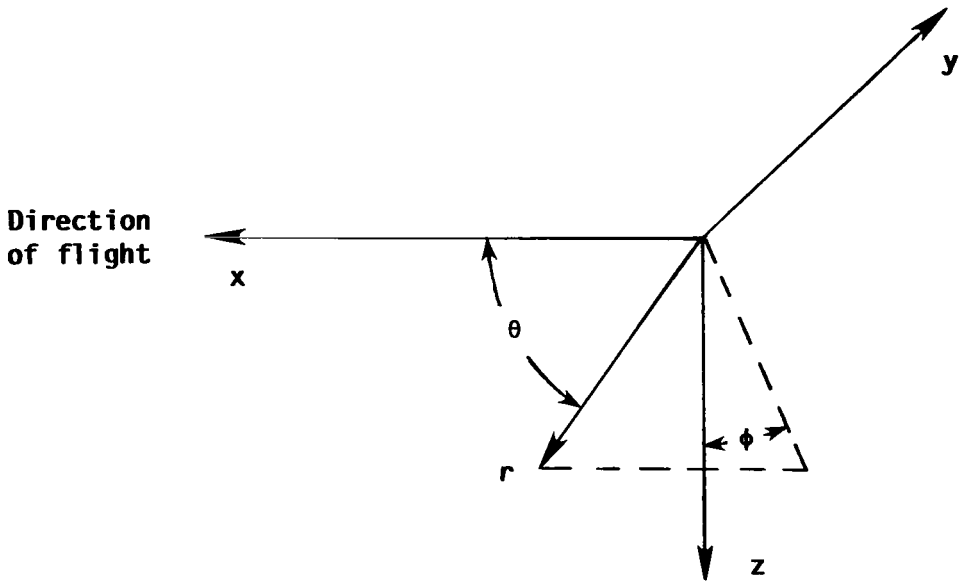

Spherical coordinates	Cartesian coordinates
$r = \sqrt{x^2 + y^2 + z^2}$	$x = r \cos \theta$
$\theta = \arccos x/r$	$y = r \sin \theta \sin \phi$
$\phi = \arctan y/z$	$z = r \sin \theta \cos \phi$

Figure 1.- Spherical coordinate system used for empirical noise prediction.

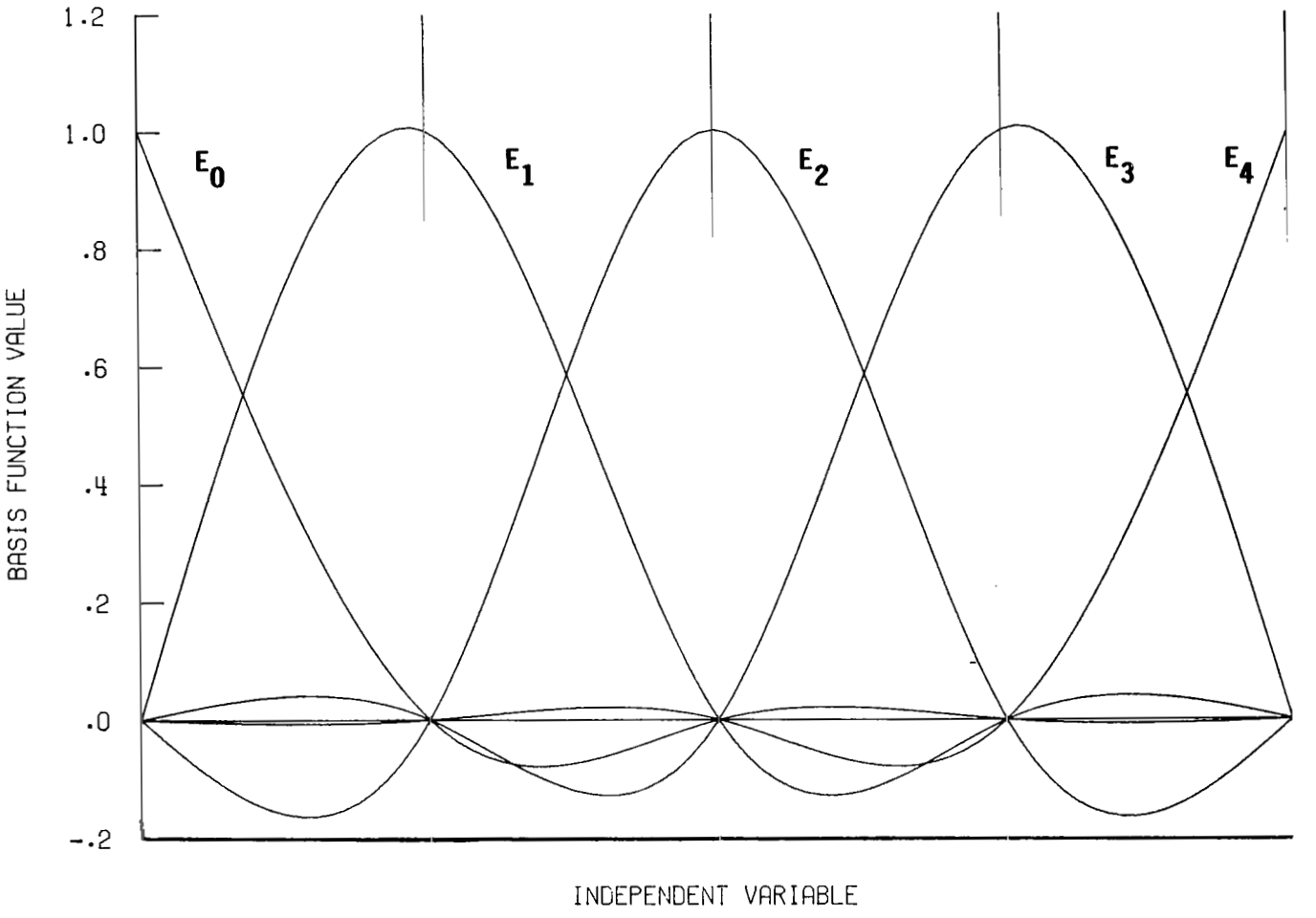

Figure 2.- Basis functions E_m for cubic spline.

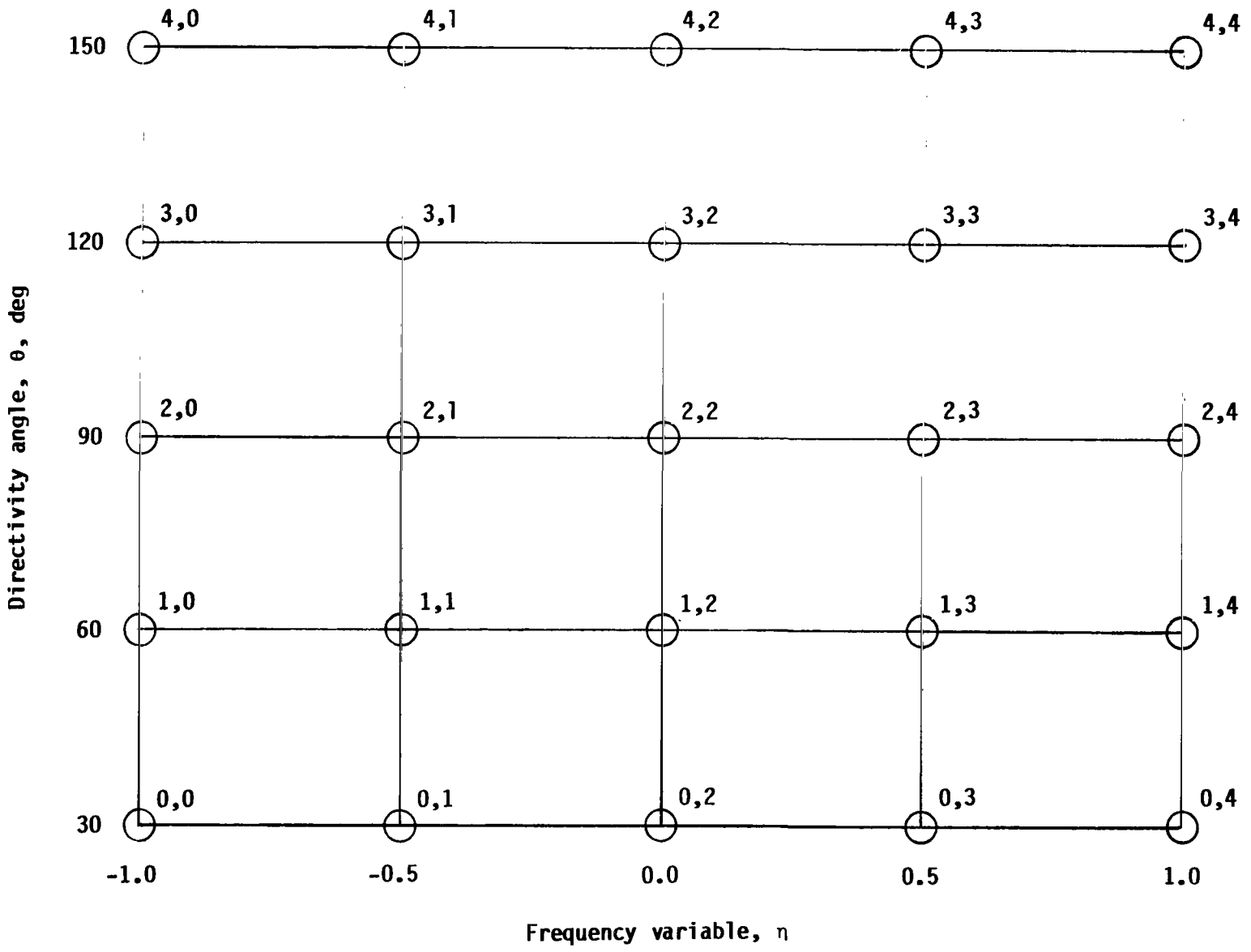

Figure 3.- Node points for bicubic spline fit to jet noise data.

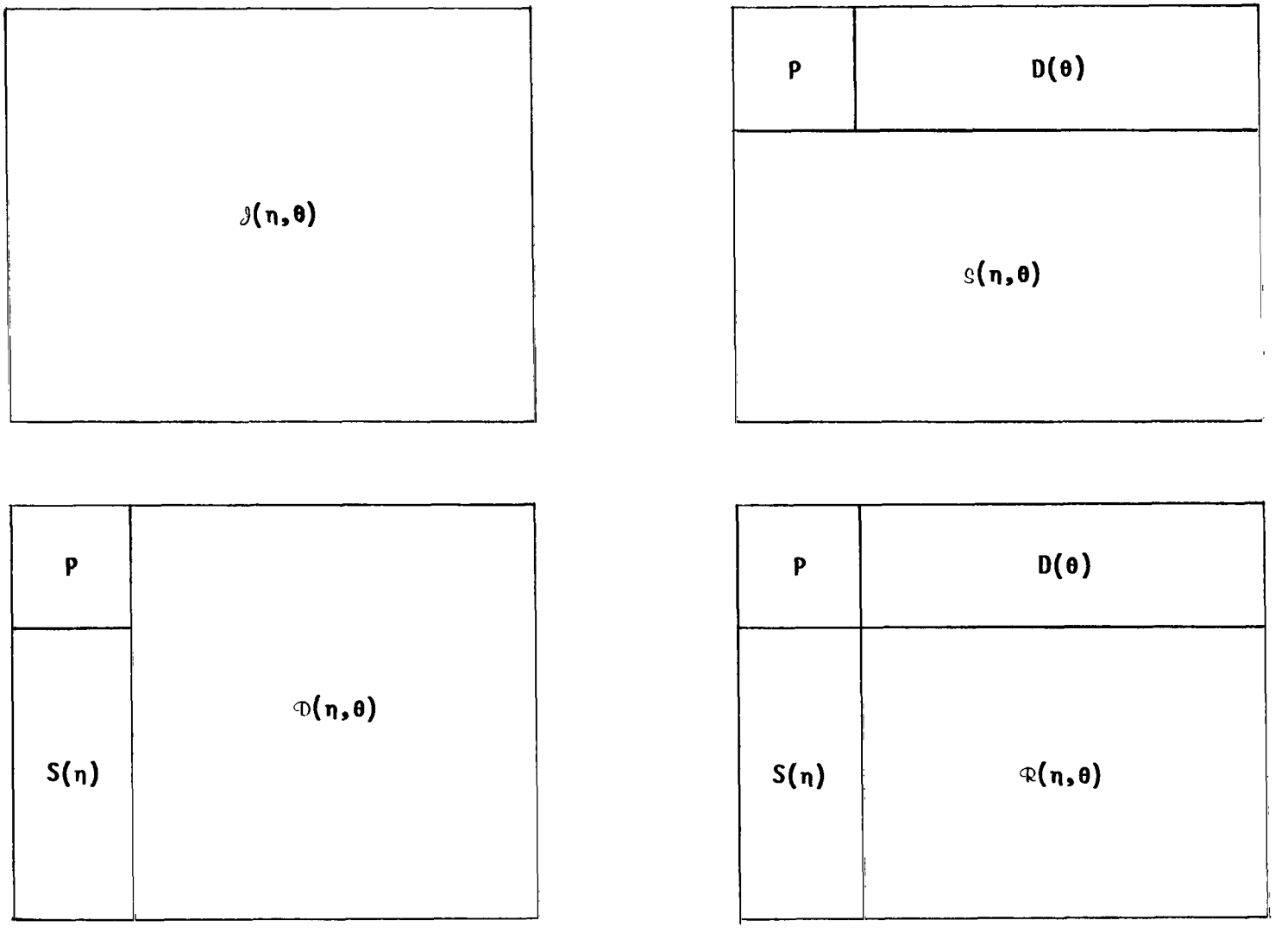

Figure 4.- Alternate sets of independent noise level coordinates.

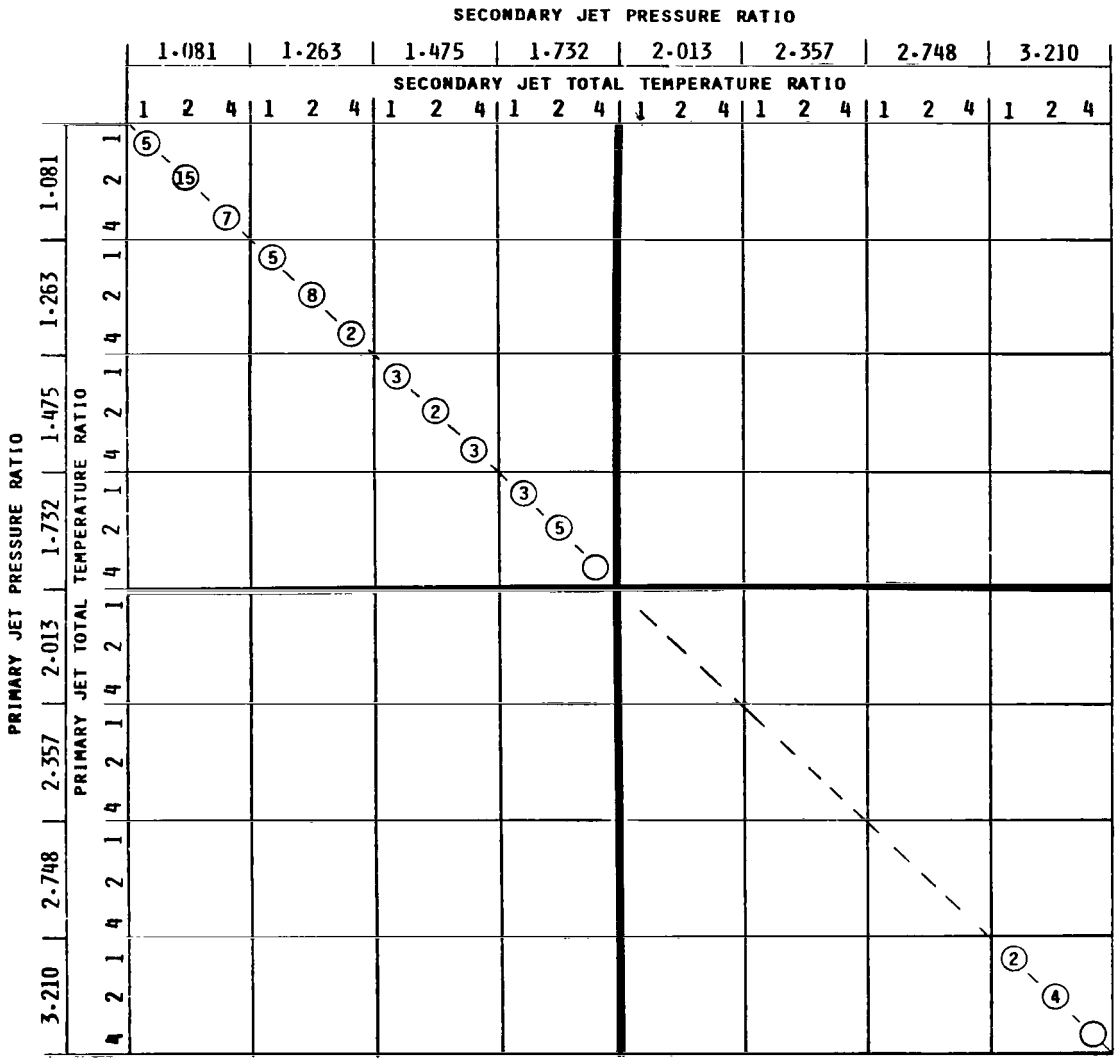

○ Circular jet

Figure 5.- Jet noise test points for GALAC data.

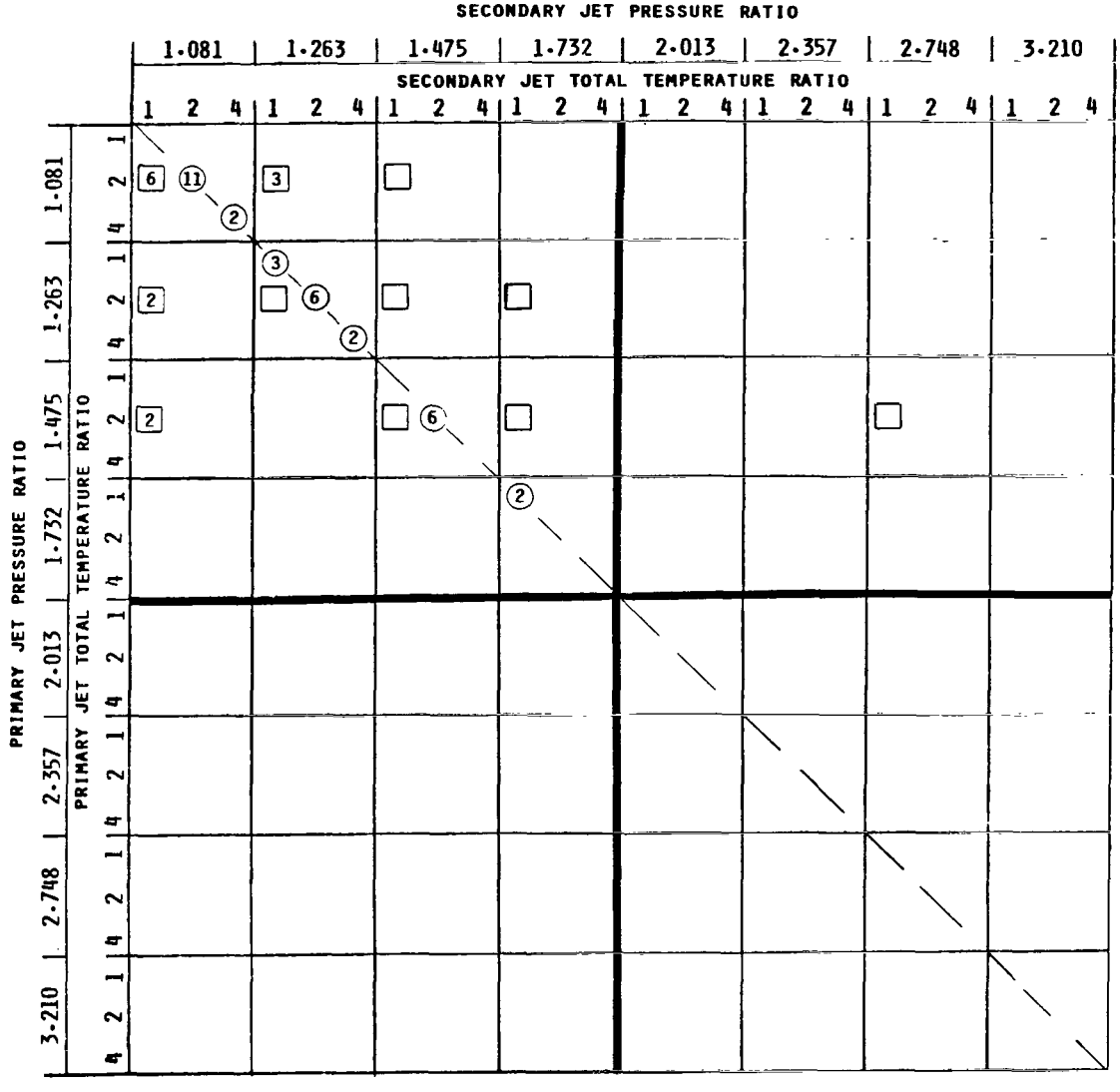

Figure 6.- Jet noise test points for NGTE data set A.

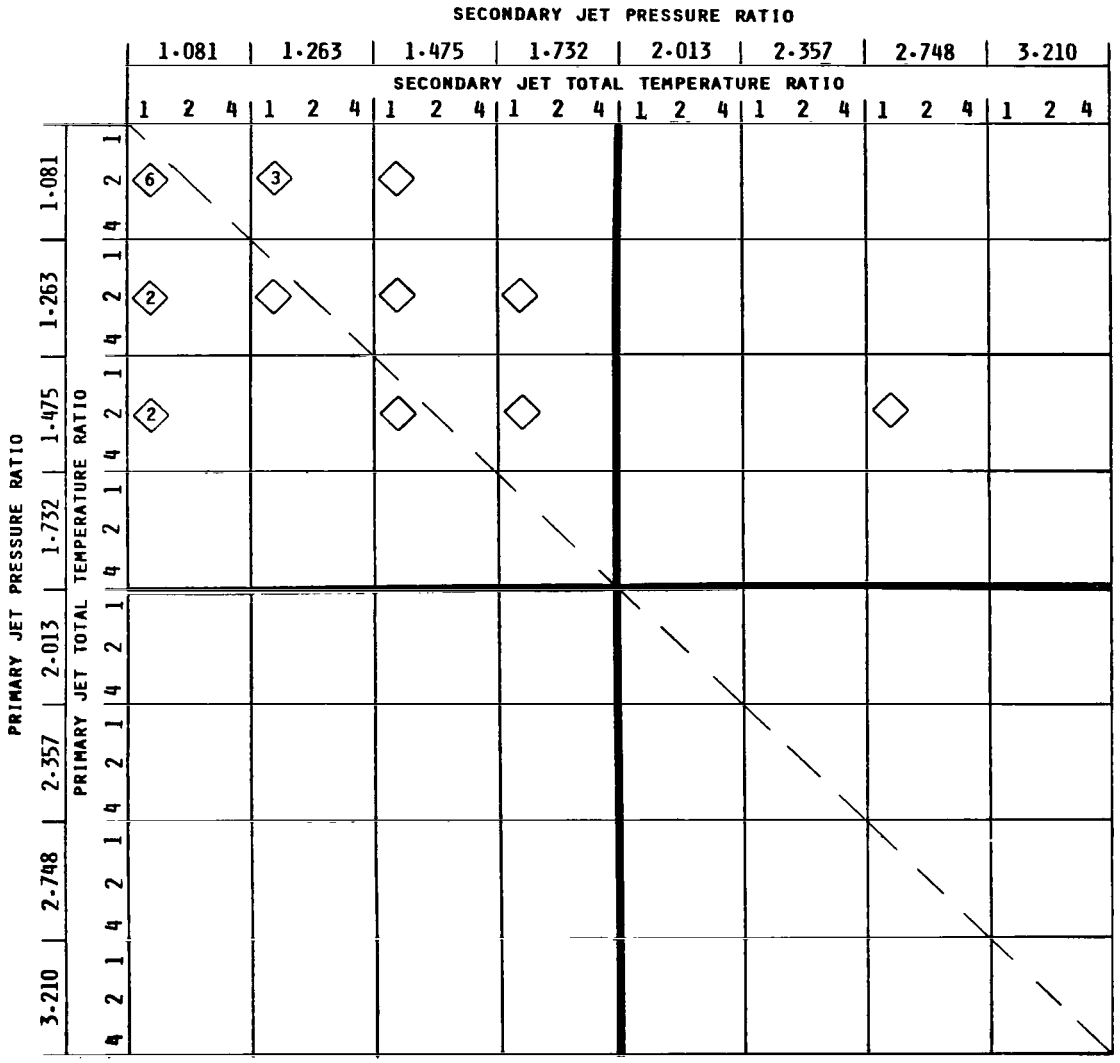

Figure 6.- Continued.

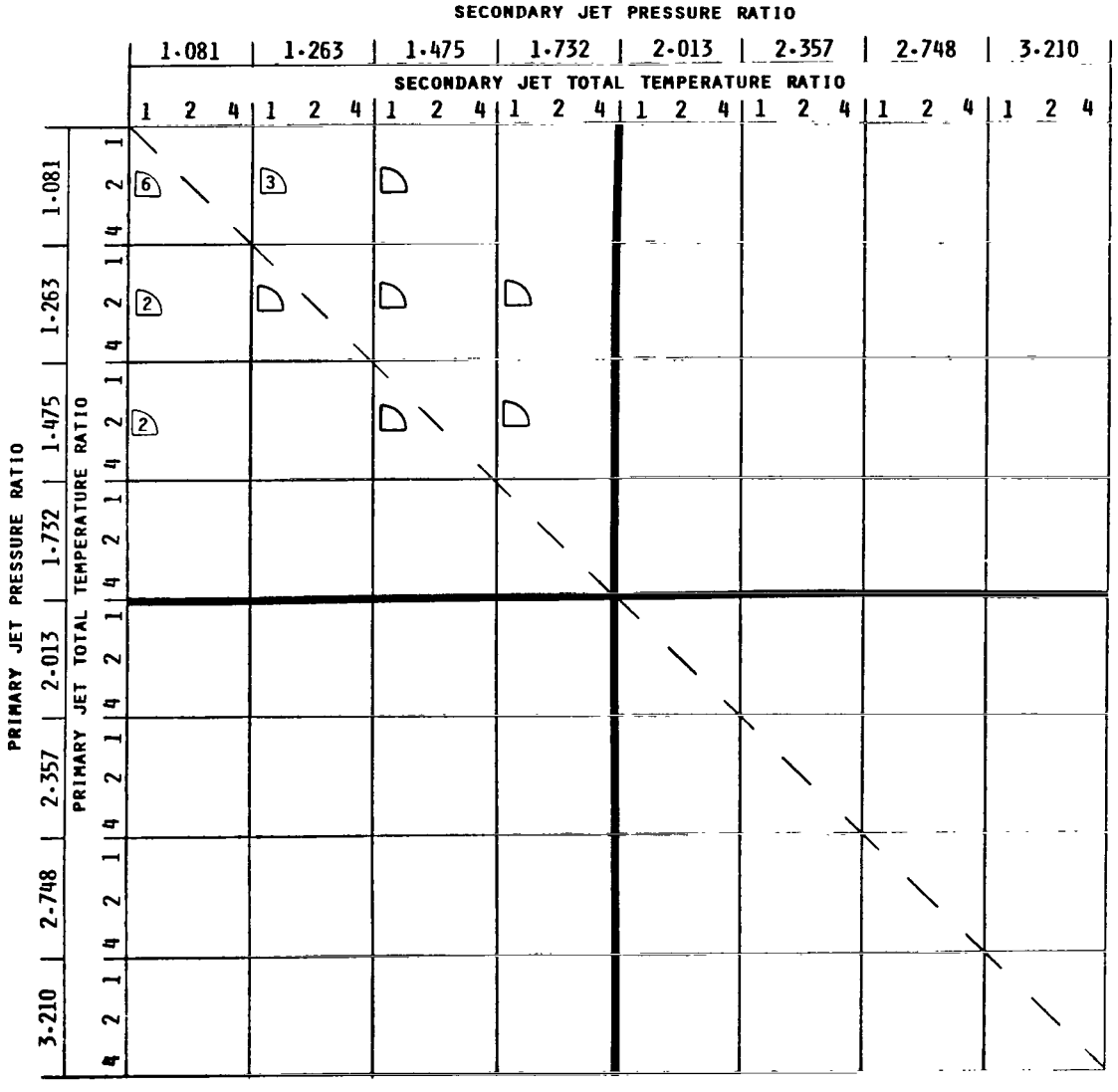

Area ratio = 6.0 jet

Figure 6.- Concluded.

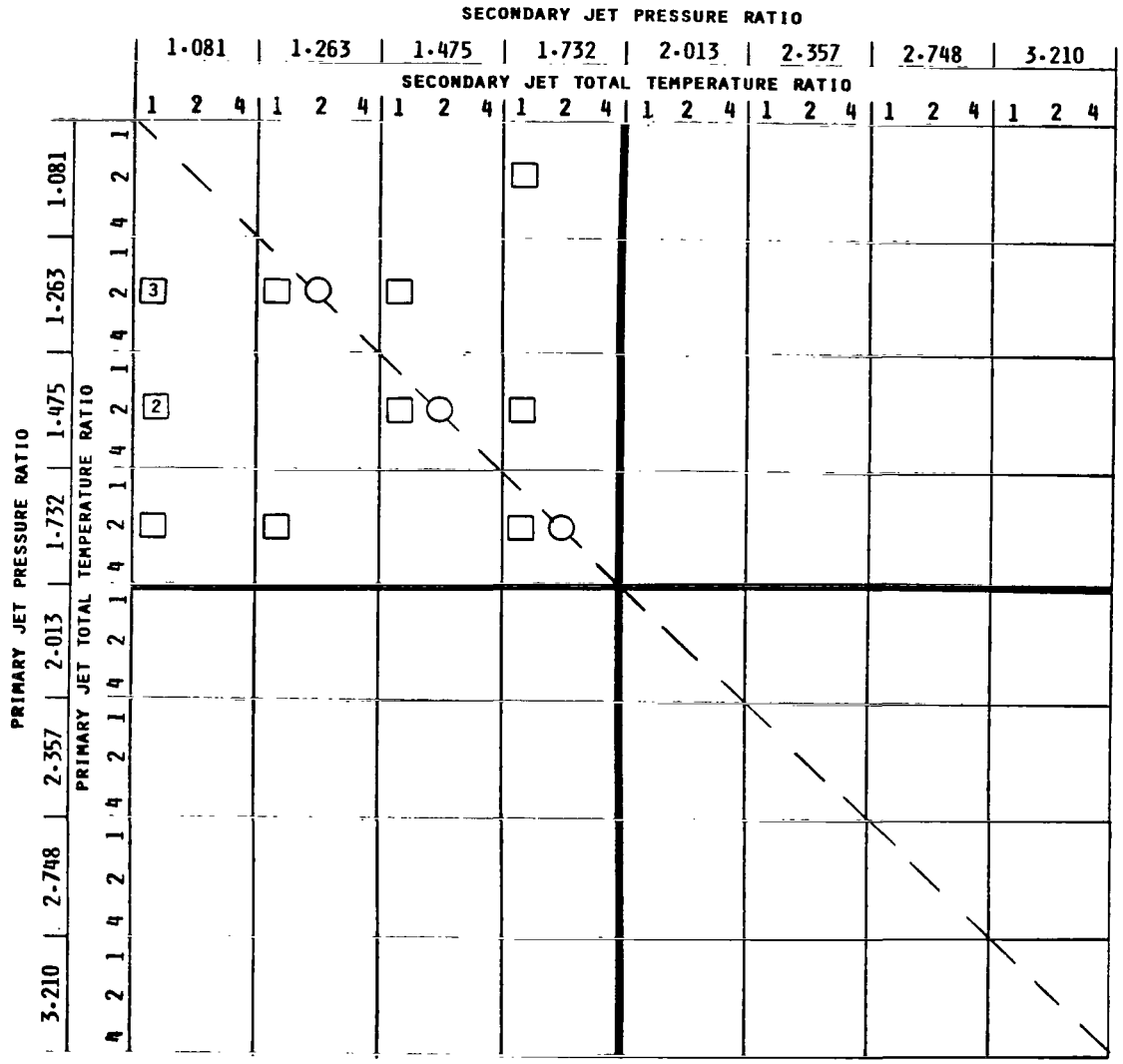

○ Circular jet □ Area ratio = 4.0 jet

Figure 7.- Jet noise test points for NGTE data set B.

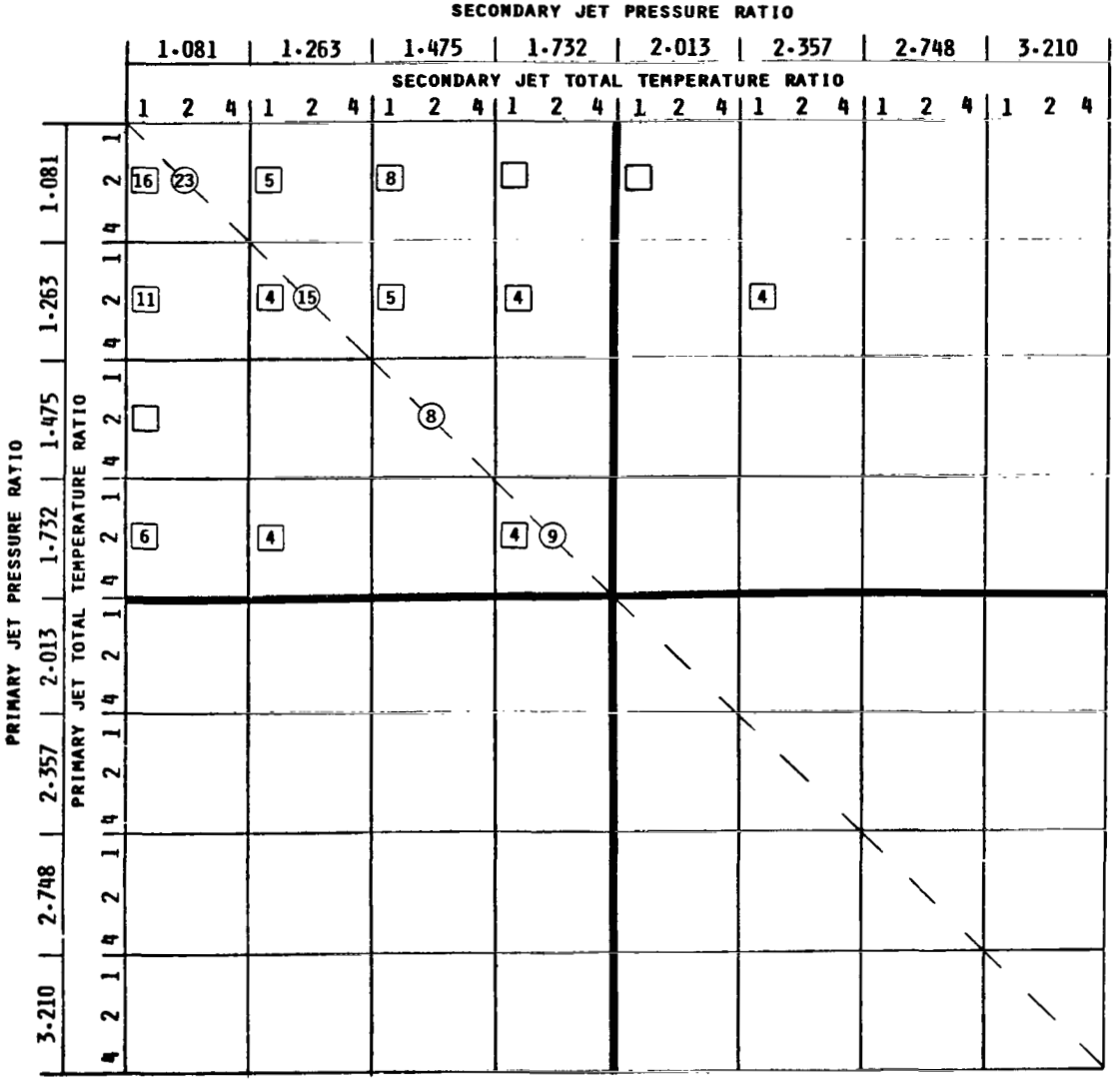

○ Circular jet □ Area ratio = 1.4, 1.5, and 1.6 jets

Figure 8.- Jet noise test points for NGTE data set C.

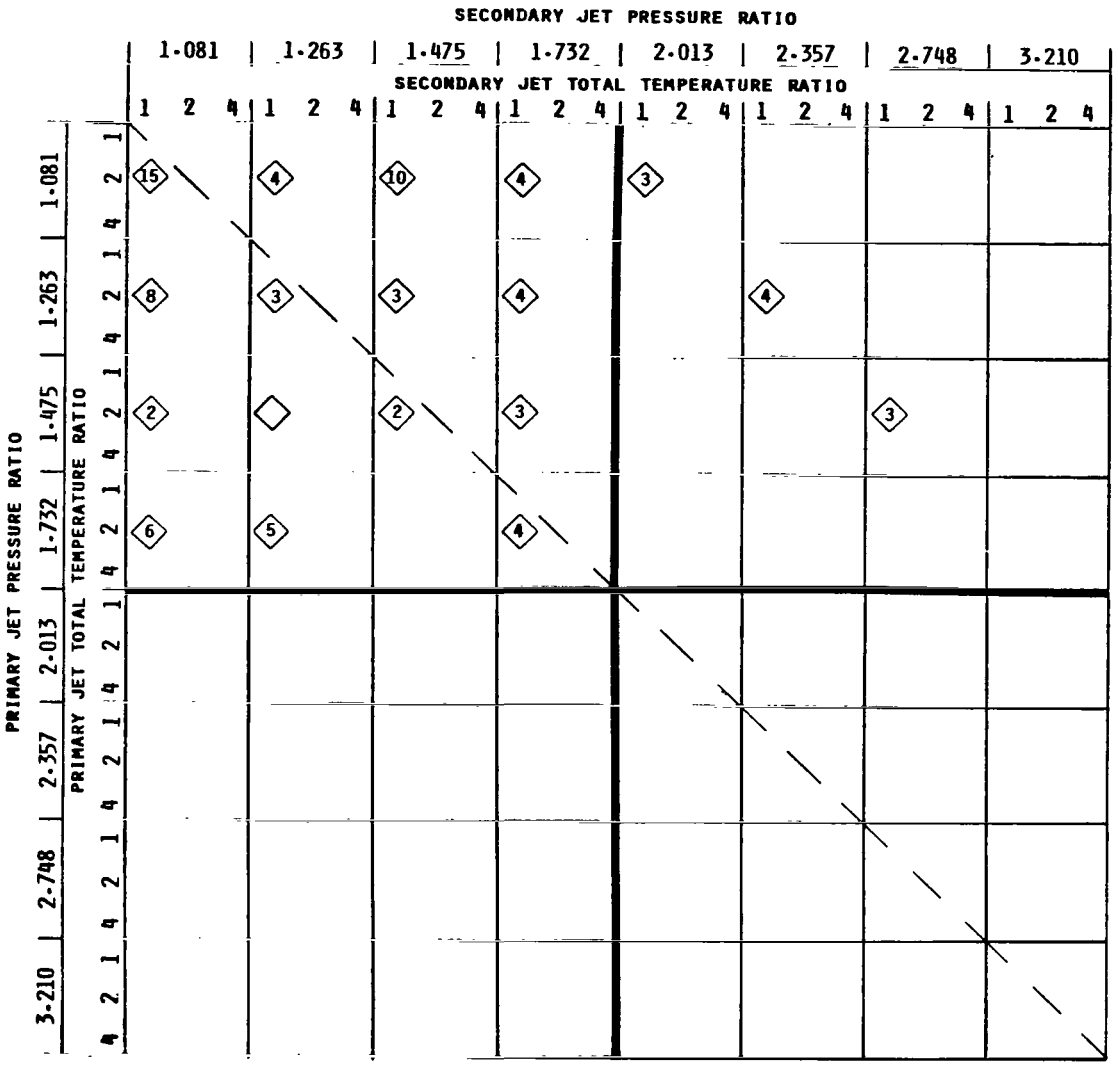

◇ Area ratio = 1.9 and 2.0 jets

Figure 8.- Continued.

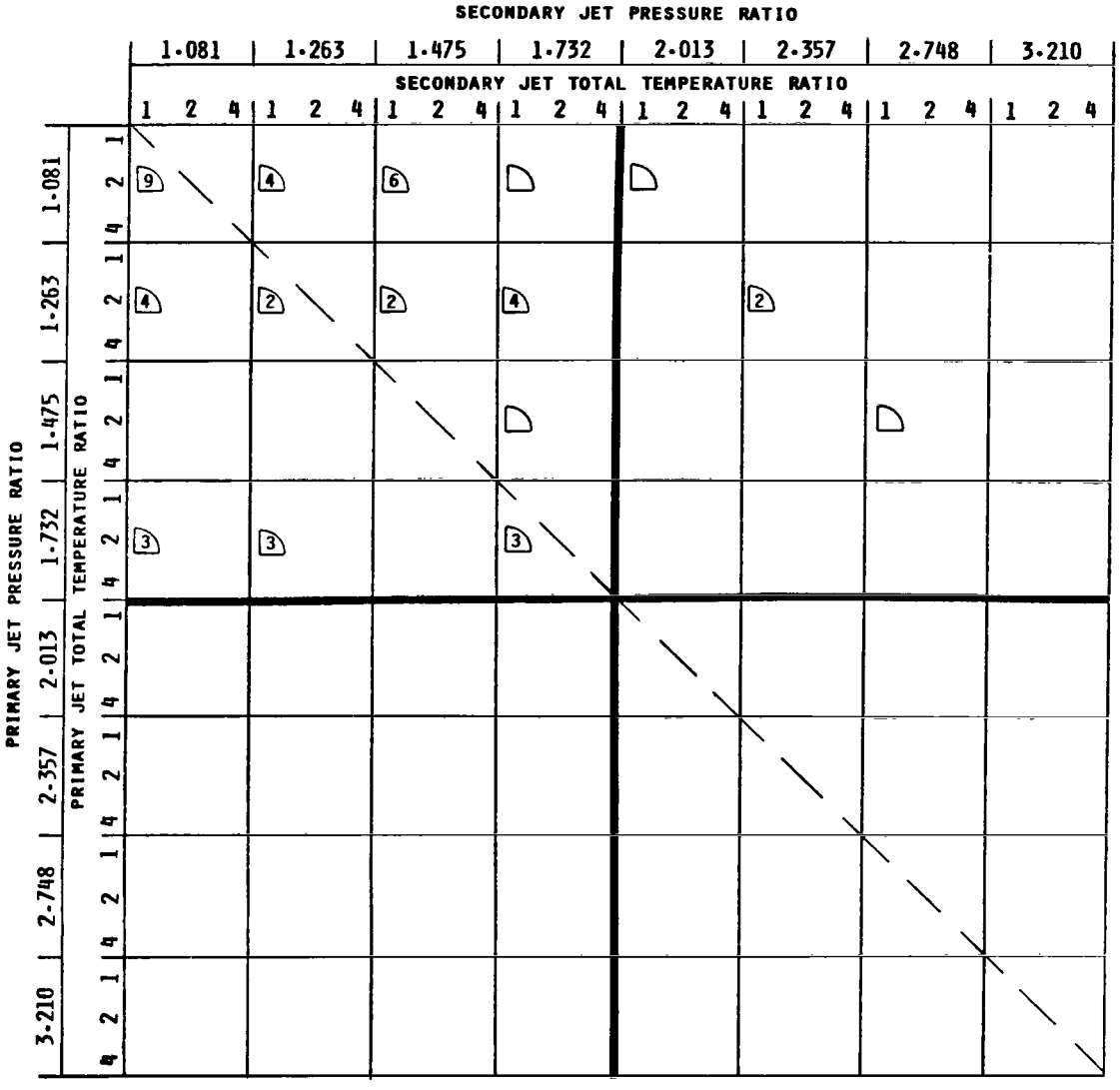

Area ratio = 4.0, 4.1, and 4.3 jets

Figure 8.- Continued.

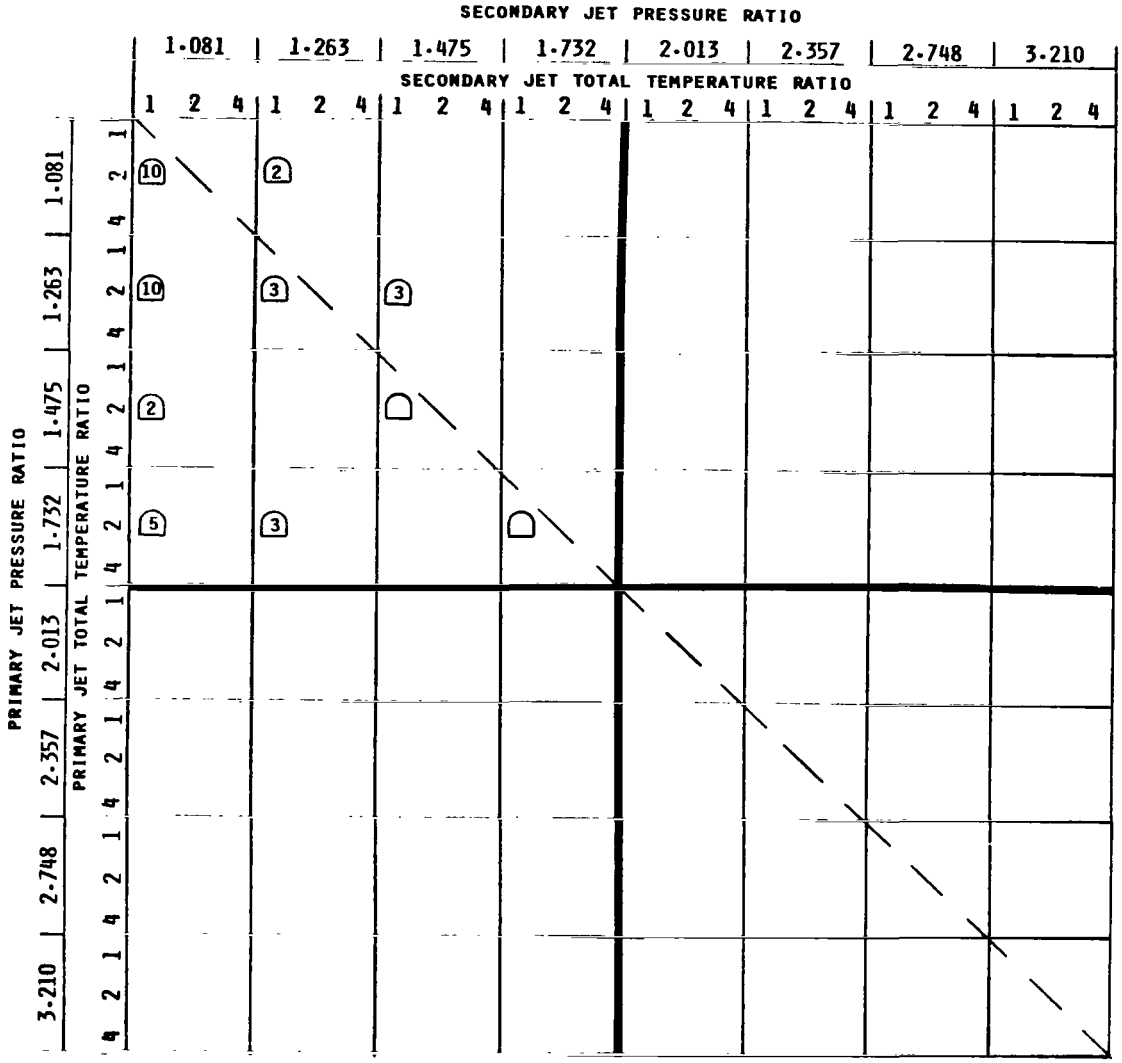

⌂ Area ratio = 7.9, 8.0, and 8.1 jets

Figure 8.- Concluded.

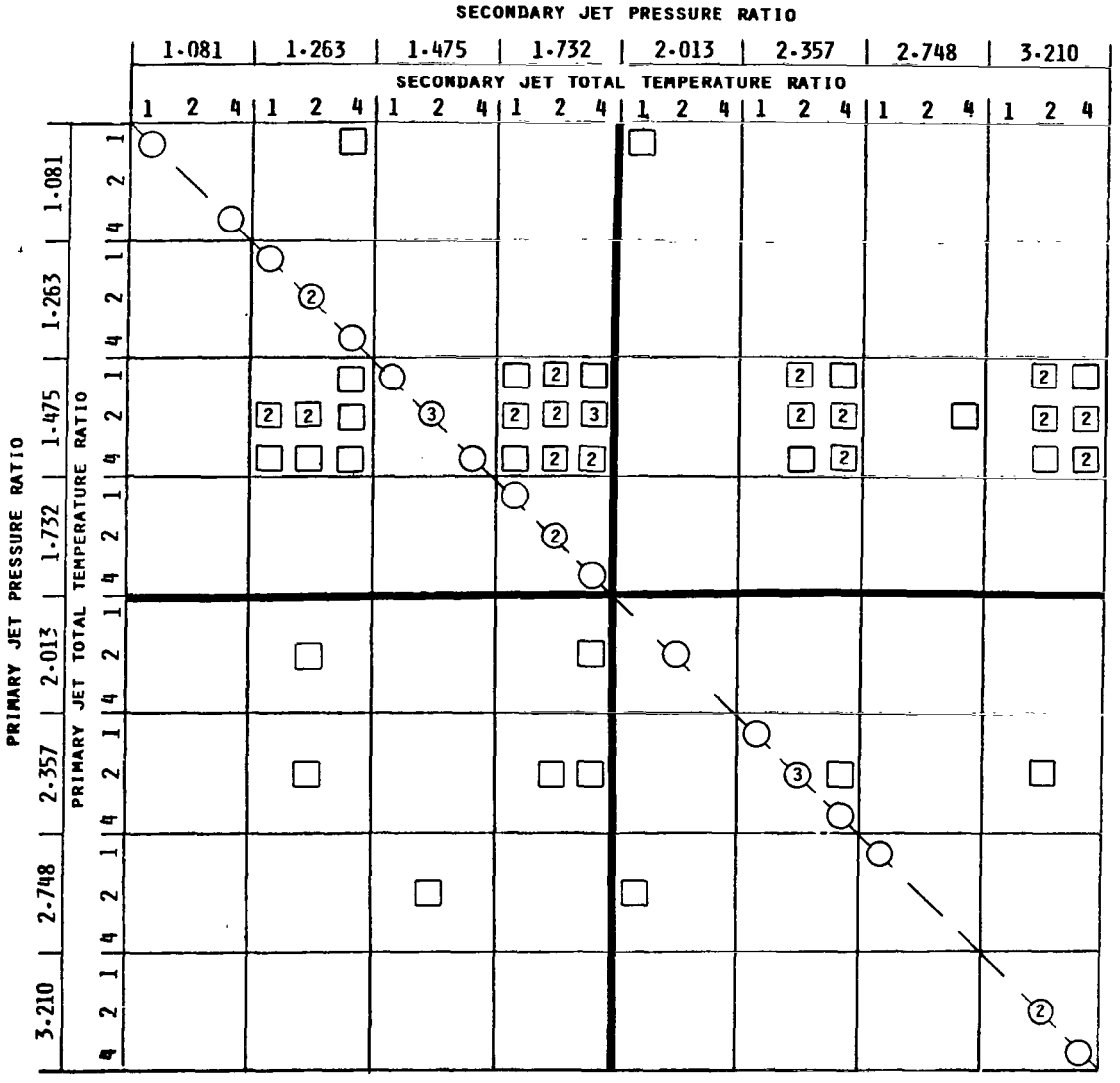

○ Circular jet □ Area ratio = 0.75 jet

Figure 9.- Jet noise test points for P&W data.

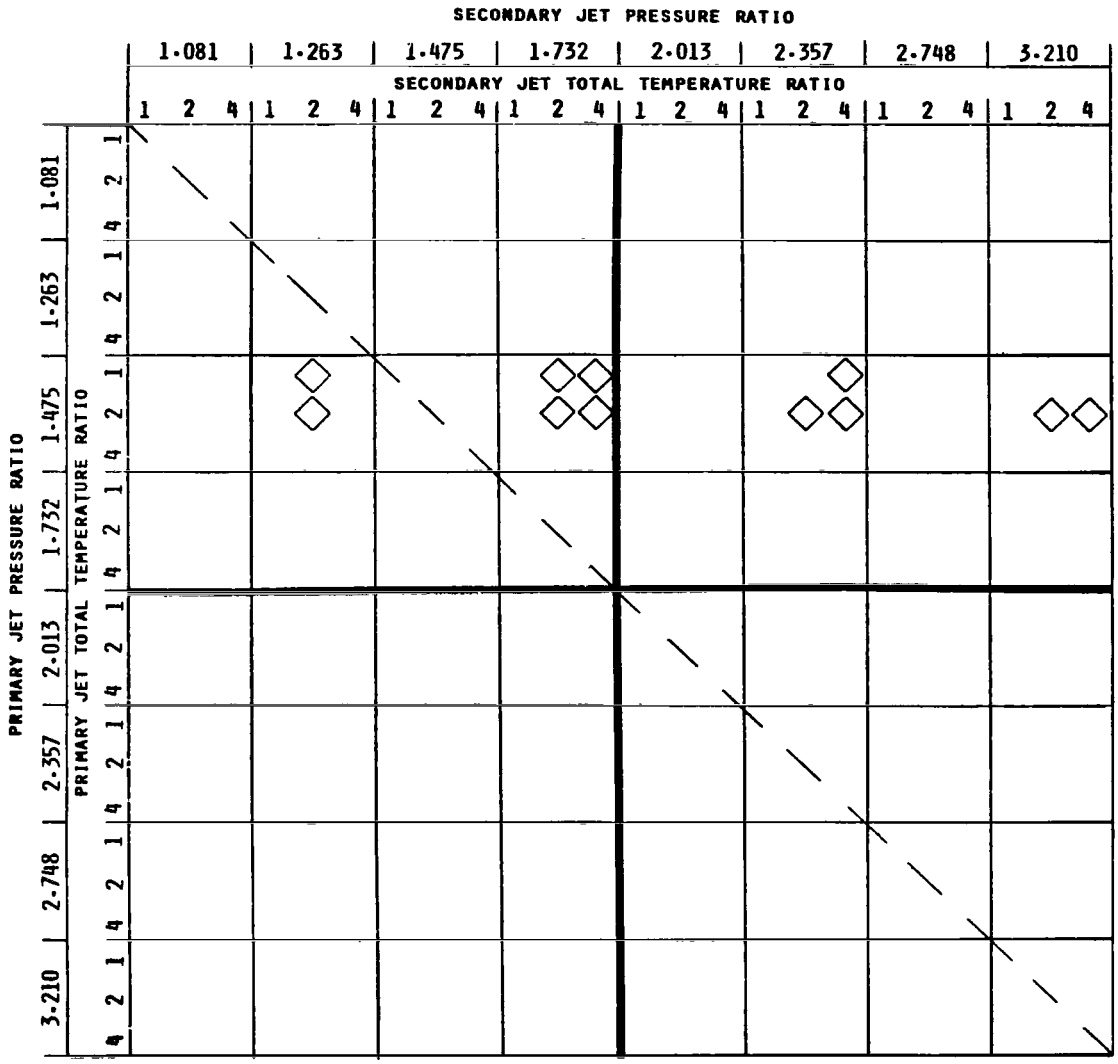

Figure 9.- Concluded.

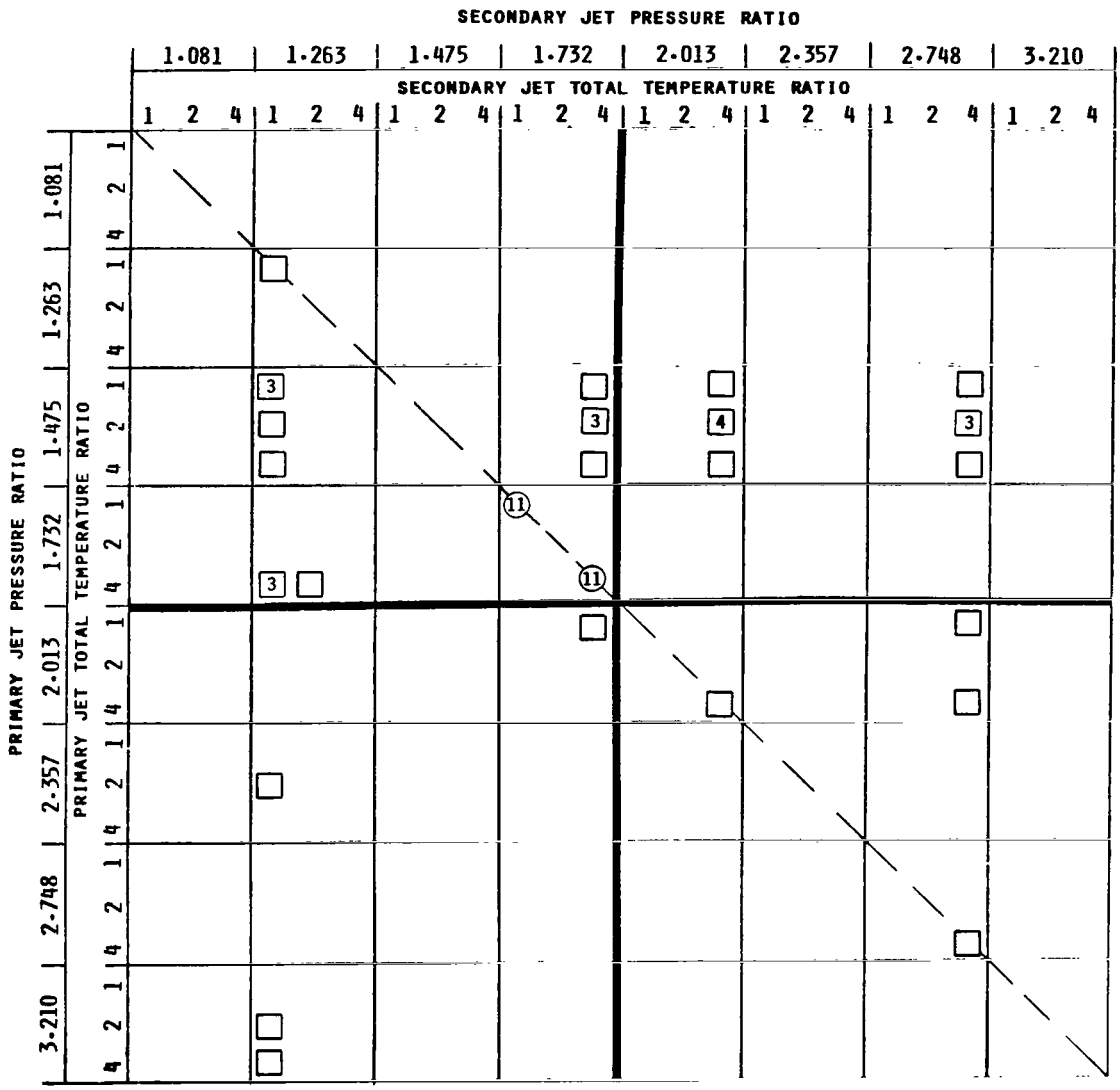

○ Circular jet ☐ Area ratio = 1.2 jet

Figure 10.- Jet noise test points for LeRC data.

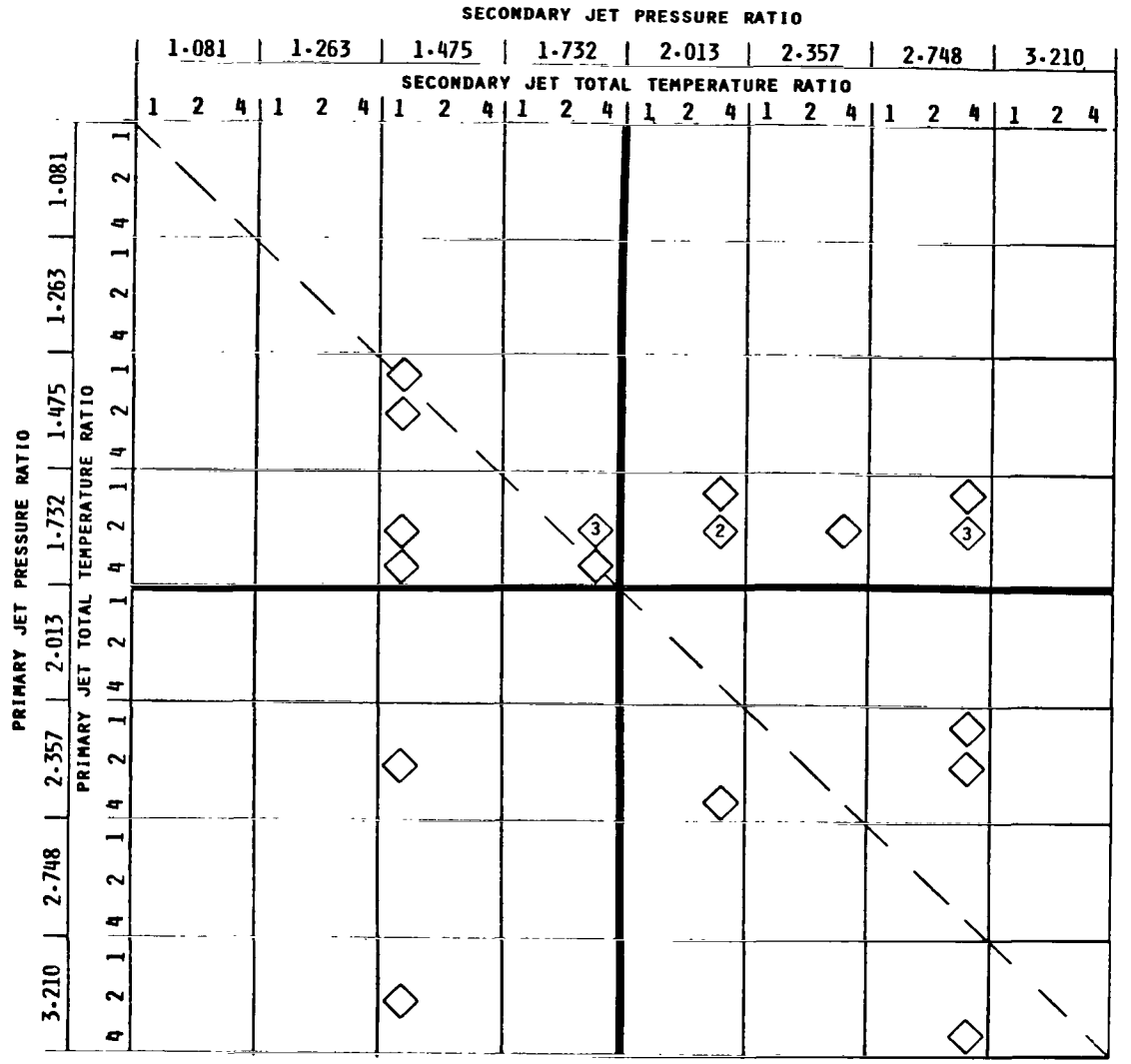

◇ Area ratio = 1.5 jet

Figure 10.- Continued.

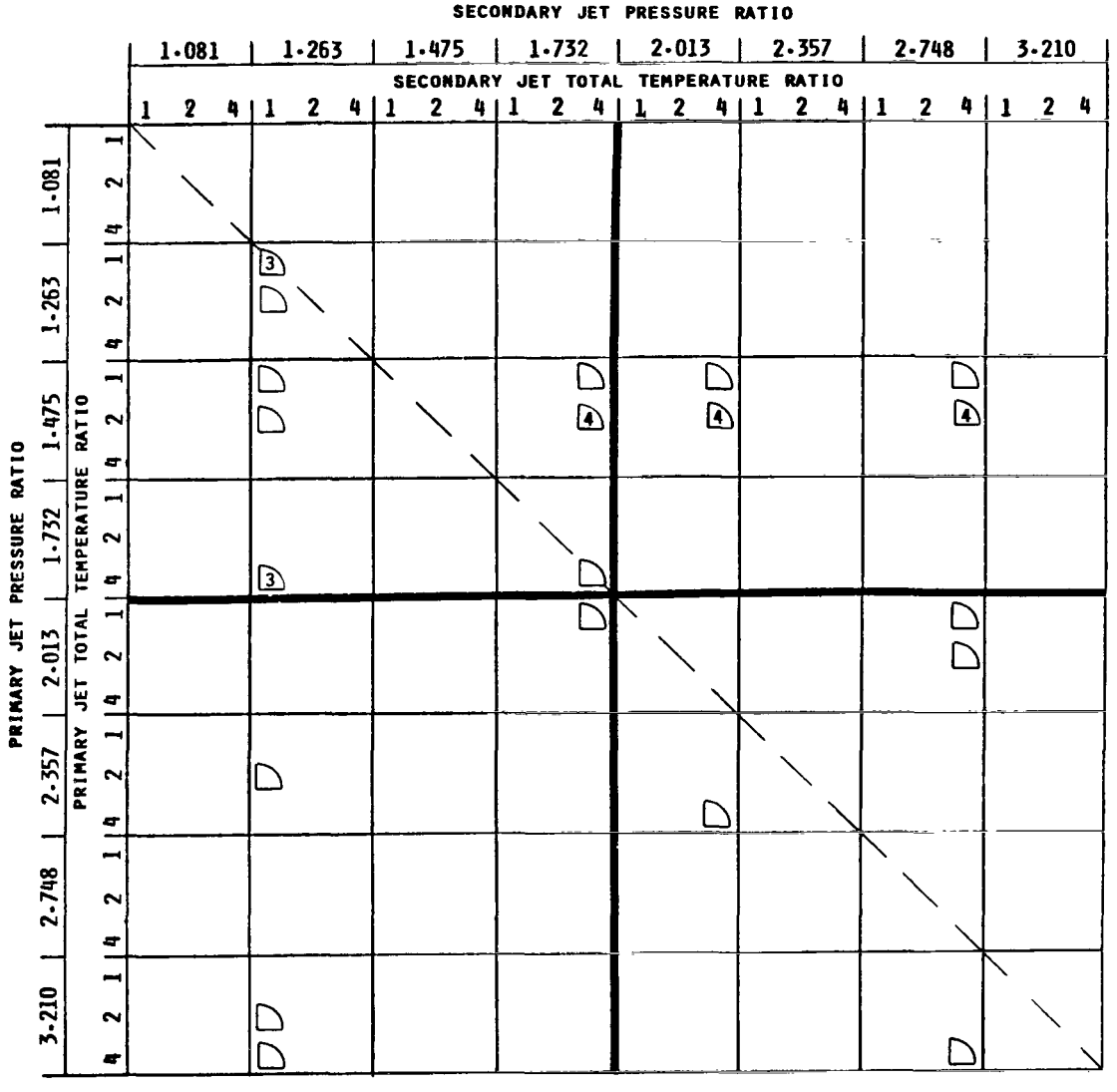

Area ratio = 2.0 jet

Figure 10.- Continued.

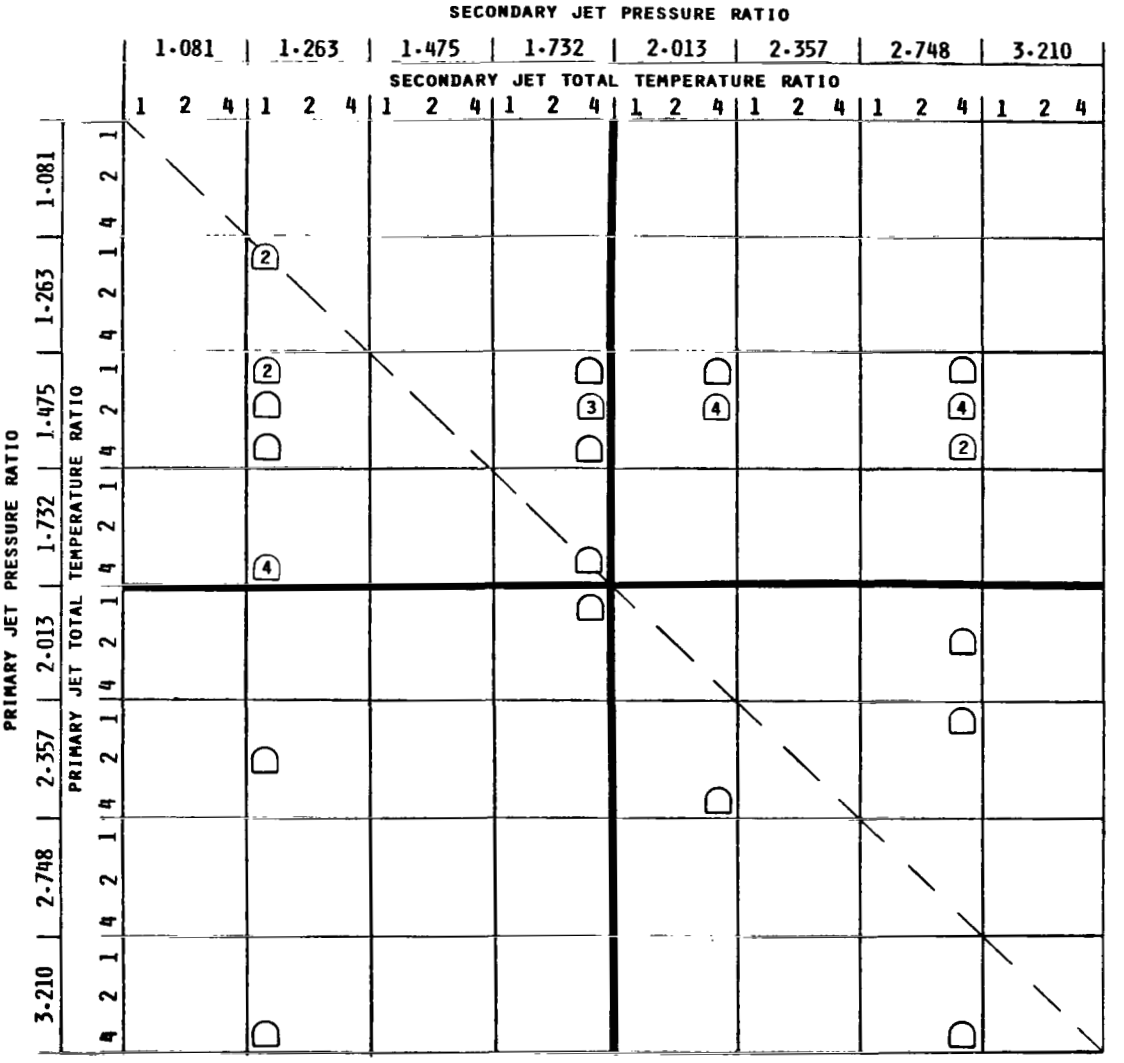

Area ratio = 3.33 jet

Figure 10.- Concluded.

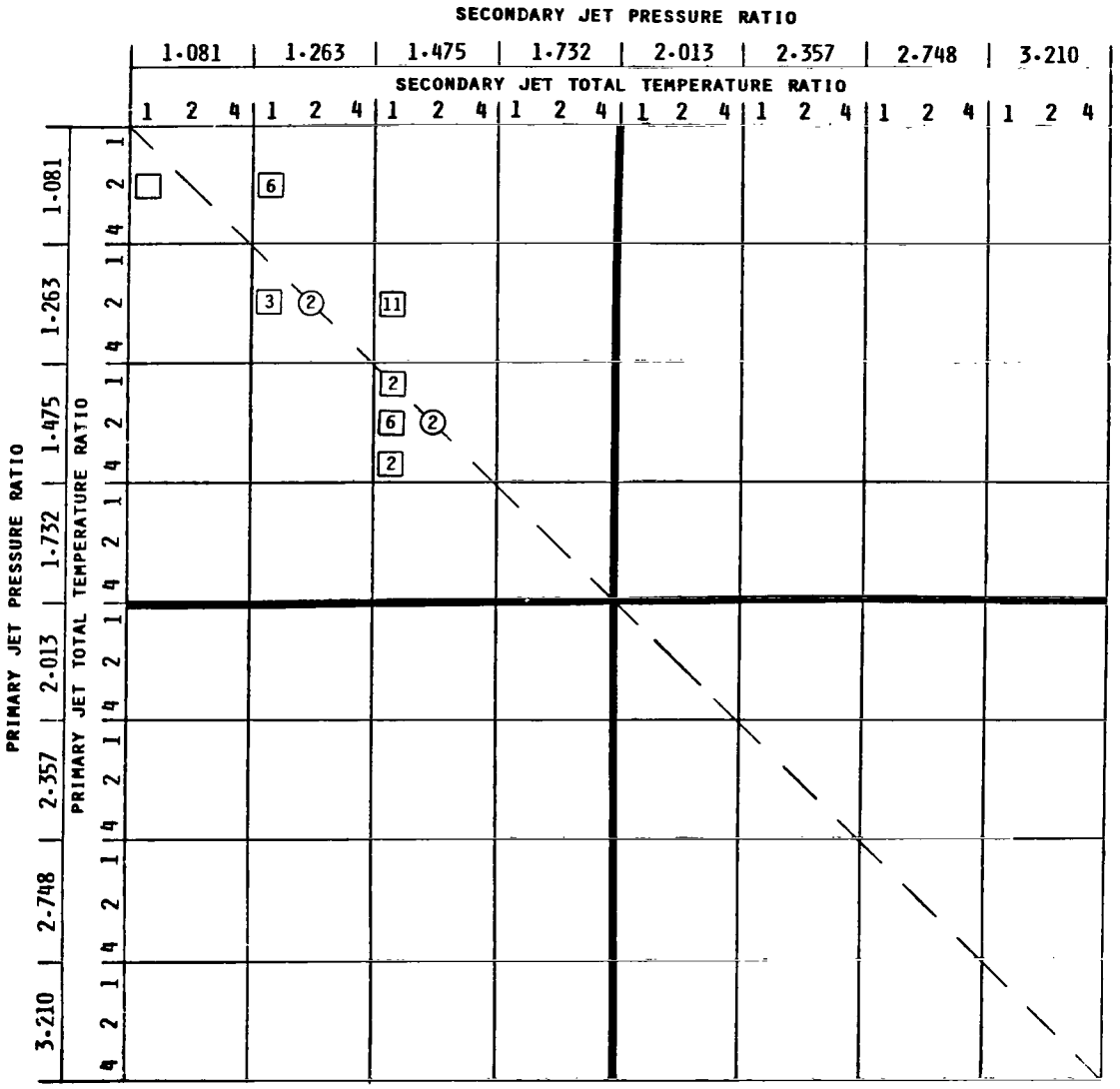

○ Circular jet □ Area ratio = 3.52 jet

Figure 11.- Jet noise test points for SNECMA data.

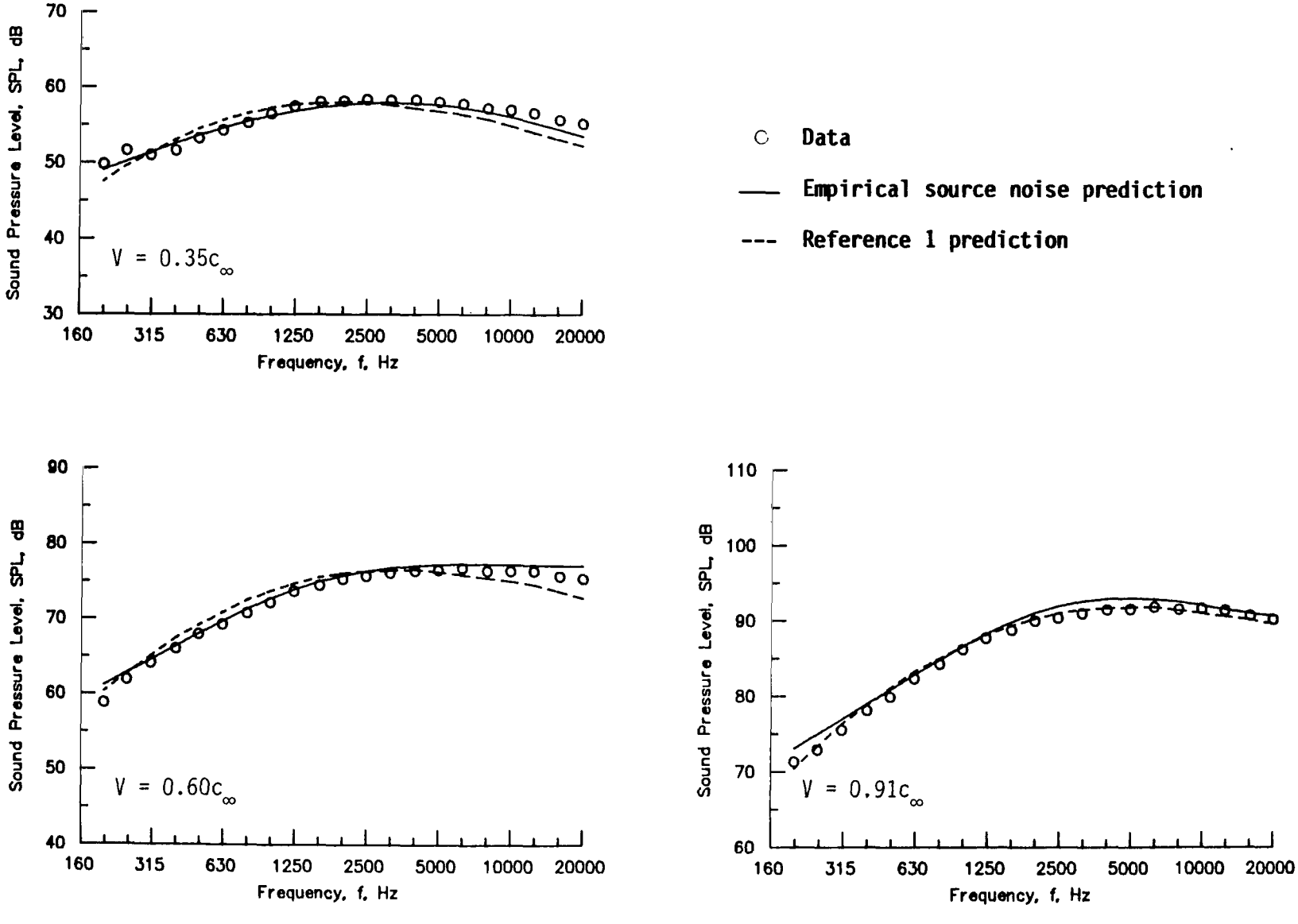

(a) $\theta = 120°$; $T_t = 1.0T_\infty$.

Figure 12.- Comparison of prediction methods for GALAC single jet data set.

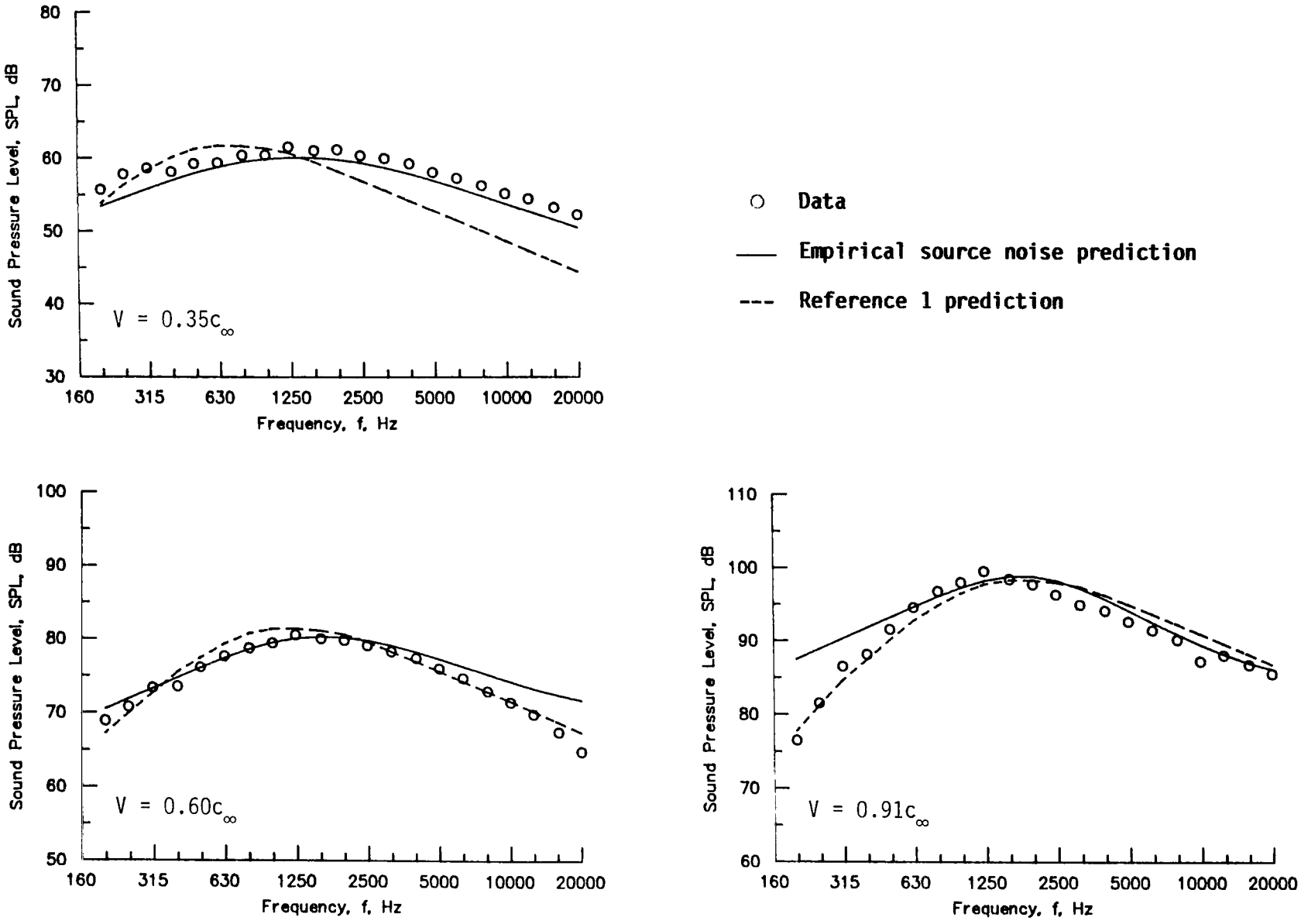

(b) $\theta = 150°$; $T_t = 1.0T_\infty$.

Figure 12.- Continued.

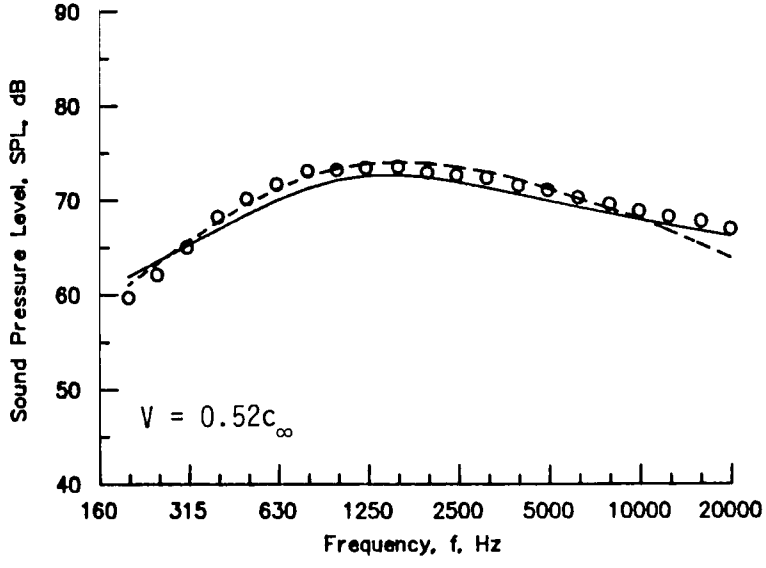

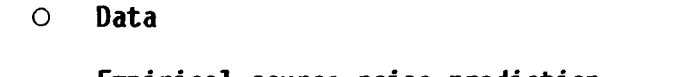

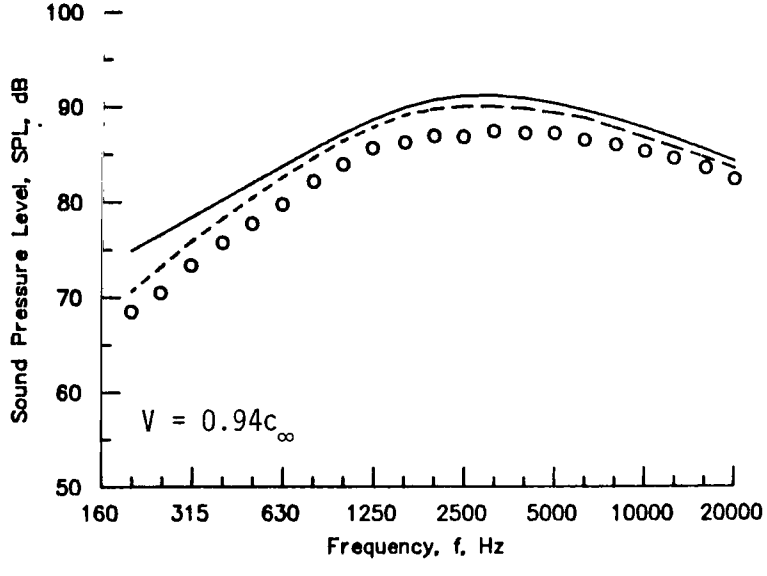

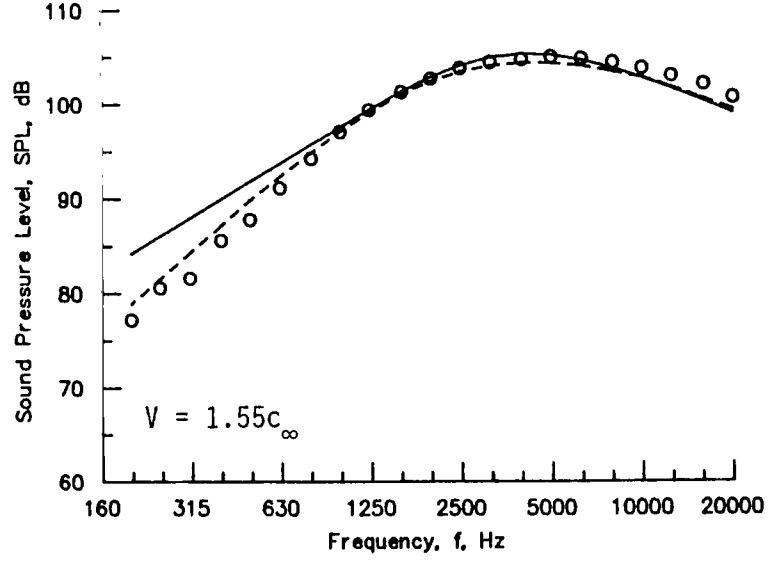

(c) $\theta = 120°$; $T_t = 3.5T_\infty$.

Figure 12.- Continued.

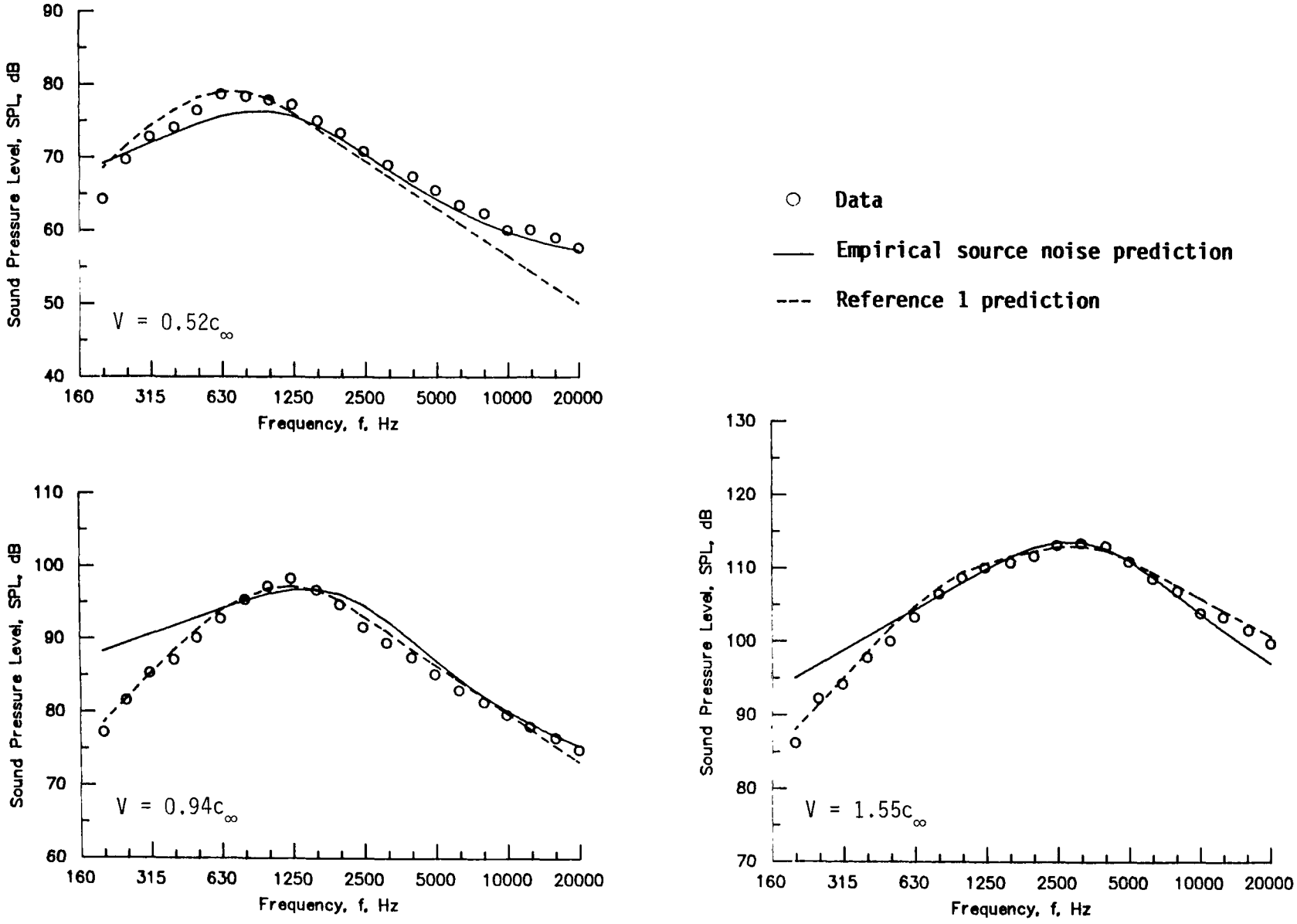

(d) $\theta = 150°$; $T_t = 3.5T_\infty$.

Figure 12.- Concluded.

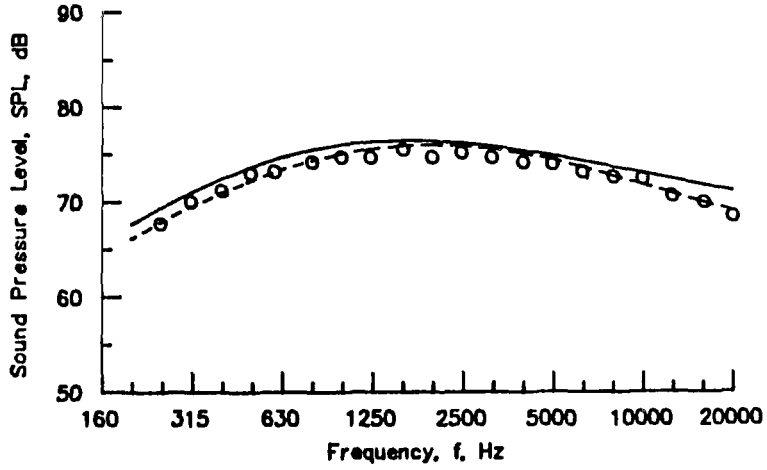

(a) $T_{t,1} = 1.0T_{\infty}$.

○ Data

—— Empirical source noise prediction based on all data sets

--- Empirical source noise prediction based on NGTE Data Set A only

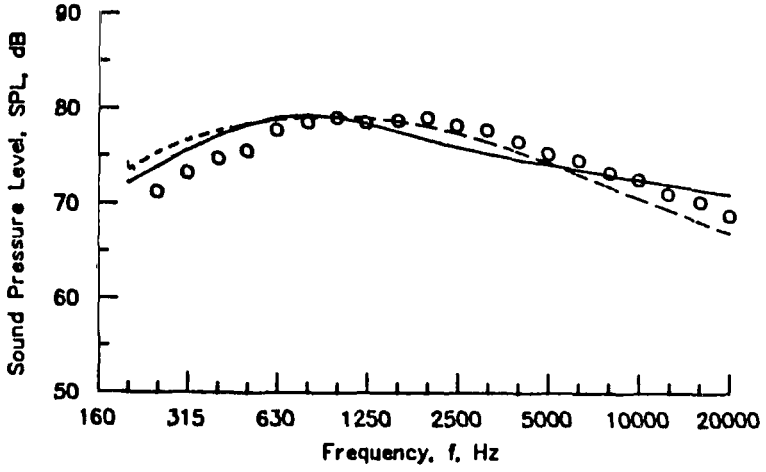

(b) $T_{t,1} = 2.4T_{\infty}$.

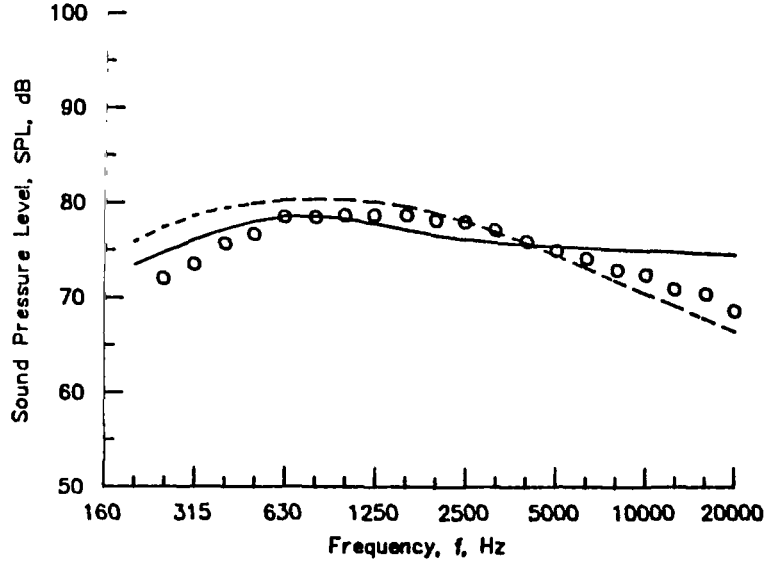

(c) $T_{t,1} = 3.1T_{\infty}$.

Figure 13.- Effect of primary jet temperature on sound pressure level for a coaxial jet with NGTE data set A. $V_1 = 0.6c_{\infty}$; $V_2 = 0.2c_{\infty}$; $T_{t,2} = 1.0T_{\infty}$; $A_2/A_1 = 6.0$; $\theta = 120°$.

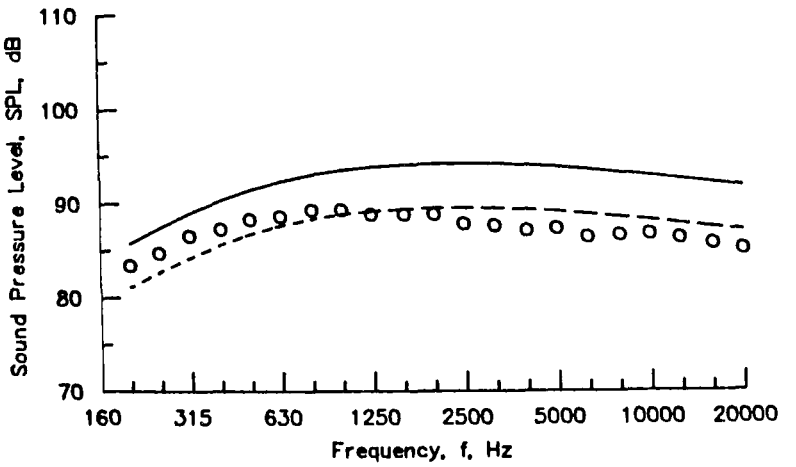

(a) $V_1 = 0.7c_\infty$.

○ Data

—— Empirical source noise prediction based on all data sets

--- Empirical source noise prediction based on NGTE Data Set B only

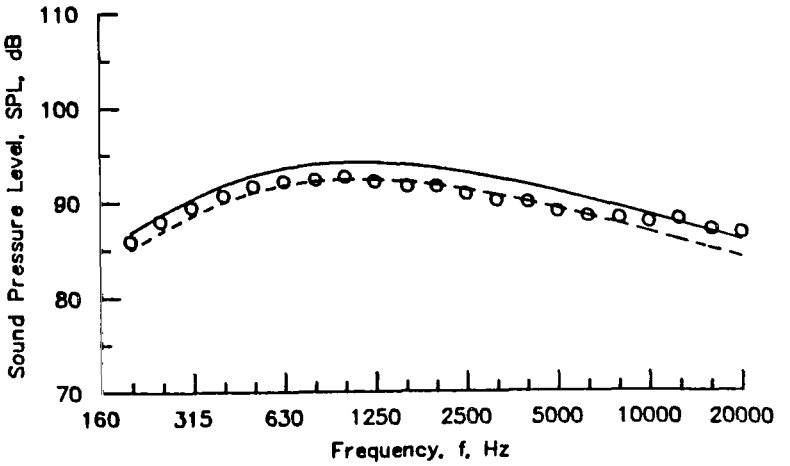

(b) $V_1 = 1.1c_\infty$.

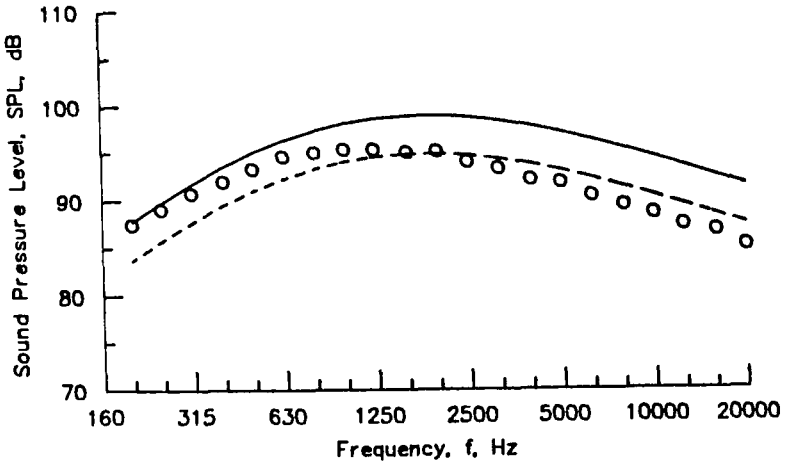

(c) $V_1 = 1.4c_\infty$.

Figure 14.- Effect of primary jet velocity on sound pressure level for a coaxial jet with NGTE data set B. $V_2 = 0.9c_\infty$; $T_{t,1} = 2.4T_\infty$; $T_{t,2} = 1.0T_\infty$; $A_2/A_1 = 4.0$; $\theta = 120°$.

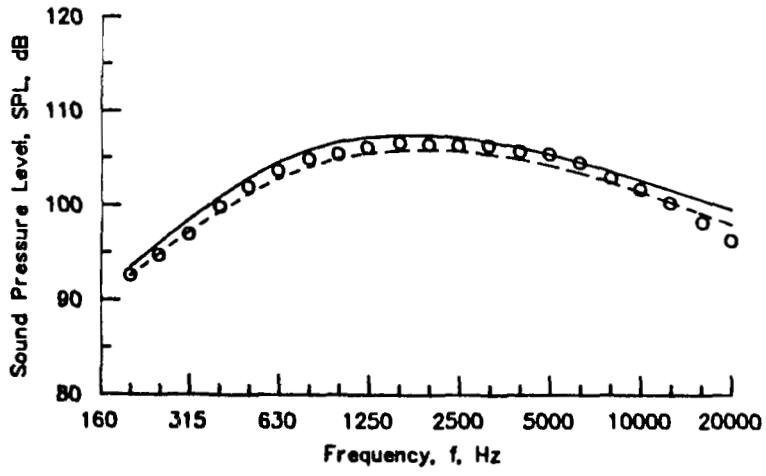

(a) $A_2/A_1 = 2.0$.

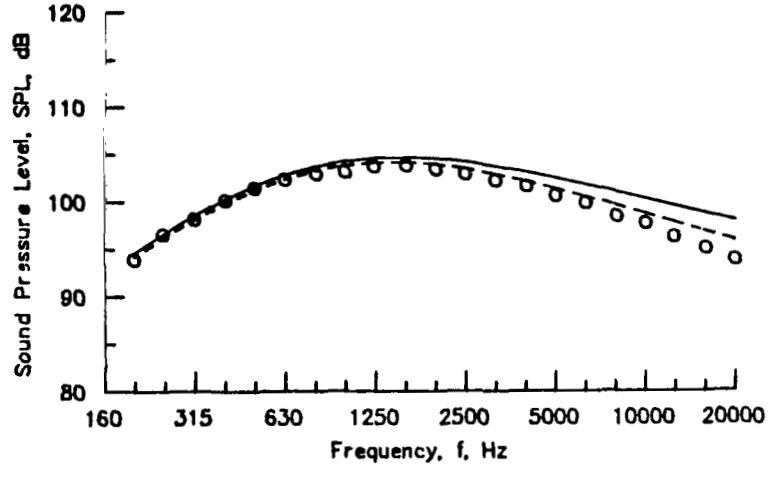

(b) $A_2/A_1 = 4.3$.

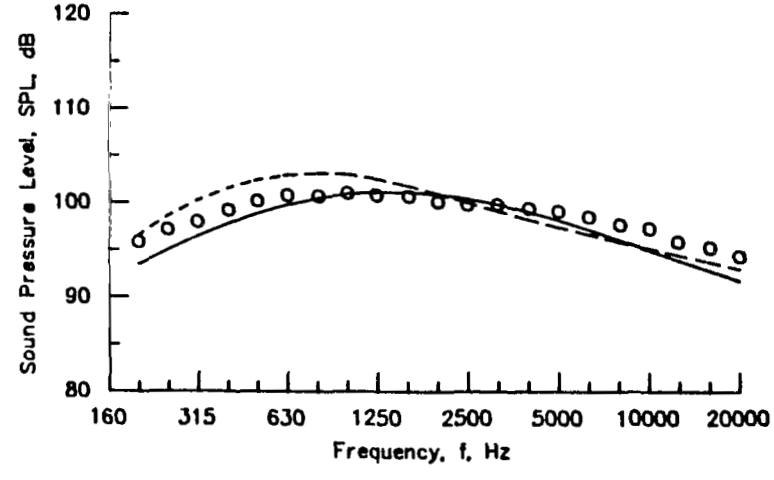

(c) $A_2/A_1 = 8.0$.

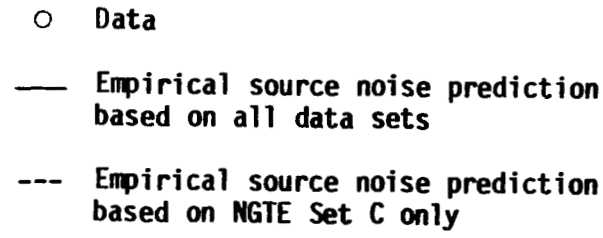

Figure 15.- Effect of area ratio on the sound pressure level for a coaxial jet with NGTE data set C. $V_1 = 1.5c_\infty$; $V_2 = 0.9c_\infty$; $T_{t,1} = 2.8T_\infty$; $T_{t,2} = 1.0T_\infty$; $\theta = 120°$.

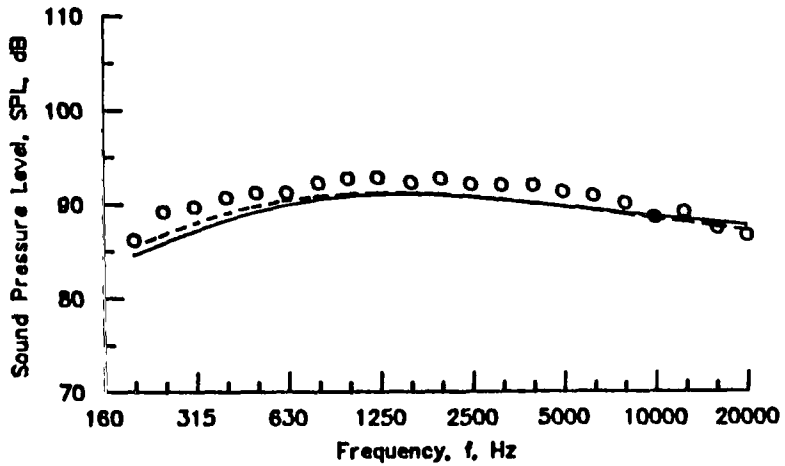

(a) $V_1 = 0.6c_\infty$; $V_2 = 0.6c_\infty$; $T_{t,1} = 1.0T_\infty$; $T_{t,2} = 1.0T_\infty$.

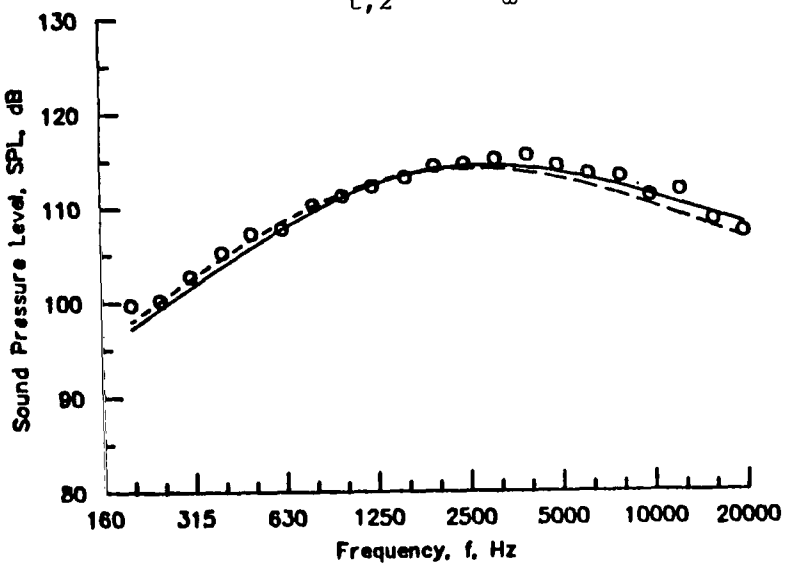

(b) $V_1 = 1.7c_\infty$; $V_2 = 0.6c_\infty$; $T_{t,1} = 3.9T_\infty$; $T_{t,2} = 1.0T_\infty$.

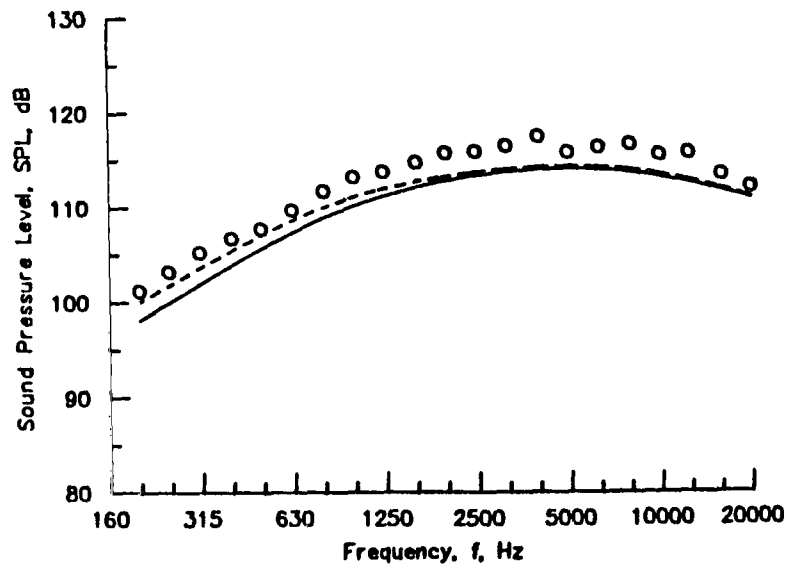

(c) $V_1 = 0.8c_\infty$; $V_2 = 1.7c_\infty$; $T_{t,1} = 1.0T_\infty$; $T_{t,2} = 3.8T_\infty$.

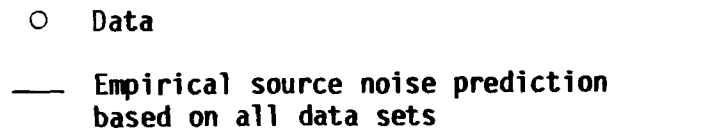

Figure 16.- Predictions of sound pressure level for widely separated states of coaxial jet with LeRC data set. $A_2/A_1 = 2.0$; $\theta = 120°$.

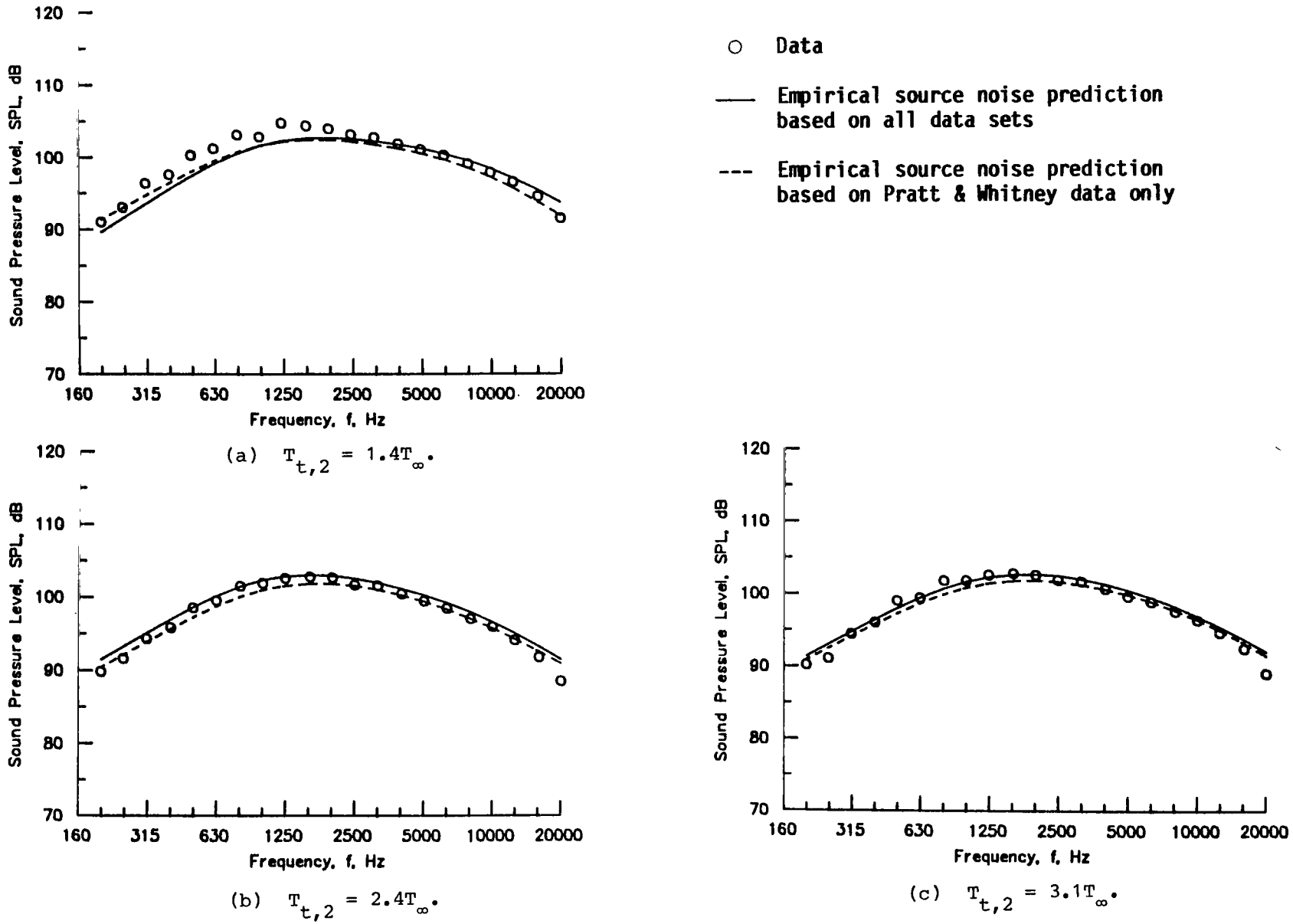

(a) $T_{t,2} = 1.4T_{\infty}$.

(b) $T_{t,2} = 2.4T_{\infty}$.

(c) $T_{t,2} = 3.1T_{\infty}$.

Figure 17.- Effect of secondary jet total temperature on sound pressure level for coaxial jet with P&W data set. $V_1 = 1.3c_{\infty}$; $V_2 = 1.0c_{\infty}$; $T_{t,1} = 2.8T_{\infty}$; $A_2/A_1 = 0.75$; $\theta = 120°$.

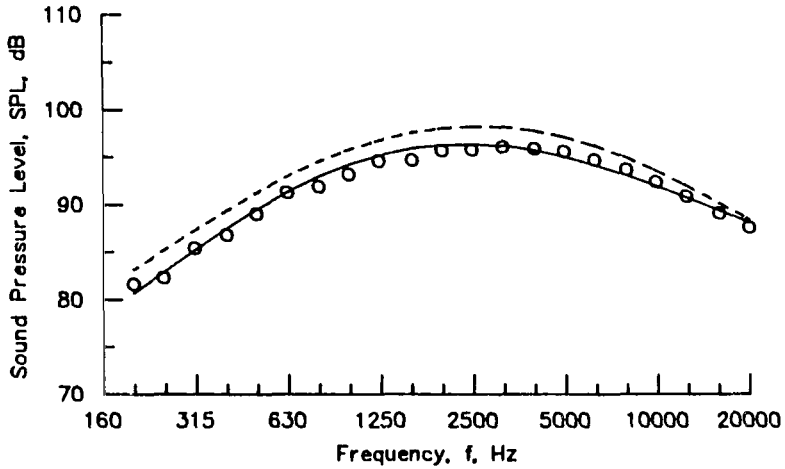

(a) $V_1 = 1.3c_\infty$; $V_2 = 0.8c_\infty$; $T_{t,1} = 2.9T_\infty$; $T_{t,2} = 1.0T_\infty$.

○ Data

—— Empirical source noise prediction based on all data sets

--- Empirical source noise prediction based on SNECMA data only

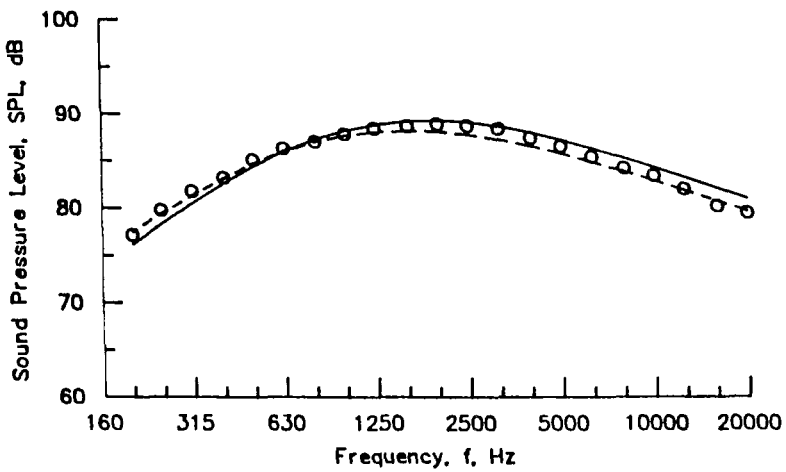

(b) $V_1 = 1.0c_\infty$; $V_2 = 0.7c_\infty$; $T_{t,1} = 2.7c_\infty$; $T_{t,2} = 1.1T_\infty$.

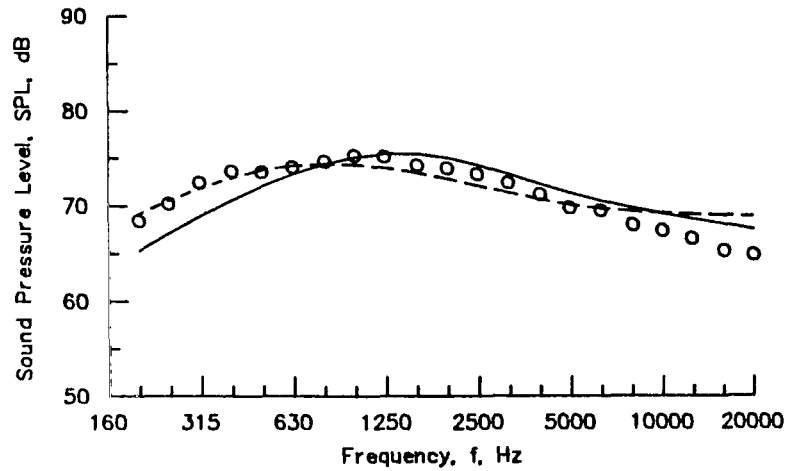

(c) $V_1 = 0.6c_\infty$; $V_2 = 0.6c_\infty$; $T_{t,1} = 2.0T_\infty$; $T_{t,2} = 1.2T_\infty$.

Figure 18.- Effect of thrust on sound pressure level for coaxial jet with SNECMA data set. $A_2/A_1 = 3.5$; $\theta = 120°$.

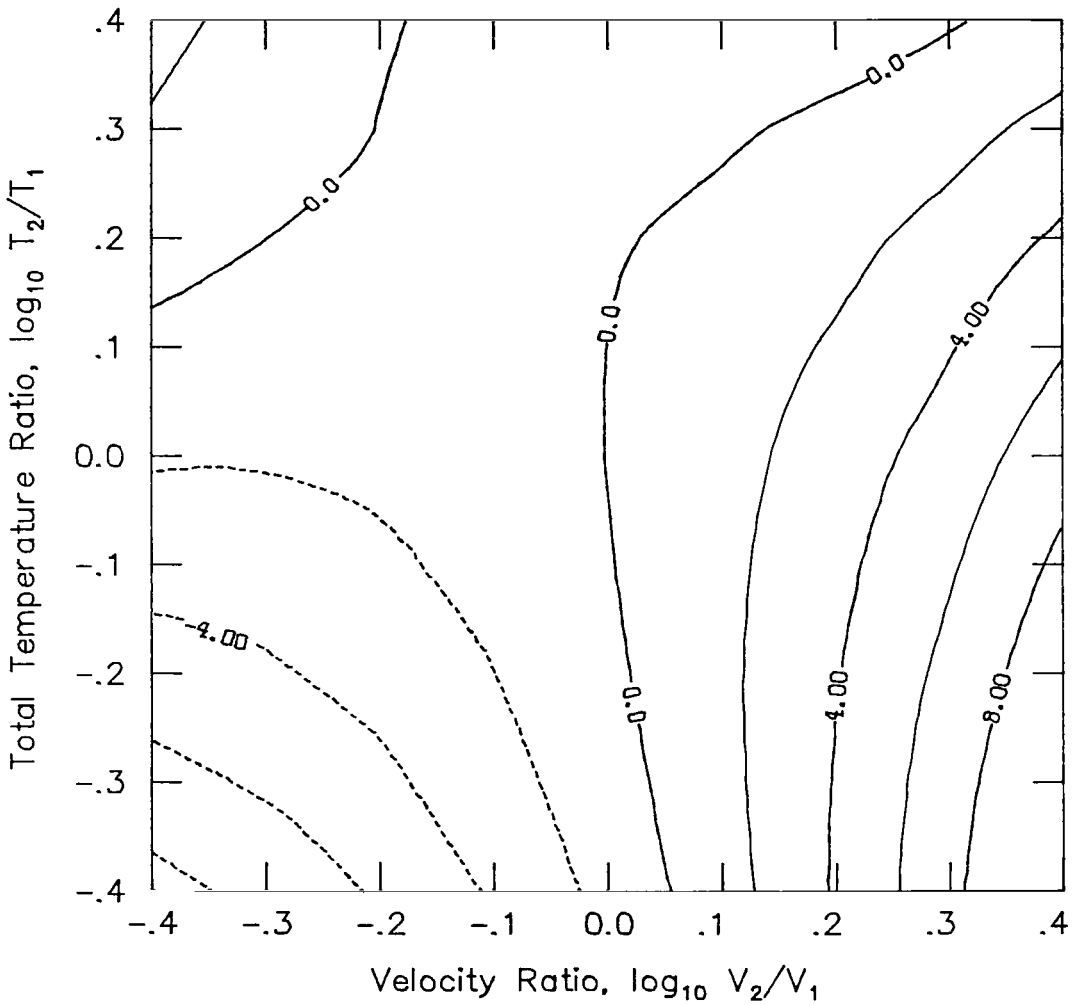

Figure 19.- Contour plot of coaxial benefit for equivalent velocity ratio of 1.0, equivalent total temperature ratio of 2.0, and area ratio of 1.0.

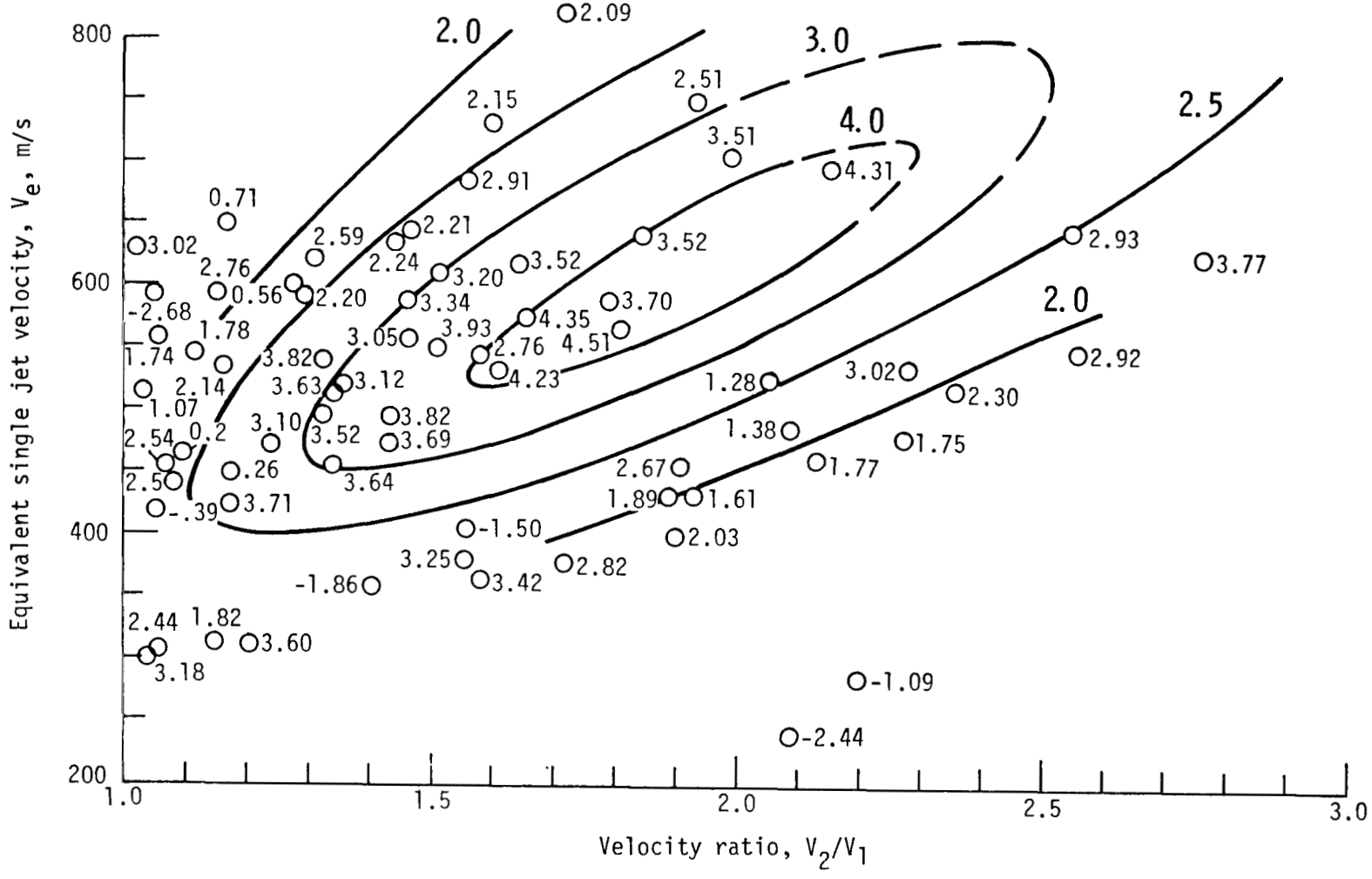

Figure 20.- Contour plot of coaxial benefit from P&W data set from Pao (ref. 9).

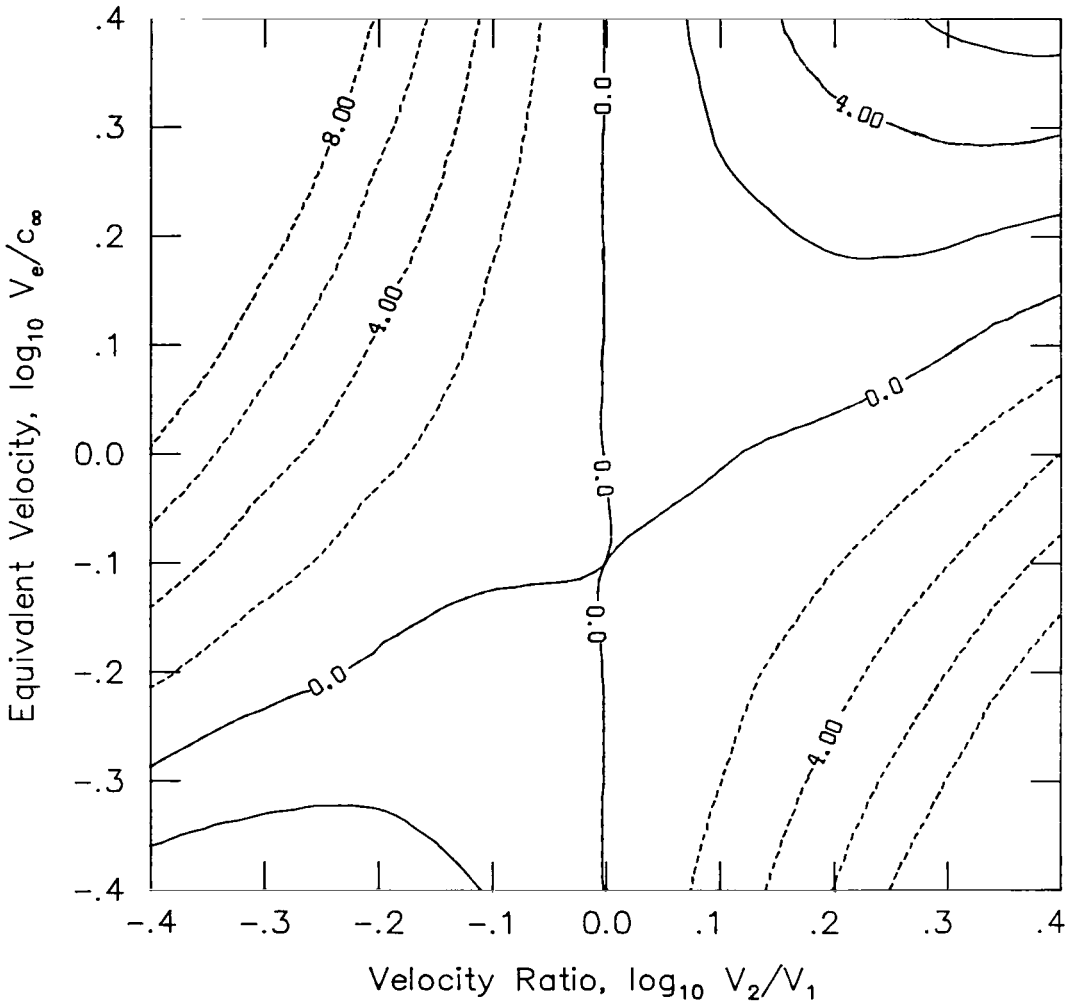

Figure 21.- Contour plot of coaxial benefit from P&W data set using the empirical source noise prediction method.

1. Report No.	2. Government Accession No.	3. Recipient's Catalog No.
NASA TP-2084		

4. Title and Subtitle	5. Report Date
EMPIRICAL SOURCE NOISE PREDICTION METHOD WITH APPLICATION TO SUBSONIC COAXIAL JET MIXING NOISE	December 1982
	6. Performing Organization Code: 505-32-03-01
7. Author(s): William E. Zorumski and Donald S. Weir	8. Performing Organization Report No.: L-15382
	10. Work Unit No.
9. Performing Organization Name and Address: NASA Langley Research Center, Hampton, VA 23665	11. Contract or Grant No.
	13. Type of Report and Period Covered: Technical Paper
12. Sponsoring Agency Name and Address: National Aeronautics and Space Administration, Washington, DC 20546	14. Sponsoring Agency Code

15. Supplementary Notes

16. Abstract

A general empirical method is developed for source noise predictions. This method uses tensor splines to represent the dependence of the acoustic field on frequency and direction and Taylor's series to represent the dependence on source state parameters. The method is applied to prediction of mixing noise from subsonic circular and coaxial jets. A noise data base of 1/3-octave-band sound pressure levels (SPL's) from 540 tests was gathered from three countries: United States, United Kingdom, and France. The SPL's depend on seven variables: frequency, polar direction angle, and five source state parameters - inner and outer nozzle pressure ratios, inner and outer stream total temperatures, and nozzle area ratio. A least-squares seven-dimensional curve fit defines a table of constants which is used for the prediction method. The resulting prediction has a mean error of 0 dB and a standard deviation of 1.2 dB. The prediction method is used to search for a coaxial jet which has the greatest coaxial noise benefit as compared with an equivalent single jet. It is found that benefits of about 6 dB are possible.

17. Key Words (Suggested by Author(s))	18. Distribution Statement
Jet noise Noise prediction Noise reduction	Unclassified - Unlimited Subject Category 71

19. Security Classif. (of this report)	20. Security Classif. (of this page)	21. No. of Pages	22. Price
Unclassified	Unclassified	76	A05

For sale by the National Technical Information Service, Springfield, Virginia 22161

NASA-Langley, 1982

1 1 1U,H, 821215 S00903DS
DEPT OF THE AIR FORCE
AF WEAPONS LABORATORY
ATTN: TECHNICAL LIBRARY (SUL)
KIRTLAND AFB NM 87117

S